Nonlinear Dynamic Analysis of Lateral Soil Pile Structure Interaction via the Continuum Modeling Approach

Mohammad Ghorbanzadeh

Submitted to the
Institute of Graduate Studies and Research
in partial fulfillment of the requirements for the degree of

Doctor of Philosophy
in
Civil Engineering

Eastern Mediterranean University
September 2021
Gazimağusa, North Cyprus

Approval of the Institute of Graduate Studies and Research

Prof. Dr. Ali Hakan Ulusoy
Director

I certify that this thesis satisfies all the requirements as a thesis for the degree of Doctor of Philosophy in Civil Engineering.

Prof. Dr. Umut Türker
Chair, Department of Civil Engineering

We certify that we have read this thesis and that in our opinion it is fully adequate in scope and quality as a thesis for the degree of Doctor of Philosophy in Civil Engineering.

Asst. Prof. Dr. Eriş Uygar
Co-Supervisor

Prof. Dr. Serhan Şensoy
Supervisor

Examining Committee

1. Prof. Dr. Kemal Önder Çetin
2. Prof. Dr. Ali Koçak
3. Prof. Dr. Serhan Şensoy
4. Assoc. Prof. Dr. Mehmet Cemal Geneş
5. Assoc. Prof. Dr. Giray Özay
6. Asst. Prof. Dr. İsmail Safkan
7. Asst. Prof. Dr. Eriş Uygar

ABSTRACT

Structures equipped with semi-active Tuned Mass Damper (STMD) have recently become popular because of the high efficiency attained against lateral loading. Although it is easy to use, the search for the optimized STMD parameters to mitigate the dynamic response of structures founded on deep foundations is usually complicated. The search for accurate soil-pile-structure interaction (SPSI) estimation has a greater impact on the STMD configuration. The use of lateral load-displacement curves (p-y curves) recommended in the American Petroleum Institute (API) guideline is typically used as a design approach for soil-pile-structure interaction analysis due to its simplicity. The soil-pile-structure interface has two separate parts of interaction; kinematic and inertial interaction. Both types of interaction must be accurately measured for structures with dampers to determine the optimal parameters for design. For structures equipped with semi-active tuned mass dampers (STMD) on a deep foundation, the determination of the optimal STMD characteristics is completely related to the dynamic behavior of the structure. Therefore, in this study, the accuracy of the general p-y equation for buildings with STMD having a short period on deep foundations is first evaluated. Then, the three-dimensional continuum method (finite element method) is used and the general p-y equation is updated to provide compatibility.

Keywords: Soil pile structure interaction; Deep foundation; Finite element method; Semi tuned mass damper; p-y backbone curves; Spring method.

ÖZ

Yarı aktif Ayarlı Kütle Sönümleyicisi (STMD) ile donatılmış yapılar, yanal yüklemeye karşı elde edilen yüksek verim nedeniyle son zamanlarda popüler hale gelmiştir. Kullanımı kolay olmasına rağmen, derin temeller üzerine kurulmuş yapıların dinamik tepkisini azaltmak için optimize edilmiş STMD parametrelerinin araştırılması genellikle karmaşıktır. Doğru zemin-kazık-yapı etkileşimi (SPSI) tahmini arayışı, STMD konfigürasyonu üzerinde daha büyük bir etkiye sahiptir. Amerikan Petrol Enstitüsü (API) kılavuzunda önerilen yanal yük-deplasman eğrilerinin (p-y eğrileri) kullanımı, basitliği nedeniyle tipik olarak zemin-kazık-yapı etkileşim analizi için bir tasarım yaklaşımı olarak kullanılır. Zemin-kazık-yapı arayüzünün iki ayrı etkileşim kısmı vardır; kinematik ve eylemsizlik etkileşimi. Tasarım için en uygun parametreleri belirlemek için damperli yapılar için her iki etkileşim türü de doğru bir şekilde ölçülmelidir. Derin bir temel üzerinde yarı aktif ayarlı kütle damperleri (STMD) ile donatılmış yapılar için, optimal STMD özelliklerinin belirlenmesi tamamen yapının dinamik davranışı ile ilgilidir. Bu nedenle bu çalışmada, öncelikle derin temellerde kısa periyodu olan STMD'li binalar için genel p-y denkleminin doğruluğu değerlendirilmiştir. Daha sonra üç boyutlu süreklilik yöntemi (sonlu elemanlar yöntemi) kullanılmış ve genel p-y denklemi uyumluluğu sağlayacak şekilde güncellenmiştir.

Anahtar Kelimeler: Zemin kazık yapısı etkileşimi; Derin Temel; Sonlu elemanlar yöntemi; Yarı ayarlı kütle damperi; p-y omurga eğrileri; Yay yöntemi.

DEDICATION

To my parents and my wife, I couldn’t have done this without you.

Thank you for all your support along the way.

ACKNOWLEDGMENT

First and foremost, I am extremely grateful to my supervisor, Prof. Dr. Serhan Şensoy, and my co-supervisor, Assist. Prof. Dr. Eriş Uygar, for their expertise, ideas, feedback, time and patience during my doctoral studies.

I would like to thank all the members of Civil Engineering Department, especially Prof. Dr. Umut Türker and also Assoc. Prof. Dr. Mehmet Cemal Geneş. It is their kind help and support that made my study in the university a wonderful time. Finally, I would like to express my deepest gratitude to my parents Abbas and Zarrin and my lovely wife Marjan. Without their tremendous understanding and encouragement over the past few years, it would have been impossible for me to complete my studies.

TABLE OF CONTENTS

LIST OF TABLES

LIST OF FIGURES

LIST OF SYMBOLS AND ABBREVIATIONS

B	Modulus of Bulk
C	Damping ratio of device
D	Pile diameter
G	Shear modulus of soil
K	Stiffness ratio of device
P	Mass density
P_u	Lateral force
Y	Lateral displacement
Ø	Friction angle of soil
μ	Mass ratio
ATMD	Active Tuned Mass Damper
API	American Petroleum Institute
DBG	Displacement Based Ground hook algorithm
DOF	Degree of Freedom
FEM	Finite Element Method
GHA	Ground Hook Algorithm
STMD	Semi active Tuned Mass Damper
SSI	Soil Structure Interaction
SPSI	Soil Pile Structure Interaction
TMD	Tuned Mass Damper
THA	Time History Analysis

Chapter 1

INTRODUCTION

1.1 General

It is common knowledge that if structures are not properly designed, when earthquakes they will be subjected to significant damage. In order to build more resilient cities, assessing earthquake risk and developing infrastructure techniques to minimize damage should be primary aim. Geologists, seismologists, and engineers continue to focus on updating seismic codes, creating accurate records and updating knowledge for design and analysis earthquake-resistant structures. For the engineers, the ultimate goal should be to build cost-effective, damage-free systems that function in a predictable and reasonable manner to mitigate risks and achieve safety.

Recently it became possible to control the effects of building vibrations caused by earthquakes or wind loads by various basic methods. The conceptual background to the methods relies on modifying stiffness, strength, damping, and provisions of active or passive object devices. Up to now, several approaches to structural vibration control have been widely employed. The recently introduced approaches discussed to offer a lot of potential in terms of field of application and also enhancement of seismic behavior.

Remarkable improvement has been prepared in nonlinear dynamic analysis of earthquakes and structural response in recent years. Improving structural configuration

requires optimal determination of the size and shape of various elements, understanding of building materials and improvement techniques for vibration suppressing [1–6].

Conventionally, structures have been designed based only on the stiffness of their structural elements under seismic excitations. Increasing the dimensions of structural elements was typically used to increase the robustness of buildings, which resulted in greater force being moved through the structural elements, increasing required strength, again increasing the elements dimensions and this vicious circle is repeatedly create. Regarding to this challenge, control design technology is introduced, in which control system tools are added to the main structure to increase the seismic resistance of structures and help the structure dissipate more energy. Recently, the use of this technology is widely expanded to design new buildings and even retrofit current buildings. Control devices and systems are classified into four types: Active, semi-active, reactive and combined dampers. In this study, Semi Active Tuned Mass Damper (STMD) is used as an additional damping system on top of the buildings. In this system, in order to resist the lateral excitations such as wind and earthquake, the natural frequency of the STMD adapts to the main mode shape of the structure, which results in a large amount of vibration energy being transferred to the STMD and subsequently greatly increases the safety and strength of the main structure. Thus, if the STMD parameters are optimized well, the structure can perform better to mitigate the structural responses [7].

A fixed base structure behave quite different from a structure which is supported by flexible foundation when earthquake event happened. This is because of wave

propagation, and also dynamic interaction between the structure and soil. Hence, the record motion which is altered by soil conditions, transferred to the structure and has different effect on the dynamic attitude of structure, which in turn alters the input motion characterizations by its lateral movement and rotation. This phenomenon is called soil-foundation-structure interaction or usually soil-structure interaction (SSI). This interaction can be boosted when the structure is founded on a pile foundation. In this case, a superstructure-soil interaction and pile-soil interaction occurs, which is called soil-pile-structure interaction (SPSI).

The soil-pile-structure interaction, has two main mechanisms [8]:

- Inertial interaction which occurs when the inertia energy of superstructure are shifted to the foundation and eventually to the soil block and vice versa, creating initial stresses in the structure.
- Kinematic interaction which occurs in the foundation due to displacement of the ground, which increase the vertical and lateral stresses causing forces and bending moments in the foundation.

Two methods are commonly used to simulate soil structure interaction: The substructure (spring) method and the continuum (finite element) method. The spring method is a simple method for representing soil-structure interaction with a set of nonlinear unconstrained springs and dashpots. Continuum method is a complex and more accurate method in which all structural components, foundation and soil block are simulated by using finite mesh of coupled nodes without the need for defining the springs or dashpots.

1.2 Problem statement

The primary aim of this thesis is to demonstrate the effectiveness of the semi-active tuned mass damper (STMD) system by considering the soil-pile-structure interaction. For this purpose, the exact interaction between soil-pile and also soil-structure must first be simulated. The continuum finite element method for better estimation to achieve an accurate evaluation of the interaction of both components of soil structure interaction (inertial and kinematic interaction) with respect to the spring method is provided. In general, the p-y curves proposed by API recommendation [9] were obtained from experimental centrifuge studies, and later researchers extended the curves for large-scale simulation using the continuum finite element method widely used in substructure method. These general curves, simplified with API guideline [9] are produced to use for all types of structures. Therefore, there is lack of research for analysis dynamic soil-pile-structure interaction of buildings equipped with semi-active tuned mass dampers.

The existing knowledge on this topic needs to be developed according to the following problems:

- Due to the complexity of the three-dimensional continuum finite element method, structures are rarely modeled and evaluated with nonlinear time history analysis.
- The accuracy of the substructure method is evaluated for dynamic purposes. Since the reliability of the substructure method for small-scale SSI problems has been discussed repeatedly, the applicability of the substructure (spring) method for a large-scale simulation (midrise structure with STMD and SPSI) is investigated and evaluated.

- Application of semi-active structural control schemes with different mass ratios is evaluated considering flexible multilayered foundation using both substructure and continuum finite element methods.

Although, based on previous researches, structures with fundamental periods between 0.3 and 1 s are more sensitive in comparison with other structures [10], the intensity of SSI effects on structural seismic responses depends on different parameters including soil and structure relative stiffness. The investigations have also shown that for those groups of structures found on soil with shear wave velocity lower than 600 m/s, interaction between soil and structure may modify seismic responses more than other cases especially for moment resisting frames [11,12].

Therefore, in this study, the focus is on the seismic behavior of mid-rise STMD steel buildings with short periods (T<1s) incorporating the SPSI phenomenon on soil layers with shear wave velocity lower than 600 m/s with the improvement of the general determined equation recommended by the API guideline [13] by using the nonlinear time history analysis.

1.3 Reporting structure

The thesis is organized into several chapters to achieve the research objectives:

In Chapter 2, a literature review of the various methods of structural control is presented, with a focus on the semi-active tuned mass control device (STMD). In addition, a literature review of the main research on numerical methods for the simulation of SPSI is given.

Chapter 3 presented a fundamental design of STMD building systems. In this chapter, dynamic parameters and also details of design about semi-active means and its optimization by Groundhook algorithm are described. Then the simple and practical substructure method (spring method) along with simulation of springs and dashpots for the seismic behavior of structures is explained and finally, the procedure of the continuum finite element method is explained in detail by presenting the structural and non-structural elements used in the constitutive system, such as steel, concrete and the dynamic response of the soil.

Chapter 4 includes three parts: at first part, the p-y curves proposed by the API recommendation evaluated by assessing the output data of the spring and continuum methods, then presents the improved p-y curve for STMD structures founded on sandy soil developed for the results of this study. In the second part, evaluated the performance of STMD and the effects of SPSI on the dynamic behavior of the structure using the continuum (finite element) method and in the last part, the mass ratio parameter of STMD is optimized by using the simple method (substructure method) applying updated p-y curve which is investigated in last chapter.

Conclusions are presented in Chapter 9, along with recommendation for future research.

Chapter 2

LITERATURE REVIEW

2.1 Introduction

Frustrating vibrations might be cut down by revising the structure, and/ or presenting auxiliary damping into the system. In past years, considerable attention is given to the use of energy dissipation systems to suppress structural vibrations. Amongst the numerous commonly used structural control systems, Tuned Mass Damper (TMD) is deemed to be more useful due to its simple mechanism, durability and low energy consumption. Nevertheless, its reliability in vibration control is typically proportional to the ratio of its allowed frequency to the main frequency and vibration damping of the structure. Hence numerous types of TMD damping equipment are established, including semi-active tuned mass dampers (STMD), which are generally used to reduce the extreme vibration of the seismic behavior of structures excited by earthquakes. Many types of research are performed about this class of reactive energy dissipation devices (so-called Semi-Active Tuned Mass Dampers) which have low power demand, low operational charge and simple hardware requirements [7,14–19]. Semi-active control systems are actually passive control systems, which are modified to permit the adjustment of their mechanical properties during earthquakes. However, due to the high complexity of modeling, the Soil-Structure Interaction (SSI) analyses usually ignore the influence of SSI on the dynamic excitation of STMD-engineered structures, particularly for those which are supported by pile foundations [17,20–25]. Lou and Wang [26] investigated that although the TMD concept for seismic retrofitting

is intuitive, it is important to accurately evaluate the SSI influence on the seismic response of the system associated with the TMD to assess any need for seismic retrofitting if the system is to be located on soft soil such as loose sand. In fact the reaction force of the structure to the earthquake motion will differ on the basis of the ground conditions (fixed base or flexible foundation). Several research studies have demonstrated that SSI dramatically alters a structure's dynamic mechanics such as mode shapes, frequencies and damping [6,27–29]. Ali and Mahamid [30] evaluated the dynamic response of the compressor crank-foundation system by performing the three dimensional finite element method on dynamic attitude of structure such as the fundamental natural frequencies, mode shapes and also mass participation ratios of the soil foundation system and discussed how their properties will be altered. Liu et al [31] investigated the dynamic soil structure interaction with both shaking table and numerical three dimensional simulation and concluded that SSI effects clearly reduces the structural response under seismic excitations. They also stated that SSI significantly effects structure's attitude when the frequency of ground motion and structure are closer.

The efficiency of an active or passive energy dissipation mechanism such as STMD depends entirely on the dynamic characteristics of the structure. Several researchers concluded that the non-linear interaction of the soil foundation connection could play a vital role in modifying the seismic specifications of the building and neglecting the effects of the soil layers may lead to design in unreasonable and unprogressive configurations of STMD with detrimental effects [31–36]. Elias [35] considered the soil structure interaction including soil types on seismic response of structure by dispersed tuned vibration dampers and concluded that the efficiency of dampers will

be altered by considering the SSI and soil types. Zhao et al. [37] developed simplified numerical model by analysis of soil-structure interaction (SSI) results on structures fitted with viscoelastic dampers (VEDs) on pile foundations for both SDOF and MDOF structures. They found out that the competence of the viscoelastic dampers (VEDs) on pile foundation reduces as the soil stiffness decreases. Yang et al. [38] used results of two large-scale shaking table tests for tall buildings with group pile in soft soil for investigation of the seismic soil-pile-structure interaction. They concluded that, whilst some dynamic responses of the structure is improved, there were cases where soil-pile-structure interaction yielded unfavorable results.

In most of the previous studies, the soil-pile interaction is simulated by using the spring and dashpot, namely Winkler spring method. The accurate estimation of load-deformation responses at the soil-pile-structure interaction plays a significant role in Winkler spring method. In this study, the pile is modelled as an elastic beam supported with nonlinear springs called p-y springs. While clear and useful, the evaluation of appropriate coefficients for the nonlinear springs is time consuming and inefficient in practice [39].

The American Petroleum Institute (API) [9] recommends a few basic equations for estimation of nonlinear curves for piles, which can be derived based on the ground type. These were initially established for the design of offshore steel piles with a diameter of approximately 40 cm based on static and slow cyclic loading. However, in practice, due to the ease of use, these are utilized regardless of the pile type, pile dimensions or the type of loading and, especially structure type. Several investigators have performed sensitivity analyses and confirmed high concentrations of

inaccuracies, mainly in the pile response, when the API curves are used in both static and dynamic load analyses [34,35,40,41].

Some of the studies have been investigated in an attempt to discover other procedures for the soil pile interaction of the determination curves under static loading. Gm. N. [42] proposed the Strain Wedge Model (SWM) which was subsequently modified by Ashour et al. [43]. This methodology was presented to provide better results than the p-y springs of API under static loading. They also relieved that the proposed p-y curve can be used for slow cyclic loading. Elmeliegy and Rashed [44] suggested preconditioned two-iteration substructure method over the raft foundation and presented the efficiency of their method in various numerical models. Although their methodology was extended to apply in piled raft, it had some limitations such as exclusion of the damping and nonlinearity of soil. In most of the previous studies on dynamic analysis of structures, in order to estimate soil-pile-structure interaction, researchers have in fact simulated discrete modelling by applying pushover analysis. Designers mostly tend to use basic soil modes through representing the soil by sets of springs for the load-deformation response in a soil-pile interaction analysis. In terms of the sensitivity of STMD characteristics with respect to the structural dynamic attitude, further analysis of the reliability of API curves is required.

Another method which is used by researchers is the continuum Method, the reliable approach that is commonly used to model soil-structure systems in coupled manner. In this process, structural elements and the surrounding soil can be modelled together without an extra need for the use of springs. Although it is a more challenging and tedious process, it potentially offers a more accurate way for the assessment of both

inertial and kinematic interactions [45]. With the development of the continuum method, the spring method is likely to be less popular in the long term. Finn [46] used various methods (BNWF and Continuum model) in the dynamic estimation of soil-pile interactions and revealed that the API guidance results are very poor for estimating the seismic behavior of piles. Their analyses revealed that the soil-pile system in the continuum model greatly improved the estimation of kinematic and inertial interactions. After years of demanding revisions, there is still a significant gap in SSI analytical models utilized between SSI specialists and civil engineers. Tyapin [47] and Kim et al. [48] reported disagreement over the prediction of lateral displacements and bending moments for piles in clay soil by following the API Curves. A Rahmani et al. [46] investigated the p-y seismic response of the soil pile interaction using a comparison of the API model and continuum model. The results showed that the ultimate resistance, initial slope, and load–deflection loops are all weakly correlated when Winkler springs are used. Behnamfar et al. [49] and Bayat et al. [50] offered an enhanced p-y curve method by investigating carefully the effect of the excitation frequency on offshore wind turbine monopile foundations. Dash et al. [51] revealed that p-y curve for liquefiable soil has an unlike form, for instance, uphill concave with basically-zero original rigidity. The success of the BNWF method, is therefore extremely dependent on the precise assessment of the load–deflection curves. Besides, an accurate estimation of the soil pile interface is necessary to determine an optimized set of STMD device characteristics.

2.2 Tuned Mass Damper devices

2.2.1 TMD systems

Various technologies can be provided to control building vibrations caused by wind or earthquakes loads. A range of such devices have been studied by many researchers to

evaluate the benefits and weaknesses of control systems [31,52–56]. One of the most advantageous of these devices, which has been proved recently to be effective in suppressing structural vibration, especially for mid-rise and high-rise buildings, is the Tuned Mass Damper (TMD) [57]. Frahm [58] was the first researcher who introduced the concept of TMD to control the vibration. Later, Den Hartog [57] presented a complete description of TMD and a design formula in a book called Mechanical Vibrations to study the optimal parameters of damping and undamping tuned mass damper. TMD composed of two main parts, an added mass and a tuned spring damping system that increases the damping ratio of the main structure through frequency dependent hysteresis as depicted by the model shown in Figure 1.

In this figure C_1, C_2 and K_1, K_2 are damping and stiffness of primary structure and TMD damper respectively. When lateral vibrations are applied to the structure, the TMD contracts them and reduces the energy introduced into the structure [52]. In reality, TMD devices are often steel or concrete chunks bodies set up in skyscrapers or other buildings and moved by springs, fluid, or pendulums against the resonant frequency vibrations of the structure. The springs of a TMD are attuned to the principle building in such a way that the interaction of the TMD and the principle building results in amplified damping of the principle building. In this manner, the vibration excitation of the primary system is diminished. Figure 2 illustrates the largest Tuned Mass Damper, located in Taipei 101 in Taiwan.

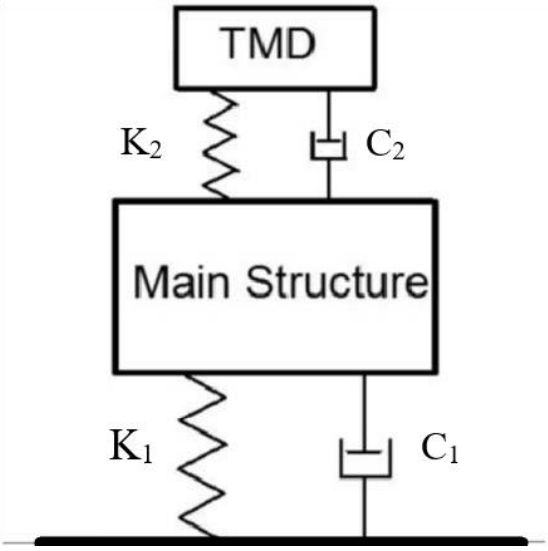

Figure 1: Tuned Mass Damper (TMD) linked to the main structure.

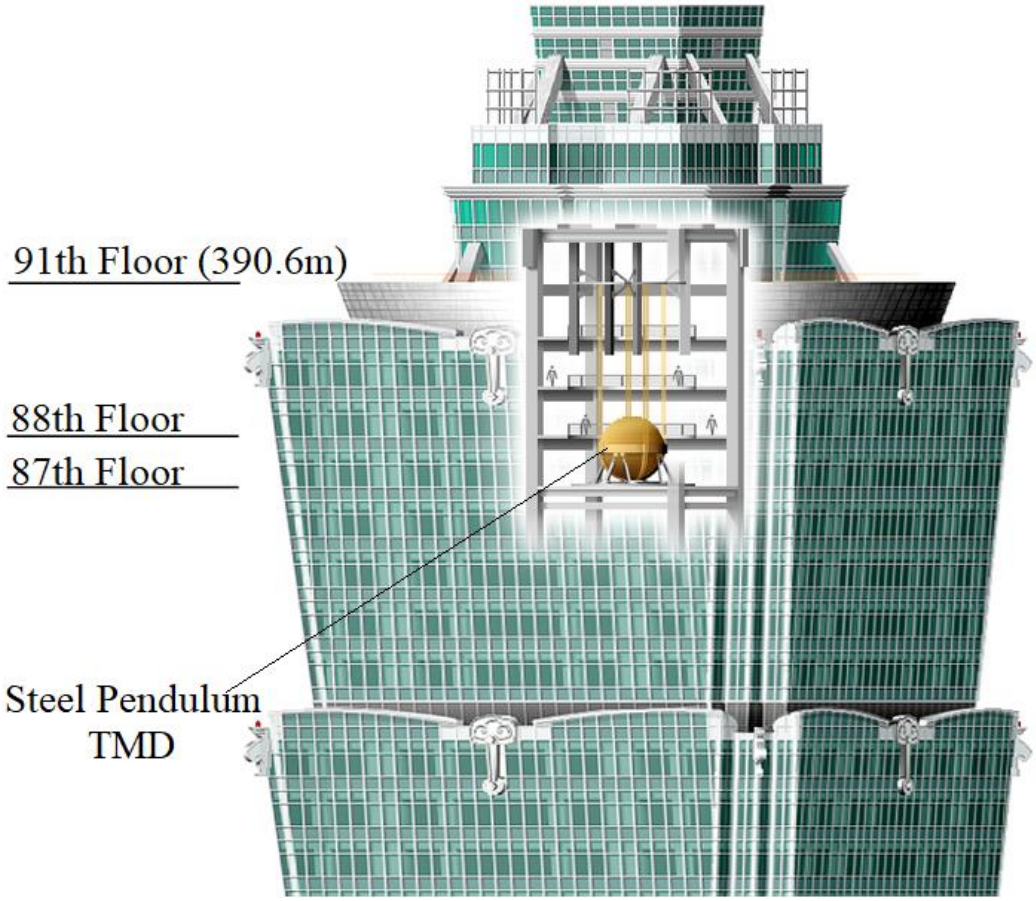

Figure 2: The largest TMD damper suspended from the 92nd to the 87th storey.

The advantages of TMD systems as a passive device can be listed as; low cost, easy installation and maintenance, ability to dissipate energy without external power source

and fast and simultaneous response to input vibration [54]. About disadvantages of this system, low efficiency in the non-main mode of the structure and loss of tuning damping which leads to reductive in the ability to absorb the energy of the structure can be listed. Loss of tuning can considerably decrease the effectiveness of the TMD, leading to the conclusion that it is not completely reliable [59].

TMD works more effectively when the ground motion has a substantial spectral contribution to the main mode frequency. Hence, it is hard to make general statements about the seismic efficiency of TMDs when the behavior of the structure is elastoplastic because in this case, passive TMD has constant parameters and con not adjust its parameters [60].

In an attempt to improve the performance of TMD and to cover the disadvantages of passive control, another type of TMD has been titled Active Tuned Mass Damper (ATMD) was introduced by Chang and Soong [61], which was shown to be more useful for elastoplastic attitude of structures. In this system, an active force is applied in the middle of the main building and the TMD device to control the system. Abdel-Rohman [62] investigated a method to improve the efficiency of ATMD by applying pole assignment design process to control high-rise buildings subjected to stationary random wind forces. This research recommended that in any case, parametric revision is required to tune the ATMD characteristics during lateral loading energy. In addition, some other studies have been conducted to investigate the effectiveness of ATMD by studying the displacement, velocity and acceleration response of the building equipped by ATMD [53,63,64]. Although ATMD is more advantageous compared to passive TMD, fully active systems require a large external energy source and also it has

complex process to update parameters for suppressing energy during lateral loading events.

2.2.2 Semi-Active TMD systems

ATMDs have been found to mitigate structural excitations better than passive TMDs. However, ATMDs have disadvantages such as; high operation and maintenance costs, and high external energy sources.

Hence, they are not entirely trustworthy compared to the passive systems. Considering the advantages and disadvantages of both systems, a new type of semi-active tuned mass damper (STMD) was developed, which uses adjustable damping parameters or stiffness systems. STMD require a small amount of external power source to adjust the damping of the device, which was the main problem of ATMD. Moreover, STMD adjust the device parameters during the input lateral loading with wide data available library, hence, more useful possible variables by comparing to the other type of TMD [65]. Semi-active devices are very useful in cases where the device does not need to be active for an extended period of time, but needs to create significant outputs quickly [15]. The effectiveness of semi-active systems and control mechanisms in reducing damage during seismic events has been widely demonstrated. Semi-active systems can preferably be trustworthy and simple to use.

Hrovat et al [14] utilized semi-active tuned mass dampers with adoptable parameters in tall buildings to control wind-induced excitations. Abe [16] applied a variant of semi-active TMDs using pulse generators only for earthquake resistance of buildings. Later, Setareh [66] examined the Groundhook Algorithm to optimize the TMD parameters to improve the vibration part of the automobile, and again (Setareh [67]) used the adjustable semi active tuned mass damper to mitigate the ground vibrations

induced by the motion produced of live load. The evaluation of the variable damping component of the STMD under harmonic vibration was studied by Pinkaew and Fujino [15]. They offered clipped optimum mechanism law based on a semi-active optimal control. Ricciardelli et al. [68] presented an empirical algorithm to optimize the STMD parameters as a function of the response of the primary structure. They proved that TMD damping optimization just decrease the displacement of damper and cannot effect on structural response reduction.

Shen [69] investigated a semi active control strategy utilizing a practical switch that is in a position to change stiffness and also damping component for any TMD usage. Aldemir [70] examined the optimum functionality of any magnetorheological (MR) damper, as well as applied within a tuned mass damper to minimize ultimate reactions associated with a single degree of freedom structure put through a wide category of seismic inputs. Later, Mulligan et al. [71] studied spectral analyses of SATMD devices by performing probabilistically scaled measurements. Their results suggested that resettable fuse devices are the best way for tuning design which allows to account for deviations in structural criteria.

2.3 The optimization of STMD parameters

The TMDs and STMDs are developed, formulation of TMD and STMD variables started to become a challenge. For these control devices, the main aim is to find damper variables to optimize their efficiency.

A TMD, as presented in Figure 3, consists of a mass, a spring and a damping element usually tuned to the natural frequency of the main mode of the system [72]. In case of an earthquake, the TMD mitigates the vibrations of the structural system.

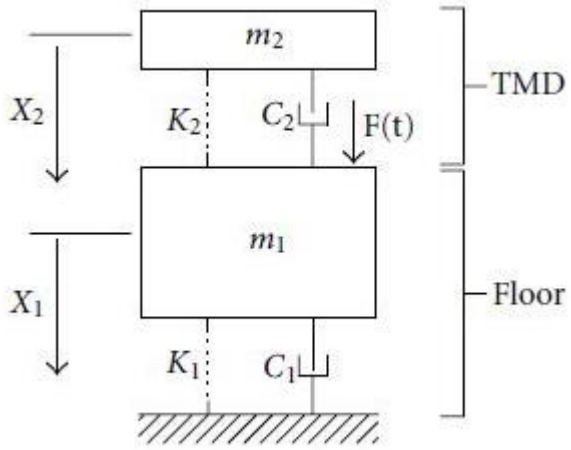

Figure 3: Diagram illustration of a two-DOF system [72]

The variables m1, k1, c1 and X1 indicate the mass, stiffness, damping and displacement of the structure, respectively; m2, k, C2 and X2 indicate the mass, stiffness, damping and displacement of the TMD, respectively; and F(t) represents the excitation force. The passive damper diminishes structural vibrations by increasing the effective damping. TMD systems usually operate in a small frequency band and must be tuned to a main natural frequency. They are inefficient if the building have had numerous small-cycle hysteresis of natural frequencies, and if they are out of tune, they can amplify the vibrations [16]. By inserting a spring mass tuned to the same main natural frequency (fn) of the main system (Figure 4), the natural frequency of the main system may be separated into lower (f1) and higher (f2) frequencies.

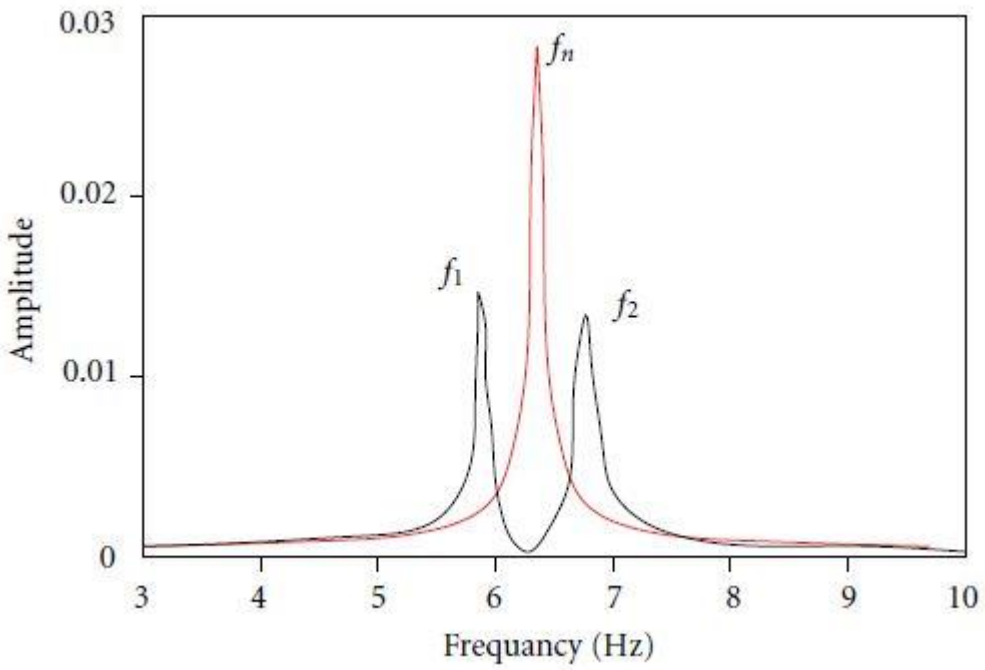

Figure 4: Model indicating the TMD efficiency [16]

One of the critical design parameters is the mass ratio. This important factor is often assumed to be in the range between 2% - 5% in practice.

Number of studies have addressed the TMD performance for obtaining absorber parameters[7,55,73,74]. General formulations for the top damping ratio and tuning ratio of an additional mass damper were extracted by Den Hartog [72]. These formulations were dependent upon reducing the displacement of an un-damped main structure through sinusoidal oscillation.

In order to achieve the most effective device variables Mark and Crandall [75] applied the normal square effect of the stationary procedure. Later, Chey [60] derived basic expressions based on Mark and Crandall (1963) theory, for the optimum values of the damping ratio and also frequency ratio of TMD based on the acceleration and displacement of structure. Ioi et al. [76] introduced an empirical formula for optimal

damping and also stiffness of any TMD, dependent on the reduction of the acceleration effect on a low damping building. Randall et al. [77] applied numerical optimization methods for analyzing the maximum TMD components, with a view to damping of the structure. Thompson [78] recommended that first the tuning ratio of TMD is optimized numerically and then, the damping ratio of TMD is obtained based on analytical investigation of TMD with optimized tuning ratio of damper. Fujino and Abe [16] used a perturbation method to obtain expressions for optimal TMD components that can be applied for mass ratios of 2% and (also for values ratios of structural damping between) 5% to10%.

In various studies, the optimized variables of TMD are obtained for different configuration to minimize response of structure [60]. A curve fitting method was typically utilized to find comprehensive expressions for the optimal parameters of the TMD device. In this method, mass ratio and frequency ratio of TMD optimized and fitted according to the Ant Colony Optimization (ACO) [79].

Warnitchai and Hoang [80] proposed a new process to develop several TMDs for reducing severe excitation of linear attitude of structure elements. The process applied a numerical variable by using a gradient based nonlinear programming algorithm to find optimal TMD components. The target response was enhanced as a quadratic operation mark that is usually efficiently computed by releasing a Lyapunov formula [81].

In order to get a TMD operative, the variables of the spring and also of the damping component have to be carefully chosen. There are already many optimization strategies aimed at making the TMD ideal under different forms of excitation causes. For

instance, Den Hartog [72] created the popular fixed point philosophy to improve dashpot and spring of a TMD linked to an un-damped building. In this theory, when the magnitude of the maximum vibration at main system and dynamic vibration absorber are equal, it can say that the absorber device is optimal. Warburton [82] analytically identified the perfect frequency ratio and also damping ratio of any TMD equipped with an damped building under white noise vibration as base acceleration. Instead of applying the structural acceleration/displacement response as the best target [72], Greco and Marano [83], Reggio and De Angelis [84] improved the TMD from a dynamic perspective to optimize the energy dissipation. That is well acknowledged that the efficiency of controlling TMD rely more on the mass ratio between main structure and TMD. Better and much more efficient control could be estimated by placing a much larger additional mass. Although, using a huge mass on the main frame not only raises the production cost significantly, also is not formally useful in many cases. It would be agreeable to be able to reach the same or even higher control performance with a small additional mass.

Besides, another issue in using STMDs as a control device is the use of the appropriate algorithm to estimate the optimized damping coefficient or stiffness ratio of the mechanism. Recently, several control algorithms, such as Lyapunov [85], Clipped-Optimal [86] and Fuzzy Inference System [64], have been proved for semi-active controllers. Some of these researches [67,87] investigated the proper control methodology for semi-active tuned vibration absorbers (TVAs) in structural vibration applications. Among them, Groundhook Algorithm investigated by Setareh M. [67] is a useful method for optimizing the STMD parameters in simple and practical way (Figure 5). In this procedure, four control techniques are considered separately or in

combination, including velocity-based, on-off ground hook control (On-Off VBG); velocity-based, continuous ground hook control (Continuous VBG); displacement-based, on-off ground hook control (On-Off DBG); and displacement-based, continuous ground hook control (Continuous DBG). The results have shown that among them, the Groundhook Algorithm variants are more efficient in shortening the excitation vibration response and On-Off DBG is the strongest of the considered control strategies, which will be further explained in the next chapter. In this study, the STMD is used to monitor the vibration of the structures considering a flexible foundation and moreover, the damping ratio of the STMD is optimized using the on-off DBG Groundhook Algorithm.

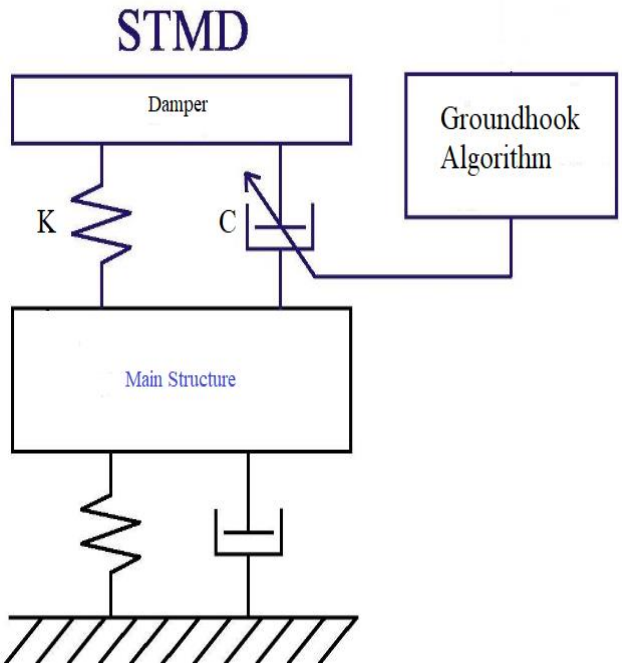

Figure 5: Adjustable damper

2.4 Dynamic SPSI analysis of structures

The popular methods continuum (finite element) method and simple substructure (spring) method are used in this thesis for simulating soil-structure interaction under nonlinear time history analysis.

2.4.1 Continuum finite element model (Direct method)

In the continuum method, the structure and the soil are modelled together with appropriate boundary condition set for equilibrium of form of displacement. The finite element method (FEM) is utilized to find solutions for the problem geometry and loading within time domain. This method is conceptually straightforward. The main problem of the continuum method is the determination of the dimensions (or perhaps the size) of the model geometry to avoid boundary effects changing results. It is also important to correctly simulate the progression of some waves within the model setup. Therefore it is customary to use a large enough model geometry, so that the reflections from the system are eliminated before reaching the boundary. Many scientific studies have been developed for setting appropriate boundaries to reduce the dimension of the soil block required. The types of boundaries developed includes (Figure 6); viscous boundary, unified boundary, , viscous spring boundary, periodic boundary and also consistent boundary [88–93].

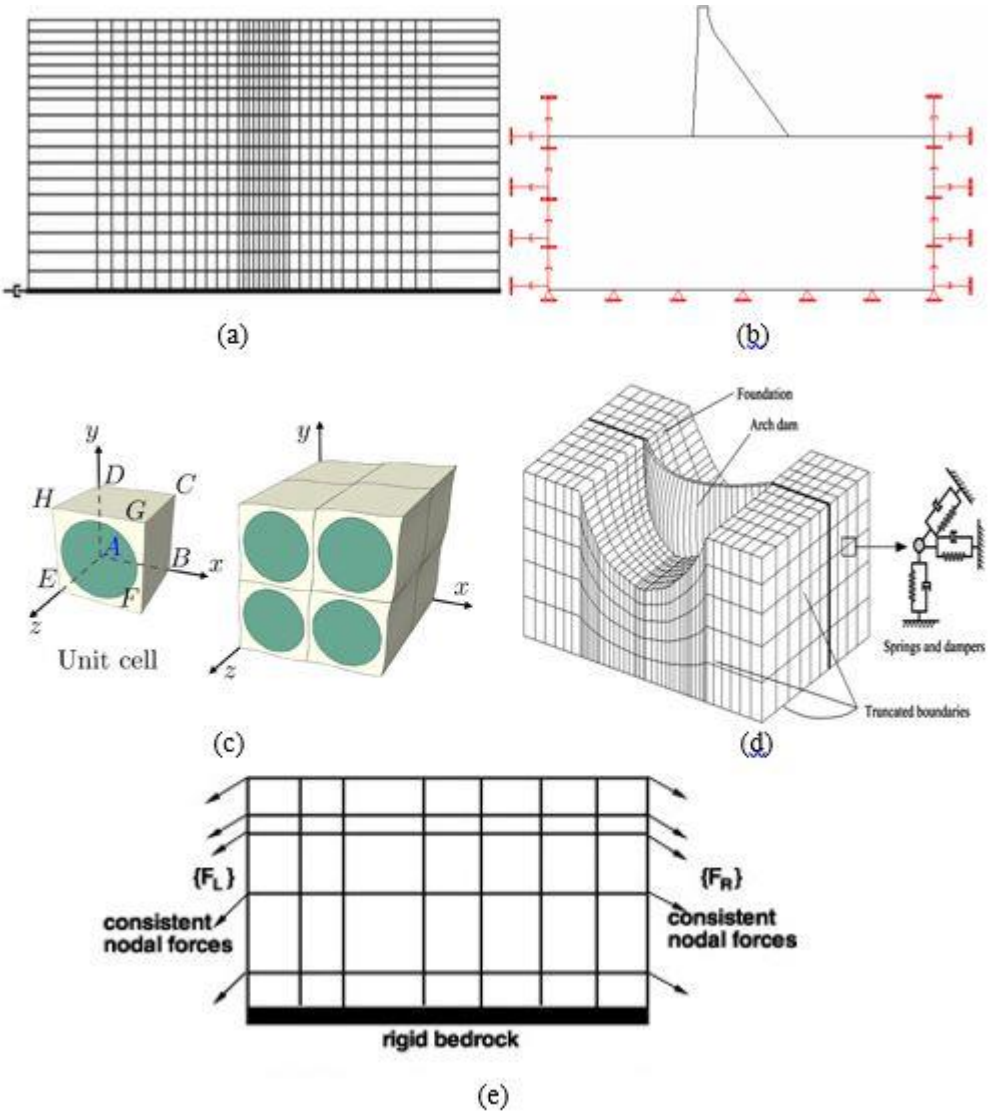

Figure 6: Types of boundary condition; (a) Unified boundary, (b) viscous boundary, (c) Periodic boundary, (d) Viscous spring boundary and (e) Consistent boundary

These boundary types often act as non-reflecting boundaries or attracting strata to keep away the reflections of the propagating output waves through the soil region. Despite the use of aforementioned boundaries, the continuum method requires with a considerable site of soil block for a proper analysis of SSI. If finer temporal resolution is necessary, the time step must decrease accordingly in addition to the component size, resulting in an analysis version with larger DOF along with a larger number of time steps. For this reason, the continuum method with three-dimensional high-

accuracy models has not been widely used. With the development of computer systems, the work with large-scale three-dimensional models has increased [94–97]. In such studies, typically nonlinearity is only considered for the soil block, not for the structure. Recently, computational methods started to allow the use of the continuum method with a complete nonlinear numerical evaluation of the soil structure system [98,99].

2.4.2 Substructure model (Multistep method)

In the substructure methodology, the structure and the soil are modeled discretely; a rigid body foundation is assumed to be located between the building and the soil. In this particular strategy, the seismic vibration analysis is performed in the following steps [100]:

- First, the determination of the specific ground motion, which is not similar to the free-field ground motion regarding the existence of the structure (named kinematic interaction);
- Second, the determination of the frequency dependent impedance functions due to the foundation by generating a harmonic vibration of stress at a certain frequency on the foundation, calculate approximately the response stress of the ground, and the ratio between the response and the input as an impedance function;
- Then, calculate of the dynamic result of the structure based on the impedance functions obtained in the previous step and by the input motion obtained in the first step (Inertial interaction).

The determination of the input ground motion involves the conditions of an elastic half-space for soil and structure with essential properties of material. In this thesis one

one-dimensional analysis are performed, which assumed stratified or uniform soil block and only vertical propagation of shear waves. Inaccurate matching between free-field ground motion and foundation resulted in kinematic interaction. The kinematic interaction occurs due to the dissimilarity in foundation rigidity and the surrounding soil, which causes deviation and reflection of seismic waves in the soil. In order to the shallow foundation, the kinematic interaction is usually neglected because of the strain-free boundary situations at the ground surface. However, for rigid embedded foundation, the free-field input ground motion is altered where it interacts with the base, resulting in rotational activity of the base. For frequency dependent impedance characteristics, the mathematical problem of the soil block is developed as a mixed boundary value problem. A number of analytical and empirical methods have been found for this particular problem [101–104]. These results have been used to model the soil block as an oscillating spring for a variety of structures. This methodology eas also developed later for SSI analysis [105–107]. It should be mentioned that the verification of these methods is limited to the determination of the frequency-dependent impedance functions. The method is applicable to a circular and rectangular rigid base on a homogeneous half-space of linear isotropic elasticity loaded by the vibration at the center of gravity of the base [108].

2.4.2.1 API guidelines for soil-pile interaction

The API curves represent a key role in the analysis methodology. These curves can be used for both static and dynamic analysis. The BNWF definition for the API backbone curve has been developed and updated by several investigators such as Matlock H [109], El Naggar et al. [110], Gohl B [111] and Wilson [112]. An effective macro-element theory on soil pile interaction was also formulated by Taciroglu et al. [113].

API standard [9] recommends the following Eq.(2.1) for laterally loaded piles in sands, so-called p-y curves, at any particular depth of H,

$$P = Ap_u \, tanh(\frac{kH_y}{Ap_u}) \tag{2.1}$$

where, lateral resistance P is computed along the pile based on horizontal displacement ″y″, and about the modulus of subgrade reaction ″k″ is derived from specific figure as a function of internal angle of friction ∅′, and p_u is the ultimate lateral soil resistance, and A is a constant related to the static or cyclic loading which can be taken as 0.9 for sand.

The lateral soil resistance is expected to occur based on two mechanism [8]: (I) wedge failure: resistance at shallow depths, a passive wedge stand against the lateral displacement of the pile; (II) flow failure: resistance at greater depths, the soil appears to shift horizontally around the pile instead of the shifting up into the wedge to extreme overload stress. These mechanisms are formulated as presented in Eq. 2.2a and Eq. 2.2b. API standard recommends the lowest p_u value obtained from these equations to be used,

$$P_{us} = (C_1 H + C_2 D)\gamma' H, \tag{2.2a}$$

$$P_{ud} = C_3 D\gamma' H, \tag{2.2b}$$

where, D is mean pile diameter from the face to depth, $\gamma'$is effective soil weight, C_1, C_2, and C_3 are coefficients obtained by the following equations as a function of Ø′ and also using Figure 7.

$$C_1 = \tan\beta\{K_p \tan\alpha + K_o\left[\tan\emptyset \sin\beta\left(\frac{1}{\cos\alpha} + 1\right) - \tan\alpha\right]\} \tag{2.3}$$

$$C_2 = K_p - K_A \tag{2.4}$$

$$C_3 = K_p^2\left(K_p + K_0 \tan\emptyset\right) - K_A \tag{2.5}$$

Where; K_0=0.4, $K_A = tan^2(45^\circ - \emptyset/_2)$ and $K_p = tan^2(45^\circ + \emptyset/_2)$, β is approximated to be 45 + ø'/2 and α is equal to ø'/2. Also K_A, K_O, K_P are lateral earth pressure coefficient at rest, active and passive condition, respectively. The input parameters and results of spring method are easily controlled implicitly due to the difficulty of appropriate characterization of springs and dashpots compared to the continuum method, though it is more difficult to setup and run to use in the analyses. API recommendation [9] also offer recommendations for the calculation of q-z and t-z curves on the basis studies of Meyer et al. [114], where the axial pile shear stress, and tip end bearing are t and q respectively, also z is the axial displacement of the pile,. Table 1 gives the nonlinear backbone curves for q-z and t-z for sand recommended by API. Also the curves are shown in Figure 8.

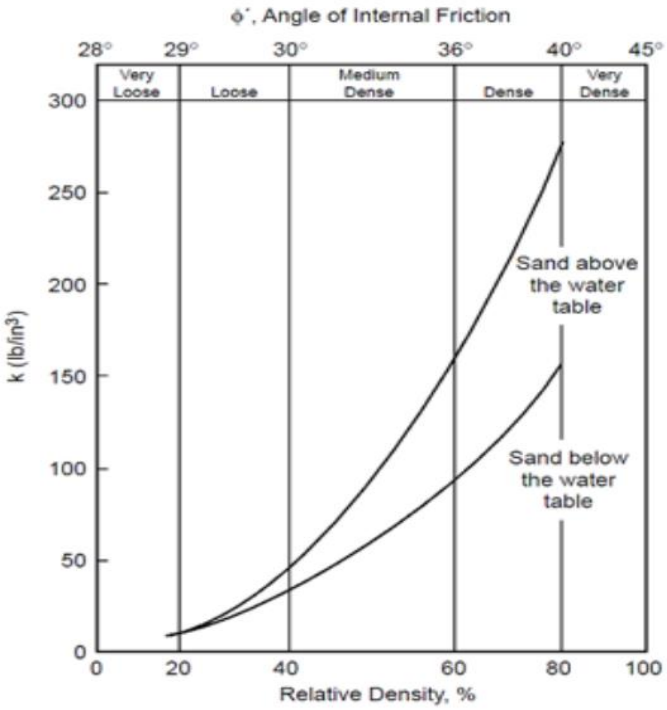

(a)

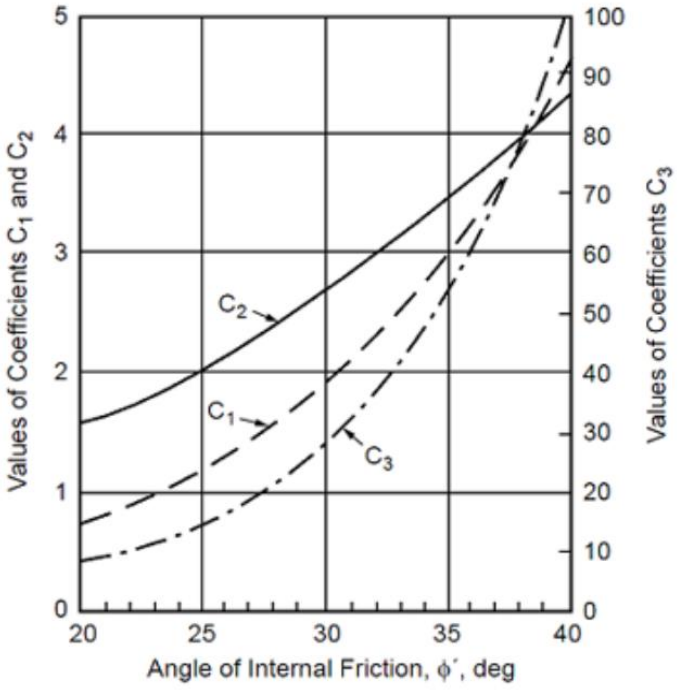

(b)

Figure 7: The diagrams offered by API (2007) for assigning; (a) initial subgrade reaction, k, and (b) the C1, C2, and C3 parameters.

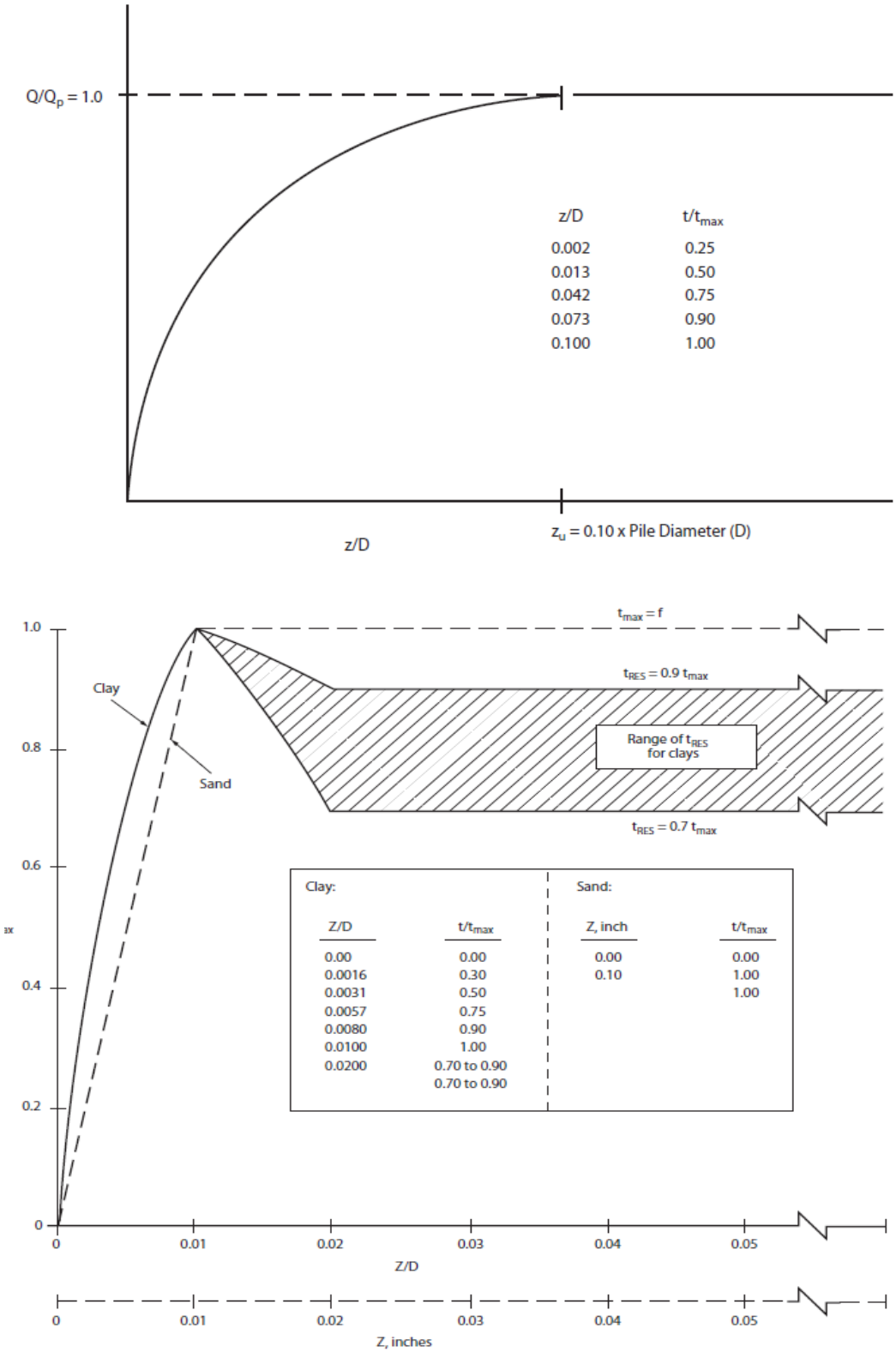

Figure 8: Representative shapes of the (a) t-z, and (b) Q-z curves as presented in API (2007).

Table 1: (q-z) and (t-z) values recommended by API (2007)

sand	z (mm)	t/t(max)
Axial Load Transfer (t-z) Curves	0.000	0.00
	0.100	1.00
	∞	1.00
sand	z/D	Q
Tip-load-Displacement Curve (q-z)	0.002	0.25
	0.013	0.50
	0.042	0.75
	0.073	0.90
	0.100	1.00

Jeong and Kim [115] realized that the application of API curves to piles embedded in clayey soils leads to a significant overestimation of pile lateral displacements and also of the bending moment profile. In accordance with the response of several powerful centrifuge experiments, Choi et al. [116] claimed that the API curves are drastically different from the experimental curves; the ultimate soil resistance is underestimated, although the soil effective modulus is overestimated for the small deflections of the piles. Tyapin [47] and Kim et al. [115] reported disagreement over the prediction of lateral displacements and bending moments for piles in clay soil by following the API Curves. A Rahmani et al.[117] investigated the p-y seismic response of the soil-pile interaction using a comparison of the API model and continuum model. The results showed that the ultimate resistance, initial slope, and load-deflection loops are all weakly correlated when Winkler springs are used. Behnamfar et al.[49] and Bayat et al.[50] offered an enhanced p-y curve method by investigating carefully the effect of the excitation frequency on offshore wind turbine monopile foundations. Dash et al. [118] revealed that p-y curve for liquefiable soil has an unlike form, for instance, uphill concave with basically-zero original rigidity.

2.5 Summary

This chapter provides a basis and literature survey for the concept of structural control for suppression and reduction of earthquake related vibration. As the second topic, due to the complexity simulation of soil structure interaction, explains about the current approach which are provided to model the soil structure interaction. The research has found both positive and negative impacts of SSI on structural response. In research and in practice, the finite element method or the 3D continuum modeling process is not often used for nonlinear dynamic SSI analysis of structures. This is mostly due to the fact that the analysis needs extensive computing effort, which is very complicated and time consuming. The multi-step method, also known as the substructure method, includes three main phases: defining the kinematic input motions through a site response analysis; evaluating the dynamic stiffness of the foundation on the soil-foundation system; and eventually applying dynamic analysis of the superstructure on entire system. The spring approach is more attractive to engineering practice than the continuum approach because of its simplicity. In contrast, the identification of springs and dashpots is extremely complex and complicated.

Chapter 3

ANALYSIS METHODOLOGY AND RESEARCH STRATEGY

3.1 Introduction

One of the most important reasons why designers prefer the STMD over the TMD is the damping ratio of the device, which can be modified during the earthquake period to damp the dynamic vibrations more. Therefore, the moderator of the device must recognize the dynamic behavior of the structure accurately to improve the efficiency of the STMD. As described earlier, the mid-rise structures equipped with semi-active tuned mass dampers (STMD) resting on a pile foundation need to be accurately modelled to achieve high structural efficiency in suppressing the dynamic loads. Therefore, estimating the accurate interaction between soil and structure can help the STMD device to improve its performance during earthquake record motion and it can be said that the STMD configuration completely depends on the dynamic structural attitude. The substructure method is the simple and convenient way to simulate the SPSI interaction using additional systems such as spring and dashpot. Although this method is widely used, determining the spring stiffness and damping values of the dashpot is still challenging and requires a lot of effort. On the other hand, the continuum method is a reliable way to find an accurate estimate of the SPSI interaction, but it is very complicated and costly. Therefore, designers prefer the substructure method over the continuum method to simulate the SPSI interaction. The

recommendation API proposed some equations for structures on pile foundations, the p-y curves, which are general and proposed for all kinds of structures. In this chapter, the three main parts of this study (STMD configuration, substructure method and continuum method) are explained in detail and the methodology is discussed. For this end, the whole methodology provided in this thesis, is shown by flowchart Figure 9.

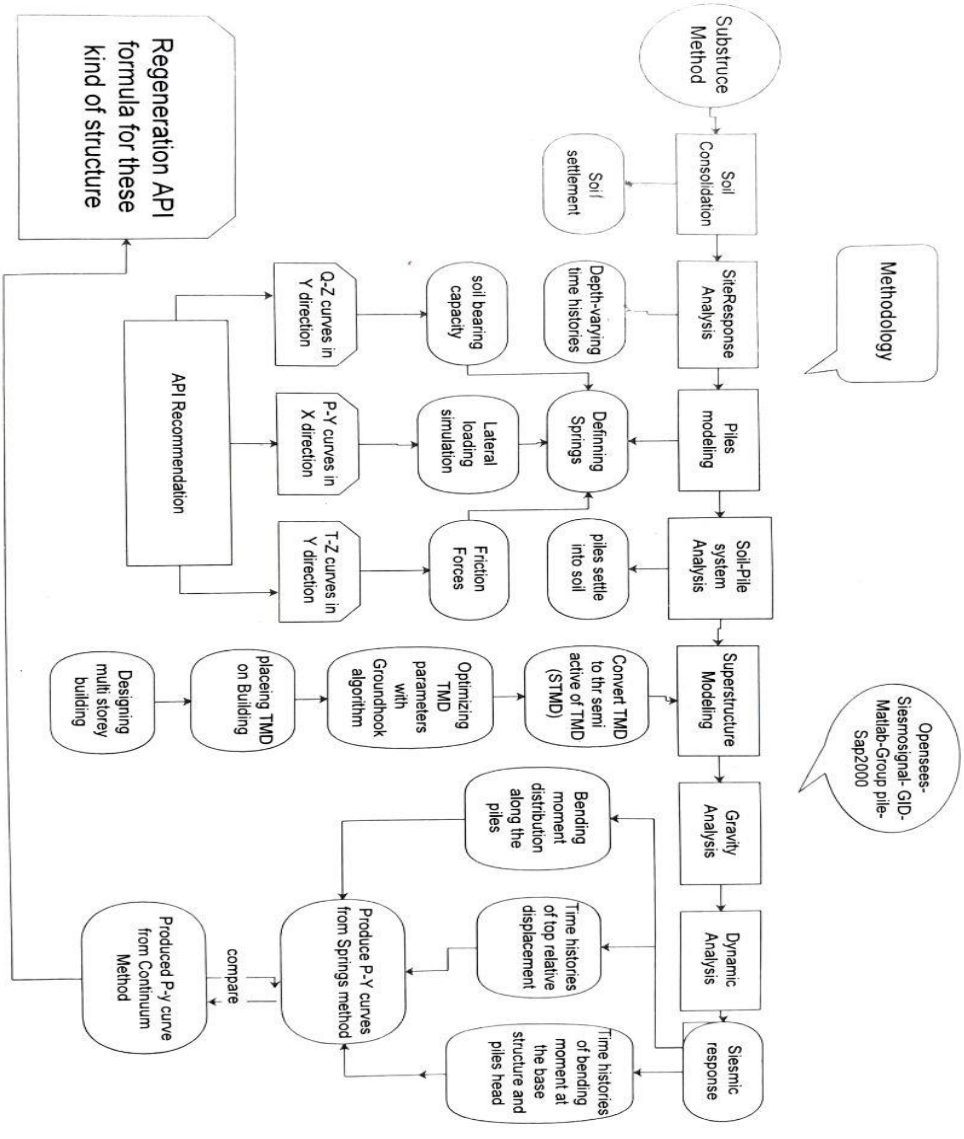

Figure 9: Thesis methodology and strategy

3.2 Semi-Active configuration

The STMD system differs from a conventional passive TMD system in that the passive damping device is replaced by a tunable semi-active damping component as explained earlier. Figure 10 (a) displays the SDOF model of the STMD. As presented in Figure 10 (b), a passive damping device has permanent damping (C_p), but a variable damping system can be modified by two damping rates called on-state (C_{on}) and off-state (C_{off}) damping. Figure 10 shows how a variable damping device can produce a wide variety of damping forces. The equivalent absorbing force for the passive damper at a given velocity is a constant force, (f_p). It means the variable damping device providing a damping force varying from (f_{off}) to (f_{on}). The variable damping device, which provides a diverse range of dynamic force, significantly enhances the dynamic response of the STMD when optimally controlled. The STMD has a mass ratio in the range of 1-10 percent.

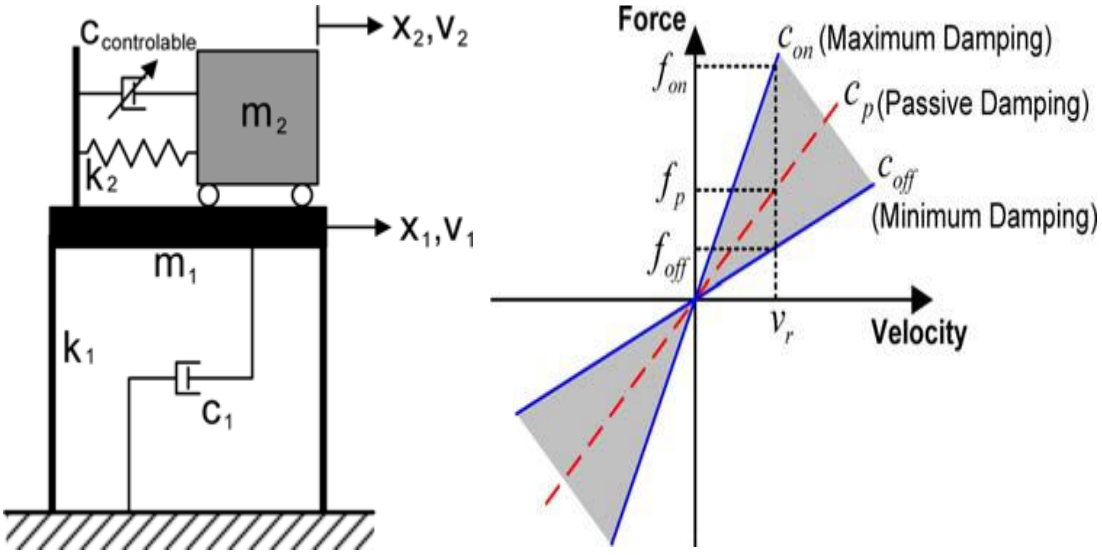

(a) (b)

Figure 10: (a) SDOF structure equipped with STMD, (b) Force-velocity diagram based on damping ratio.

3.2.1 STMD tuning parameters

In order to find the optimal parameters of the STMD and considering this point that the difference between TMD and STMD lies in the damping ratio, the methods are identical except for the variable of the damping ratio which is modified by Groundhook Algorithm. The mass ratio of the damper is the most important parameter of TMD and STMD can be calculated in (3.1).

$$\mu = {m_2}/{m_1} \tag{3.1}$$

The larger the mass ratio is, the more functional and robust the TMD is [119]. Usually, the mass ratio is considered in the range of 1-10 percent.

About the natural frequency of TMD damper design, it can be found by the following equation (3.2):

$$f_d = \frac{f_n}{1+\mu} \tag{3.2}$$

, and finally, the optimal damping ratio of TMD damper is defined by:

$$\zeta_{opt} = \sqrt{(\frac{3\mu}{8(1+\mu)^3})} \tag{3.3}$$

for STMD, with an intermediate moderator of damping such as ζ_{opt} , which lies somewhere between these extremes (high and low damping ratio) that modified during earthquake period by Groundhook Algorithm, it is possible to adopt the oscillation of the primary system over a large collection of frequencies [86].

3.2.2 Groundhook algorithm

The dynamic process associated with the harmonic base acceleration of $\ddot{x}_b = \ddot{X}_0 e^{iwt}$ is presented in Fig.4 for which m_1; k_1, and c_1 subsequently represent the mass, stiffness, and damping of the main system. In this algorithm the on-off damping regulator, in which the STMD damping ratio C_2can be converted between the strong

coefficient C_{max} and the weak coefficient $C_{min}$is used for obtaining optimum characterization of STMD. The on-off ground-hook control and its variants are assumed as the organizers for the STMD in this study. The switching is done based on the following situations:

$$x_1(\dot{x}_1 - \dot{x}_2) \geq 0 \rightarrow C_2 = C_{max} \quad \text{ON state} \tag{3.4a}$$

$$x_1(\dot{x}_1 - \dot{x}_2) < 0 \rightarrow C_2 = C_{min} \quad \text{OFF state} \tag{3.4b}$$

where x_1, $\dot{x}_1$ and $\dot{x}_2$ are the displacement and, velocity of mass m_1 and velocity of m_2 correspondingly. The controller Eq. (4.1a, 4.1b) rely on the displacement of the principal structure, and consequently, is known as the displacement-based ground hook (DBG) controller [67,87].

3.3 Substructure approach

In the last chapter it had been found that the evaluation of a linear elastic soil-structure interaction may be performed in following steps consists of Kinematic interaction and also Inertial interaction. The process of analysis is known as substructure approach. The theory of the substructure approach is based on the beam-on-nonlinear Winkler foundation (BNWF) model studied by McClelland and Focht [120] and then extended by Matlock [121] for lateral analysis of piles under static loads. Later, Allotey and Naggar [122] and Raychowdury [32] have used BNWF models to predict the two-dimensional (2D) seismic behavior of foundations with nonlinear springs including gapping and dashpot components. Briefly, BNWF models have the following reference:

One-dimensional nonlinear springs and dashpots located at the soil-foundation interface can be used to characterize soil-structure interaction phenomena. This model has high numerical efficiency in performing linear and nonlinear analysis.

At the end of foundations, a variable stiffness distribution and spring spacing can be used to account for larger responses at the end of rigid foundations and to incorporate the influence of rotational stiffness.

According to the principles of the substructure approach, Kausel et al. [123] recommended a multistep method for numerical analysis of a standard SSI issue with linear elastic attitude. This method didn't present a particular process to establish the dynamic stiffness matrix and also the input kinematic activity for a piled foundation building process under a seismic record motion. There aren't many scientific studies which offer a comprehensive description of the substructure technique for the evaluation of a pile supported STMD building. In this study, the whole analysis approach for simulating soil-pile-structure interaction is explained and evaluated. Shamsabadi [124] proposed the analysis approach for simulating the substructure method for bridge systems, therefore, this study uses this approach except the superstructure simulation method for modelling the structures with STMD including pile foundation. The analytical strategy, i.e. the substructure technique, is offered in greater clarity and detail with five sequential steps [45]. A short explanation of each of them for the evaluation of a regular pile supported STMD structure is provided in the subsequent steps.

3.3.1 First stage: Free field response analysis

Site response analysis as a first step of substructure method is conducted. In the absence of the structure, a free-field response study is performed on the foundation soil to determine depth-variable time histories is displayed in Figure 11. Equivalently, in the linear method, linear analyzes are conducted using soil characteristics which are repeatedly modified to correspond to an effective shear strain generated in the soil. Since this study focuses on the reliability of spring and dashpot simulations within dynamic SSI analysis, approximations should be minimized in the analysis of site behavior analysis. The stress-strain response of each soil element should be properly monitored in the time domain to better reflect the nonlinear, inelastic reaction of the soil. Hence, the input ground motion is used in the form of accelerations to the ties at the bottom of the soil block after a self-weight evaluation to determine the primary stress state.

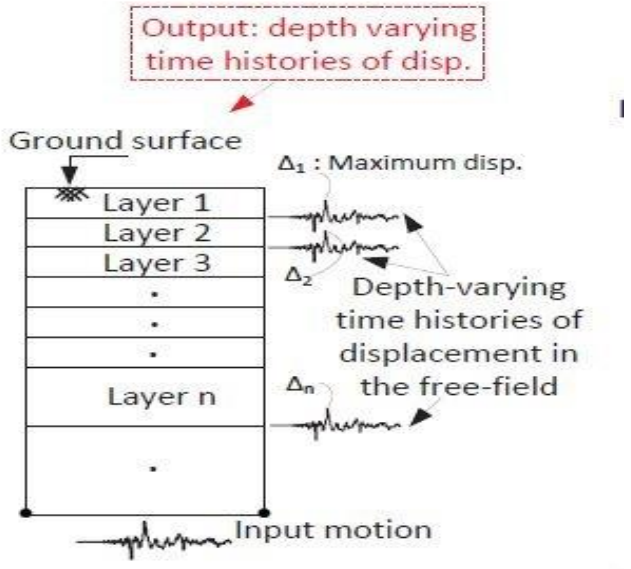

Figure 11: Determination of the depth-varying time histories of displacements [8]

3.3.2 Second stage: Effective linearization of backbone curves

The stiffness and damping properties of the foundation-soil system under dynamic loading are represented by impedance functions. To analyze the dynamic equilibrium equation of a rigid foundation, a complete process is performed includes six dynamic impedances, three translational and three rotational (three dimensional model). These impedances are determined by the geometry of the foundation, the soil parameters and the frequency of the structure-foundation-soil system. Lateral stiffness of the pile cap computed by using the described method and also by using the nonlinear backbone curves such as p-y, t-z and q-z curves offered by API recommendation. In order to consider the effects of group pile, the AASHTO [125] standards, should be utilized to calculate the group reduction factor. The procedure for calculating lateral and vertical secant stiffness for pile foundations is shown in Figure 12.

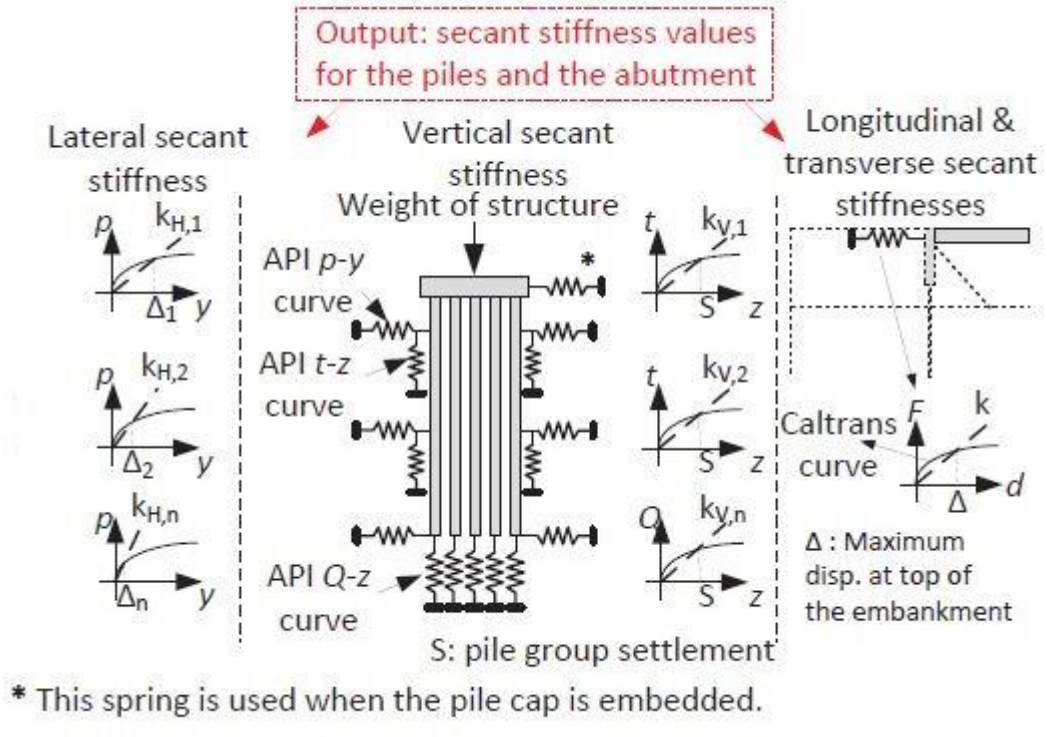

Figure 12: Effective linearization of the backbone curves[8]

3.3.3 Third stage: Determine pile head dynamic stiffness

As mentioned earlier, by simulating the 3D group pile foundation, 6 diagonal values can be calculated describing the dynamic transverse, rocking, vertical, and torsional stiffness, and four terms outside the diagonals describing the coupling elements between the transverse displacements and the rotation of the foundation. Current useful tables and diagrams can be used to achieve the relevant spring and dashpot variables, although they are only useful for modelling basic SSI issues where the foundation soil stays elastic under static or slow dynamic loading (Figure 13). Secant stiffness values can be used to better account for the nonlinear behavior of the soil-structure system in the design. The secant stiffness elements is utilized in the analyses of Lam et al. [126] to better predict the hysteretic loading, un-loading, and relieving response of the soil-pile interaction, and consequently set the standard for numerical modeling of foundations under earthquake shaking. As previously explained, the secant stiffness in the main framework is estimated using the appropriate maximum acceleration of the layered soil in the free field, which eliminates the influences of the seismic responses of the superstructure. Moreover, a damping ratio of 5% is considered for the internal structural damping.

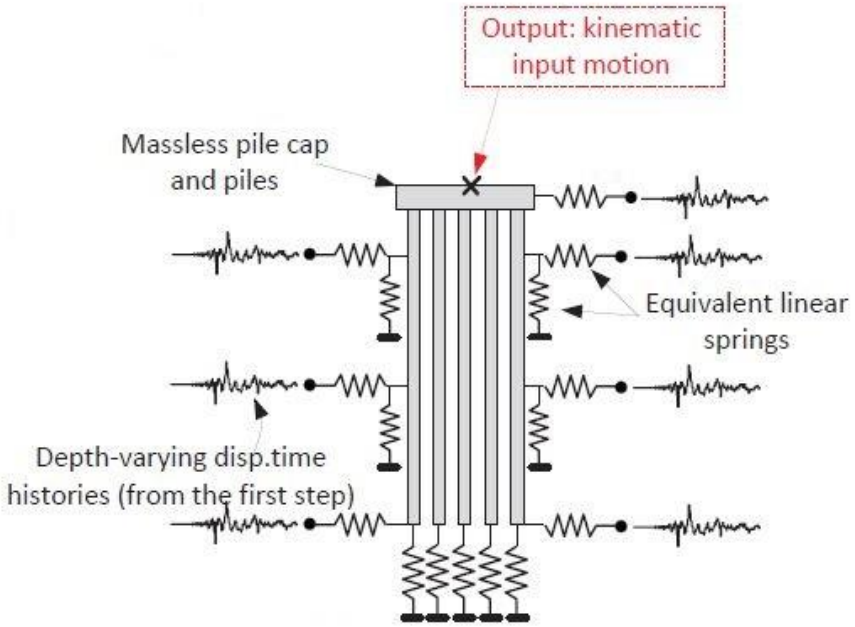

Figure 13: Characterization of the 6x6 stiffness matrix (K)

3.3.4 Fourth stage: Calculating pile cap kinematic motions

The kinematic input motion on the pile cap beneath the surface, is calculated at this stage. According to Fan et al. [127], when the system responds to low-frequency earthquake shaking, the movement on the pile cap is approximately equivalent to the free-field motion. Later, Makris et al. [128] applied free field motion (kinematic input motion) in their investigation. Based on Shamsabadi [124] analysis, the potential consequences of kinematic interactions on pile head motion can be investigated by modeling a massless pile group excluding superstructure. The corresponding linear springs and dashpots developed in the second phase are applied to model the response of the foundation soil as a practical simulation. The depth-variable time histories of acceleration generated in the first phase are then applied to the springs' ground nodes

as shown in Figure 14. The time history of the pile head displacements, named the kinematic input motion, is the result of this analysis.

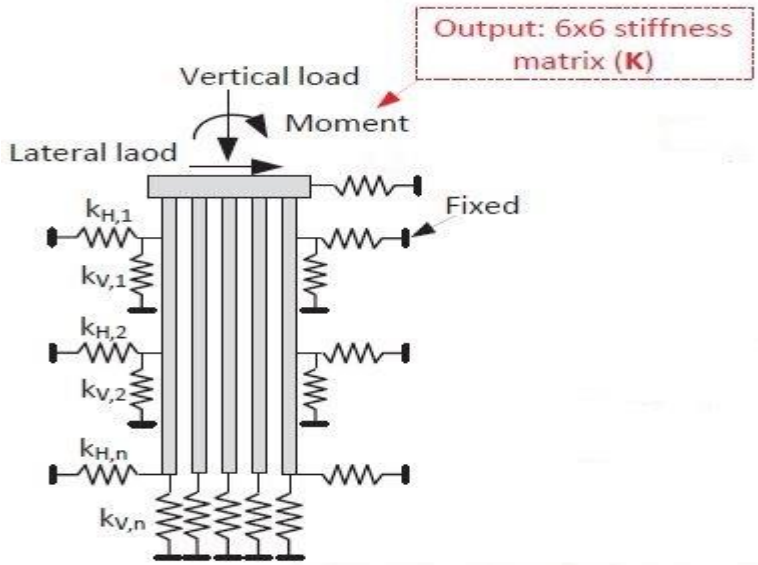

Figure 14: Characterization of the kinematic input motion at the pile head [8].

3.3.5 Fifth stage: Dynamic analysis of the superstructure model

Time history analysis is conducted to determine the seismic response of the superstructure relies by the equivalent linear springs and the dashpots generated in the previous phases. The adjustment of the dynamic parameters of a structure caused by the flexibility of the soil-foundation system is called inertial interaction. As a result, inertial forces such as base shears and moments create displacements and rotations at the foundation level. This influence has the potential to improve significant flexibility and energy dissipation to the structure-foundation-soil system. Since the dynamic parameters of a structure are modified by its support conditions, the period of vibration is assumed to change with the degree of flexibility of its supports.

3.4 Continuum approach

Continuum approach evaluates SSI by simulating a given soil profile along with the pile foundations, superstructure, radiating boundaries around the perimeter of the soil area, and interface components in the middle of the foundation area and the soil block. As a result, the direct solution addresses the entire soil-structure system and solves the problem in a single step. This approach requires the evaluation of the input ground motion at the base of the numerical model to ensure that it is compatible with the desired seismic hazard level. However, since there are few outcrop motions available, site response analyzes are often used to obtain this input ground motion with deconvolution. Further details about the finite element method and its shape function are presented in Appendix A. Nonlinear analyzes can be performed using commercial finite element programs such as ABAQUS [129], and ANSYS [130], including the open-source finite element tool OpenSees [131].

3.4.1 Sandy soil

Yang et al. [132]suggested an elastoplastic constitutive model to simulate the hysteretic nonlinear response of sand layers. A Drucker-Prager yield surface with a non-associative yield rule and a robust deviatoric kinematic hardening rule are included in the model. In OpenSees [131], this constitutive model is referred to as the pressure-dependent multi-field model (PDMY). The stress-strain relationship is linear and isotropic within the yield surface introduced in this model, while the nonlinearity should be available due to plasticity. The plasticity is expressed based on the multi-surface-plasticity in accordance with Prevost [133], in which yield surface is given as:

$$f = \frac{3}{2}[\boldsymbol{s} - (\acute{\boldsymbol{p}} + \acute{\boldsymbol{p}_0})\boldsymbol{\alpha}] : [\boldsymbol{s} - (\acute{\boldsymbol{p}} + \acute{\boldsymbol{p}_0})\boldsymbol{\alpha}] - \boldsymbol{M}^2(\acute{\boldsymbol{p}} + \acute{\boldsymbol{p}_0})^2 = \boldsymbol{0} \quad (5.1)$$

$$\boldsymbol{s} = \acute{\boldsymbol{\sigma}} - \acute{\boldsymbol{\rho}}\boldsymbol{\delta} \quad (5.2)$$

where; $\boldsymbol{s}$ is deviatoric stress tensor, $\boldsymbol{\acute{\sigma}}$ is effective Cauchy stress with second order tensor $\boldsymbol{\delta}$, $\boldsymbol{\acute{p}}$ is mean effective stress with second order deviatoric tensor $\boldsymbol{\alpha}$, $\boldsymbol{M}$ is the yield surface size and $\boldsymbol{\acute{p}_0}$ is small absolute constant applied to limit the size of the yield surface at $\boldsymbol{p} \doteq \boldsymbol{0}$, [45].

8-node hexahedral linear isoperimetric elements with 4 degrees-of-freedom (DOF), of which includes three for solid displacements and one for fluid pressure are defined for simulating the soil block in accordance with the Biot's concept of porous medium. First and second runs are carried out as soil consolidation for both elastic and plastic phases of soil block, respectively.

3.4.2 Concrete material

For constitutive modeling of concrete materials, the uniaxial Kent-Scott-Park model [135] is applied. This concrete model is typically employed in opensees software as a concrete constitutive model for those elements which are remained elastic, hence in this study, by regarding that rigid massless pile cap is used by following Shamsabadi (2013) methodology, the piles are rigidly connected to the pile cap. Same thing applies to the connection of the columns to the pile cap. The tensile strength is negligible in this model, and the unloading stiffness decreases with increasing strain. In the OpenSees platform, the model is referred to as Concrete01. The stress-strain response of the model can be seen in Figure 15. The concrete compressive strength at 28 days (σ_{max}), concrete compressive strength at crushing (σ_u), strain at maximum compressive strength (ε_y), and strain at crushing (ε_u) represent the stress-strain response, and the baseline gradient of the response (E) is represented by:

$$26_{max}/\varepsilon_y \tag{5.3}$$

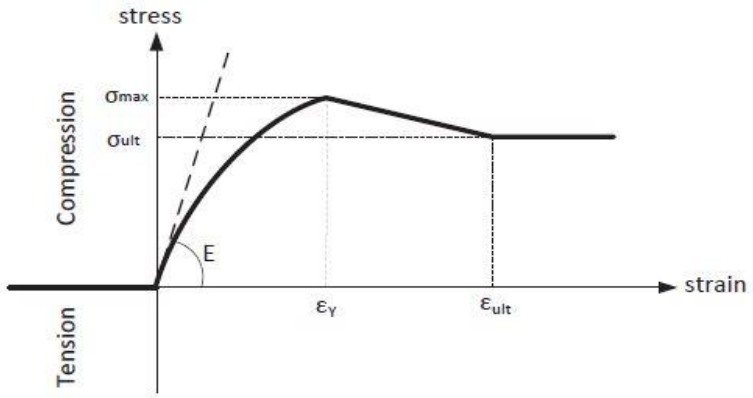

Figure 15: Kent-Scott-Park stress-strain response for concrete material [135]

3.4.3 Steel material

Uniaxial Giuffre-Menegotto-Pinto steel material object with isotropic strain hardening is considered as column and beam materials of the superstructure. In addition, in this method, Newmark time-stepping integrator object is selected for transient analysis and a Krylov Subspace Accelerated Newton Algorithm [136] is used to construct the algorithm related to the nonlinear time history analysis.

3.4.4 Modeling soil-pile interaction

The soil block is represented by solid eight-node brick components with eight Gauss points and three degrees of freedom. Pile was modeled with six degrees of freedom by displacement-based beam-column components. To develop a system of a complete soil-pile block, coupled finite elements for pile and soil are required. This is done by first removing the volume components in the pile-occupied zone and then positioning the pile-beam-column components inside the soil block. The pile nodes are horizontally connected to the soil nodes in each plane via four rigid beam-column components, as shown in Figure 16.

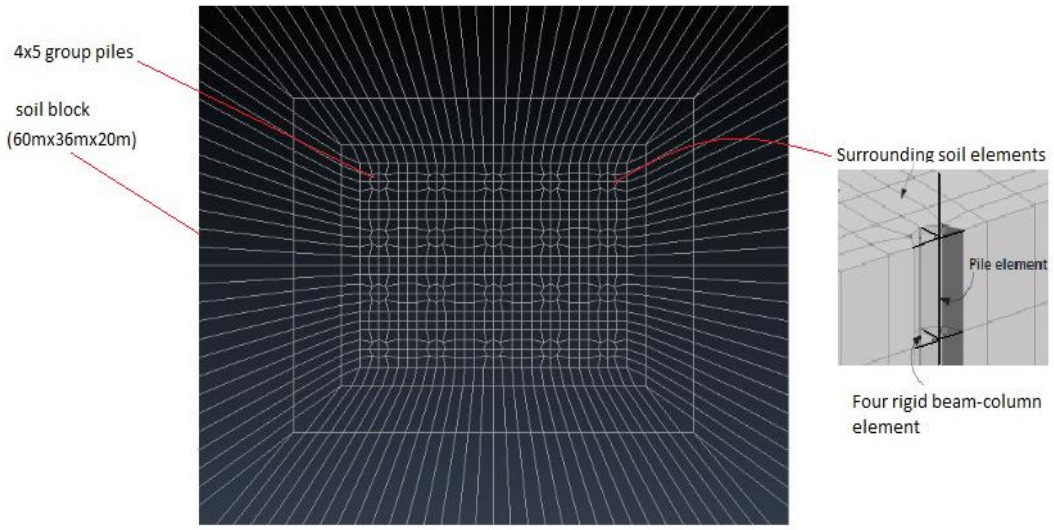

Figure 16: Finite element mesh model simulated for soil pile interaction.

3.4.5 Analysis procedure

The system analysis of the soil structure is evaluated as follows: First, the finite element model is constructed by eliminating all structural elements, and the weight of the soil is applied to all solid elements to gain the primary stress states. Then, the soil elements in the area filled by the piles are removed to identify the actual area of the piles; the structural components of the superstructure are then placed all at once, and self-weight analysis is performed to check the whole structure for stability. Eventually, the fixes are removed from the base of the finite element mesh in both the longitudinal and transverse directions, and the corresponding time histories of acceleration in these two horizontal directions are fed back to the base in OpenSees using the multi-support oscillation pattern. A static nonlinear analysis is performed for the first and second phases, and a transient dynamic nonlinear analysis with time steps of 0.01 s is performed for the third phase. To identify the series of steps to analyses the nonlinear equation, the mechanism Krylov-Newton is used. To combine the equations of motion

in dynamic analyses, the Newmark time-stepping algorithm is applied with variables g=0.5 and b=0.25.

3.5 Validation of the Continuum and Substructure methods

In this study, research data, which involve four sets of centrifuge data, to test for the ability of the spring method and continuum method in predicting pile seismic behavior. Numerical spring simulation and three dimensional finite element method procedures are used to verify centrifuge test data on steel pipe piles (diameter 57 cm) with a single pile in sand by Gohl [111]. In this test, a peak horizontal ground acceleration of PGA = 0.158g is applied to evaluate the dynamic response of system. The state of practice to model soil-pile interaction for a single pile subjected to seismic loadings consists of two consecutive steps explained in last chapter. In the first step, site response analysis is carried out to determine the depth-varying time histories of absolute displacement, and in the second step dynamic analysis of the pile is carried out by applying the time histories of absolute displacements to the ground nodes of the springs. The soil profile in the centrifuge test of Gohl [111] consisted of a single layer of dry fine-grained Nevada sand (Dr=40%) with the thickness of 12.0 m. The mass density and the friction angle of the soil were 15.0 kN/m3 and 35, respectively. The single pile was a steel pipe pile with diameter of 57.0 cm and wall thickness of 1.3 cm at the prototype scale. The pile was extended about 2.0 m above the ground surface and carries a superstructure load of 522.0 kN. The spring model of the centrifuge tests is developed in OpenSees [131] to solve the dynamic equilibrium equation. The centrifuge test are also simulated using the 3D continuum modeling method. Bending moment along the pile and acceleration response spectrum are evaluated. The results showed fairly good agreement between the measured and computed responses of the system. There was no indication of major gap formation in the outcome, but the bending moment and

acceleration response spectrum of Measured, Continuum and Spring model illustrated in Figures 17 and 18 respectively.

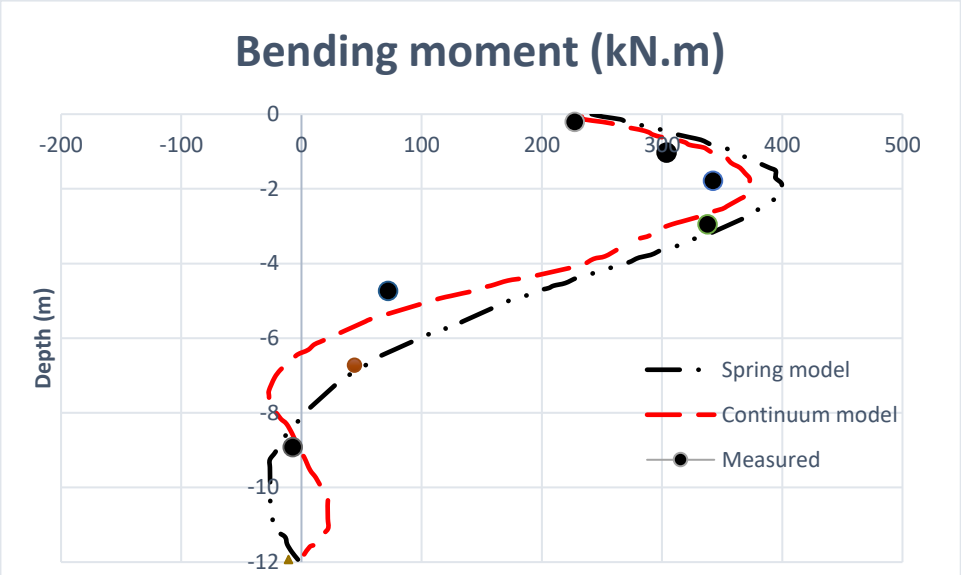

Figure 17: Bending moment at pile maximum displacement in centrifuge test of Gohl [111]; comparing the measured and the computed responses in the continuum and the spring models.

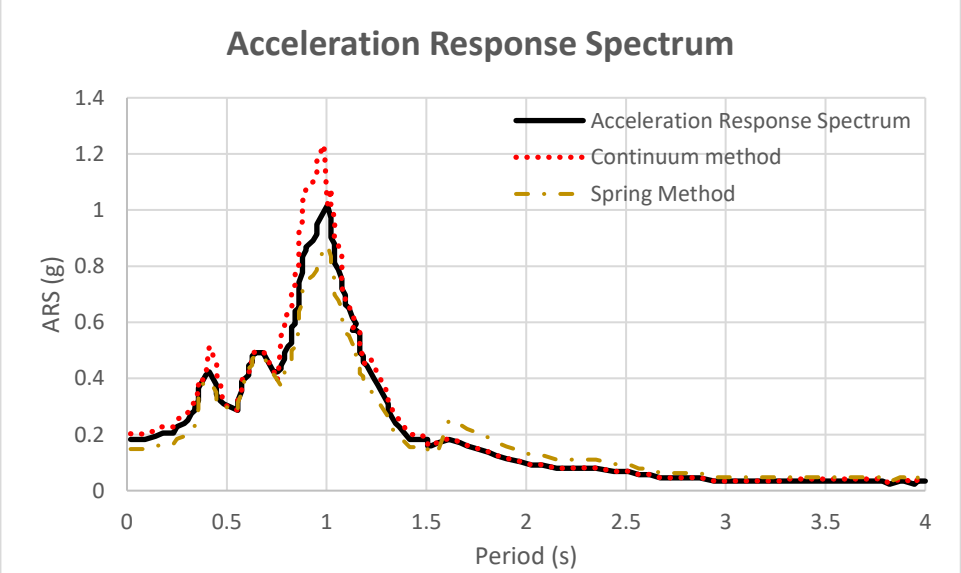

Figure 18: Acceleration Response Spectrum comparison.

3.6 Summary

This chapter first, provides an essential foundation for the construction of the structural control model as a device for reducing lateral excitation potential. Three main components of the TMD are discussed and the formulas for obtaining the optimal efficiency of the TMD are explained, mentioning that the optimal mass ratio of the device has more effect on the effectiveness of the damper for suppressing the earthquake vibration input. As briefly explained in this chapter, the concept of ground hook algorithm, which is typically used to optimize semi-active devices, is used to improve the STMD efficiency during earthquake. The on-off ground hook control is adopted as a controller for the STMD optimization in this study.

Secondly, in this chapter, dynamic analysis is contacted to the structure by using substructure approach. This approach, is detailed in five stages. First stage explained the acceleration time history in the free field foundation are calculated. In second stage, secant stiffnesses along the piles, pile heads, are calculated. The lateral and vertical secant stiffnesses of a given backbone curve are set as the stiffness at the ground acceleration in the free field and also settlement of the pile group. The group of piles are concurrently subjected for lateral and vertical stresses and simultaneously for bending moments. Fourth step explained the calculation of kinematic input motion which is produced at the cap of the pile for a massless pile group neglecting the superstructure stiffness and mass. Then, the entire simulation of the STMD structure, supported by suitable auxiliary springs and dashpots, is analyzed by the kinematic input motions in the last step.

As a last section in this chapter, the approach used in the OpenSees software to model soil-pile structures using the continuum methodology is described in detail. The extended constitutive models are proposed to analyze the nonlinear hysterical behavior of soil material under static and dynamic excitation. The pressure-dependent multi-field model (PDMY) is introduced to model sand based on multi-surface plasticity. For constitutive modeling of concrete, the uniaxial Kent-Scott-Park model, referred as Concrete01 in OpenSees, is used, while for constitutive modeling of steel, uniaxial Giuffre-Menegotto-Pinto steel material object with isotropic strain hardening, referred as Steel02 in OpenSees, is used. In the continuum model, soil volume components are linked to pile beam-column components by four rigid beam elements to model the visible dimensions of the pile.

Chapter 4

ANALYSIS RESULTS AND DISCUSSION

4.1 Substructure method evaluation

This chapter extends the direct and substructure methods which is previously mentioned by reviewing the existing models typically used in seismic analysis of soil-structure interaction problems. Domain models are often used as a direct method in research, but spring models are preferred by engineers as a simple tool for measuring the seismic behavior of structures and foundations during inertial interaction. This chapter provides a thorough examination of the components of the model. Both types of interaction (kinematic and inertial) are accurately measured for structures with dampers to determine the optimal parameters for design. For structures equipped with semi-active tuned mass dampers (STMD) on deep foundations, the determination of the optimal STMD characterizations is completely related to the dynamic behavior of the structure. Therefore, in this chapter, the accuracy of the general p-y equation for structures with STMD having a short period on deep foundations is first evaluated. Then, the three-dimensional continuum method (finite element method) is used and the general p-y equation is updated to ensure compatibility. Since the current structural models are well developed, the focus is on the geotechnical components. The strengths and weaknesses of these models are also discussed.

4.1.1 Characterization of the system

4.1.1.1 Description of building with STMD

In this study, seismic response of a 5-story, 4-bay in X and 3-bay in Y direction steel moment resisting frame building analyzed with a 5% structural damping ratio. One directional excitation is used. The building is modeled in finite element method using OpenSees software. Four bays with 6m and each story height with 3.4m is considered for this structure (Figure 19). Material properties and element details for structure and TMD are provided in Table 2 and Table 3 respectively. Newark's method has been applied for time history analysis under several earthquake excitations.

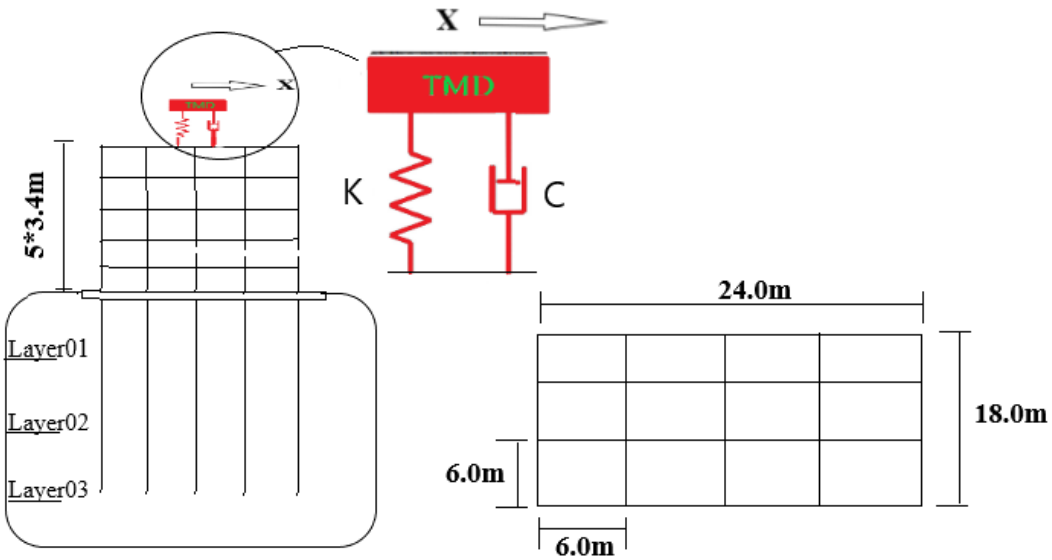

Figure 19: Five-story building controlled with STMD on a deep foundation.

Table 2: Structure properties

Structure	**properties**
Steel	St37
Column	BOX400x30,BOX350x25
Beam	IPE270,IPE320

Table 3: TMD properties

TMD	properties
Damping ratio, ζ_{TMD}	9.2%
Mass ratio, μ	2%
Frequency ratio, ω_{TMD}	9.03 rad/s

4.1.1.2 Groundhook algorithm

The dynamic process associated with the harmonic base acceleration of $\ddot{x}_b = \ddot{X}_0 e^{iwt}$ is presented in Figure 20 for which m_1; k_1, and c_1 subsequently represent the mass, stiffness, and damping of the main system. In this algorithm the on-off damping regulator, in which the TMD damping ratio C_2can be converted between the strong coefficient C_{max} and the weak coefficient $C_{min}$is used for obtaining optimum characterization of STMD. The on-off ground-hook control and its variants are assumed as the organizers for the STMD in this study. The switching is done based on the following situations:

$$x_1(\dot{x}_1 - \dot{x}_2) \geq 0 \rightarrow \ C_2 = C_{max} \qquad \text{ON state} \qquad (6.1a)$$

$$x_1(\dot{x}_1 - \dot{x}_2) < 0 \rightarrow \ C_2 = C_{min} \qquad \text{OFF state} \qquad (6.1b)$$

where x_1, $\dot{x}_1$ and $\dot{x}_2$ are the displacement and, velocity of mass m_1 and velocity of m_2 correspondingly. The controller Eq. (4.1a, 4.1b) rely on the displacement of the principal structure, and consequently, is known as the displacement-based ground hook (DBG) controller [67,87].

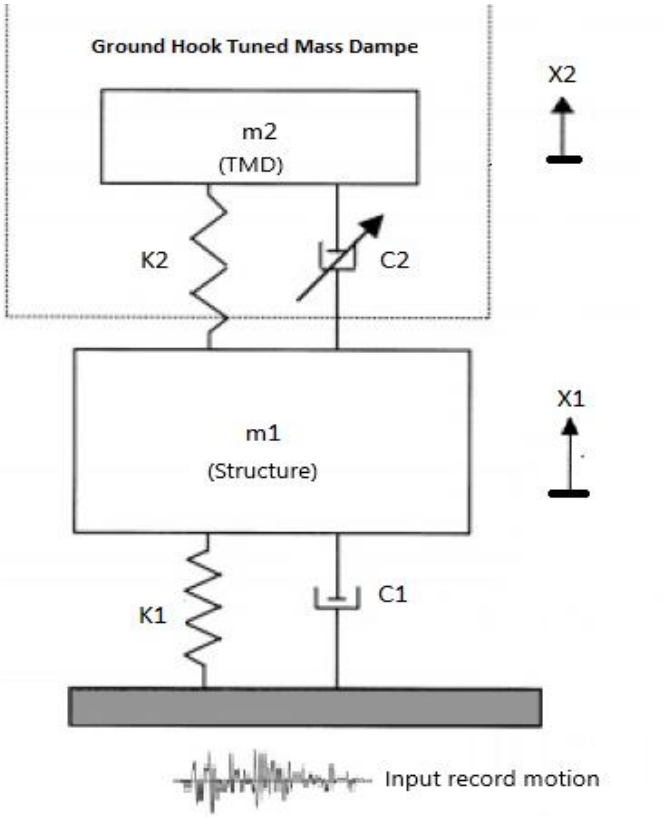

Figure 20: The vibration absorbers system with Groundhook Tuned Mass Damper algorithm.

4.1.1.3 Soil and pile properties

Some factors like friction angles and cohesion are essential for the response of large strains, however, the bulk modulus and elastic shear modulus are significant in the response of small strains. Hence, here the soil profiles consist of a layer of loose sand (Dr=15%) with a depth of 5.0 m. accordingly the mass density and the internal friction angle of the soil measured 1.94 t/m3 and 25.4°. And medium sand (Dr=25%) with a depth of 6.0 m. about second layer, The mass density and the friction angle are 1.99 t/m3 and 30.3°, respectively. Eventually, the third layer is dense sand (Dr=35%) with a depth of 9.0 m. Also the mass density and the friction angle of the third layer measured 2.06 t/m3 and 42.2°, respectively. Transition zone with 2m thickness also considered between the layers for avoiding of any suddenly changes in material properties which is lead to have more accurate result. The input soil properties for the

model are also shown in Figure 21. In this study twenty steel pipe piles with a diameter of 1.2 m and a wall thickness of 5.0 cm with spacing 6 m (center to center) and 17m height are considered.

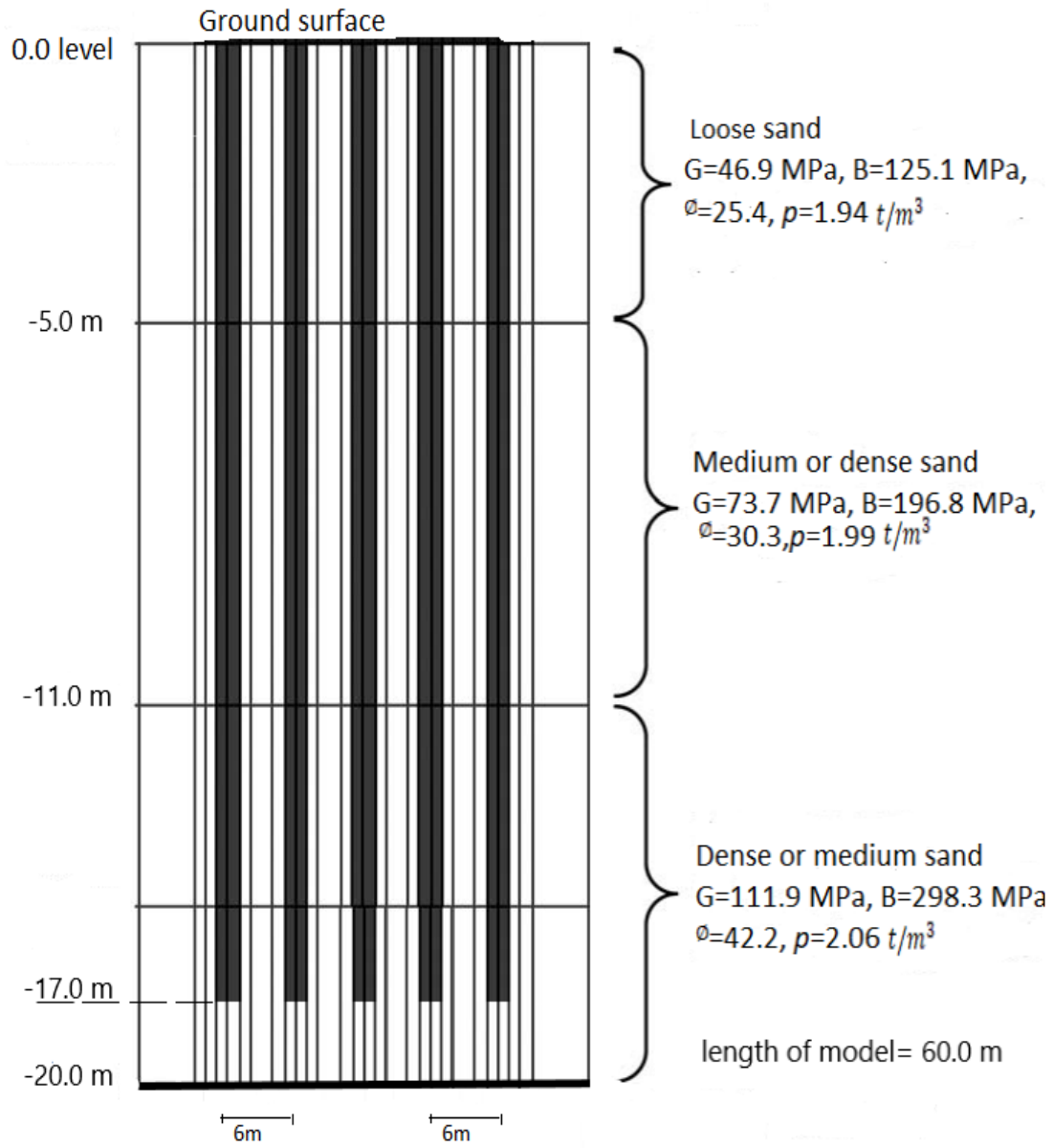

Figure 21: Soil layers properties along with pile depth.

Following the fundamental approach by Matlock H. [44], more emphasis is employed on measuring the effect of the following aspects:

(I) free-field site response, (II) nonlinear behavior regarding the soil-pile interaction throughout the length of the pile.

In order to define the spring criterion, the p–y curves (API curves without any adaptations and with adaptations which are derived from continuum finite element method) are used as a backbone curve for the definition of the parameters of nonlinear components in accordance with the Beam on Non-Linear Winkler Foundation method.

4.1.2 Substructure simulation of the system

The superposition of the linear elastic systems is applied, including two parts of the SSI interface: kinematic and inertial interface [123]. The Winkler foundation method is considered for the development of the linear spring model. The state of order for soil-pile interaction modeling subjected to seismic loadings includes two continuous steps. First, the site response analysis is subjected to an earthquake excitation for finding the depth-differing time histories of displacement, then, dynamic analysis of the pile are carried out using time histories of displacement to the nodes of soil springs [46]. In this study the two steps of aforementioned procedure is performed at one stage presented in Figure 22. Therefore, after consolidation analysis, the acceleration time histories of the far field analysis are assigned to the soil nodes of near field soil block. The Open System for Earthquake Engineering Simulation (OpenSees) computer program [131] is used for simulation purposes. The dynamic equilibrium equation for elastic beam assisted by nonlinear springs is presented by the following equation:

$$E_p I_p \frac{\partial^4 y}{\partial x^4} + m\left(\frac{\partial^2 y}{\partial t^2} + \frac{\partial^2 y_g}{\partial t^2}\right) + c\left(\frac{\partial y}{\partial t} - \frac{\partial y_{ff}}{\partial t}\right) + k_h\left(y - y_{ff}\right) = 0 \qquad (6.2)$$

where, E_pI_p is the pile's flexural stiffness, y and y_{ff} indicate relative pile's displacement and relative free-field displacement respectively at the base excitation (y_g), c is the damping percentage and k_h is the secant stiffness obtained from the p-y curves (API Standard) at each loading stage. The constitutive model used for modeling soil behavior is Pressure Dependent Multi Yield (PDMY) model for sandy soils, which describes the stress-strain association at the gauss-point of a continuum component. In this approach, different non-linear t-z, q-z and p-y models are suggested by API standard to consider the effect of soil-pile-soil interaction. Nonlinear p-y performance is characterized as elastic, plastic and gap spring components put in series [112]. Soil material is identified using 9-node quadrilateral plane-strain element. The pile itself is simulated as a series of beam-column elements, by using discrete springs linking the pile to the soil nodes.

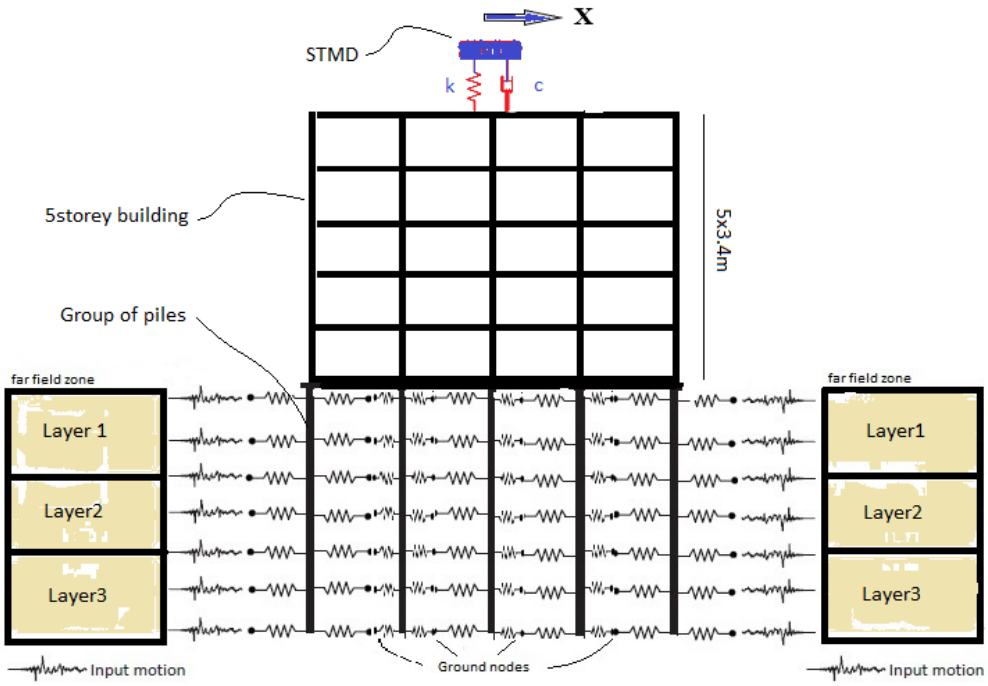

Figure 22: Configuration of the spring process used for dynamic analysis of the pile in a single region.

4.1.2.1 API guideline for soil –pile interaction

As earlier described in chapter 2, API standard [9] recommends the following equation for laterally loaded piles in sands, so-called p-y curves, at any particular depth of H,

$$P = Ap_u \tanh\left(\frac{kH_y}{Ap_u}\right) \tag{6.3}$$

where, lateral resistance *P* is computed along the pile based on horizontal displacement "y", and about the modulus of subgrade reaction "K" is derived from specific figure as a function of internal angle of friction"∅", and the ultimate soil lateral resistance is "p_u" which can be obtained for wedge failure or flow failure (equation 6.3, 2.2a and 2.2b), and A is a constant related to the static or cyclic loading. The backbone curve equation (Eq.6.3) can be obtained by substituting A with 0.9 for cyclic behavior of sand.

API standard also makes recommendations for the estimation of t-z and Q-z curves, in which t is the shear stress along pile shaft, z is axial displacement of the pile, and Q is the end bearing force which are explained in chapter 2.

However, obtaining reasonable estimates of the interaction of the pile-soil-pile is another challenge for obtaining dynamic stiffness of the foundation. Therefore, in this study, soil lateral resistance p is reduced by a scale value named p-reducer. Hence the p-reducer proposed by the American Association of State Highway and Transport Officials [125] is used to consider the effect of group interaction (Table 5). The input parameters and results of spring method are easily controlled compared to the continuum method, though it is more difficult to setup and run to use implicitly due to the difficulty of appropriate characterization of springs and dashpots in the analyses.

In this paper, authors seek to obtain confirmation about applicability of spring techniques in the preparation of dynamic SSI, hence in this phase of analyses the degree of percentage of error is either reduced or eliminated. Following up in an iterative manner though, the input parameters are updated by using the nonlinear time history analysis of the continuum model using advanced constitutive models.

Table 4: AASHTO P-reducer suggestion [125].

Spacing between adjacent piles	First row	Second row	Row 3 and higher
3D	0.80	0.40	0.30
5D	1.00	0.85	0.70

4.1.3 Continuum simulation of system

In this method, soil surrounding the pile foundations is simulated with absorb boundary conditions. These boundary conditions are set to avoid transmission of seismic waves into the soil block. The position of the transmission boundary should be set at a distance of 10 times the base width as recommended by Rosset and Kausel [137] but by using convergence curve, this boundary can set closer according to the model. The direct approach therefore takes the whole soil structure scheme into account and resolves this issue in one step. The input ground acceleration is assessed on the basis of the simulation model in accordance with the seismic design hazard level. For obtaining depth-varying time histories of ground motion, site response analyses are used.

By using Lagrange's equation, the equation of motion for a building can be expressed in matrix form for dynamic analysis as follows:

$$[m]\{\ddot{x}(t)\} + c\{\dot{x}(t)\} + k\{x(t)\} = [-m^*]\{1\}\ddot{u}_g \quad (6.9)$$

where [m], [c] and [k] indicate mass, damping and stiffness of the vibration system, in the order given. [m*] denotes acceleration mass matrix for seismic loads and $\ddot{u}_g$ is the earthquake acceleration. The finite element method can use the standard step-by-step numerical integration techniques to implement the mechanism for investigating the depth-varying time histories of record motion. For accurate estimations of inertial and kinematic interactions between foundation soil and structure, advanced constitutive models can be trusted for the application of the equation [138]. Mathematical explanation of the relation between stress and strain measurements is provided. The hysterical nonlinear reaction of the sandy soil is modeled by an elasto-plastic constitutive model [132]. Hence, the Drucker–Prager failure criterion is used with non-associative flow rule to estimate the stress state at which the rock reaches its ultimate strength. Three-dimensional meshes are generated by eight-node brick solid element which is based on tensor operation with eight gauss points. Displacement based beam-column elements are used for piles simulation in the soil block. The whole mesh included the superstructure, foundation, soil block and group piles. In order to build a standard shape of a full soil-pile framework, pile and soil components must be paired. The schematic of this method is illustrated in Figure 23.

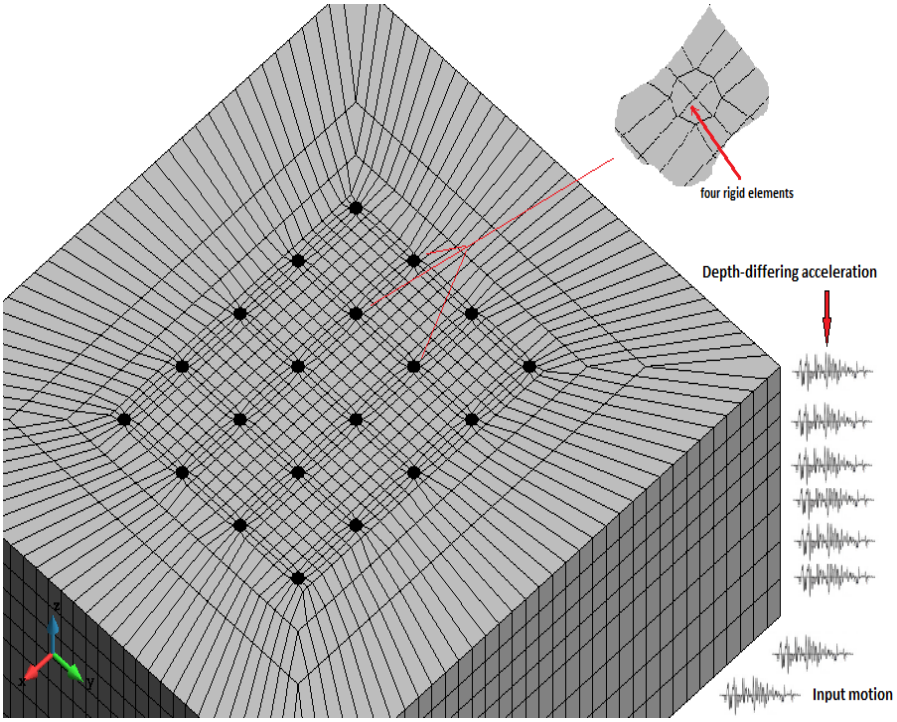

Figure 23: Schematic of the simplified continuum modeling method.

4.1.4 The p-y Curves derived in this practice

In this study, although the gap and drag factors are mostly neglected for convenience, the effect of this factors are already considered in p-y curves given by API standards. In addition, radiation damping is also ignored in the analyses, as is the case typically for the soil structure systems undergoing severe shaking [122,139].

In order to characterize soil hysteretic behavior upon lateral loading, the soil-pile interaction is modified with a nonlinear Winkler spring. These nonlinear springs are assigned the corresponding API curve value as an initial loading path and reloading or unloading in accordance with the Masing rule to model the nonlinearity of the hysteresis loops. For a short period (T<1s) of steel structures equipped with STMD founded on a deep sand foundation (piles foundation), the following equation suggests better soil-piles-soil interaction estimates. For using this equation all the

aforementioned parameters such as soil lateral resistance and subgrade reaction in API are used in revised equation except the coefficient “A”, which shows the static or cyclic loading factor. API provides this equation for both static and dynamic analysis in sandy soil, hence in this research for finding the optimum response against cyclic earthquake loads only the coefficient “A” is amended. For finding the optimum coefficient, rich data sets including 35 records are selected based on two categories (near-field and far-field) in which near-field ground motions have been characterized into two classifications: records with strong velocity pulse and records with a residual ground displacement. The characteristics of record motions are set out in Table 5.

As explained previously, in continuum method soil nodes rigidly connected to the pile nodes at same level with four rigid beam-column elements. Rigid beams are used for connection between that medium and the piles to enforce compatibility between soil and pile deflection. The computed forces in these elements are used to obtain p-y curves in which P is the summation of forces in the direction of loading, and Y is the pile deflection. On the other hand, in the substructure method, the API guidelines are used for dynamic analysis of group pile. For lateral loading, p-y curves which are provided by API used, representing the flexibility of the soil pile foundation system. These p-y curves previously investigated by last researches based on continuum method results. Hence, in this study, 3D continuum model is used for simulating the same problems. The results are compared to assess the validity of the p-y curves.

For this end, trial dynamic analysis are done with substructure method by considering the coefficient values for A, between 0.1 to 2.50 (Figure 24).

The evaluation of the data including bending moment along the pile, lateral force, lateral displacement of the piles, the top displacement and also acceleration time histories revealed that for cyclic analysis, 1.287 may be recommended rather than 0.9 mentioned in API recommendation. Hence the equation for cyclic loading becomes (6.10):

$$\hat{P} = 1.287 p_u \tanh\left(\frac{kH_y}{1.287 p_u}\right) \qquad (6.10)$$

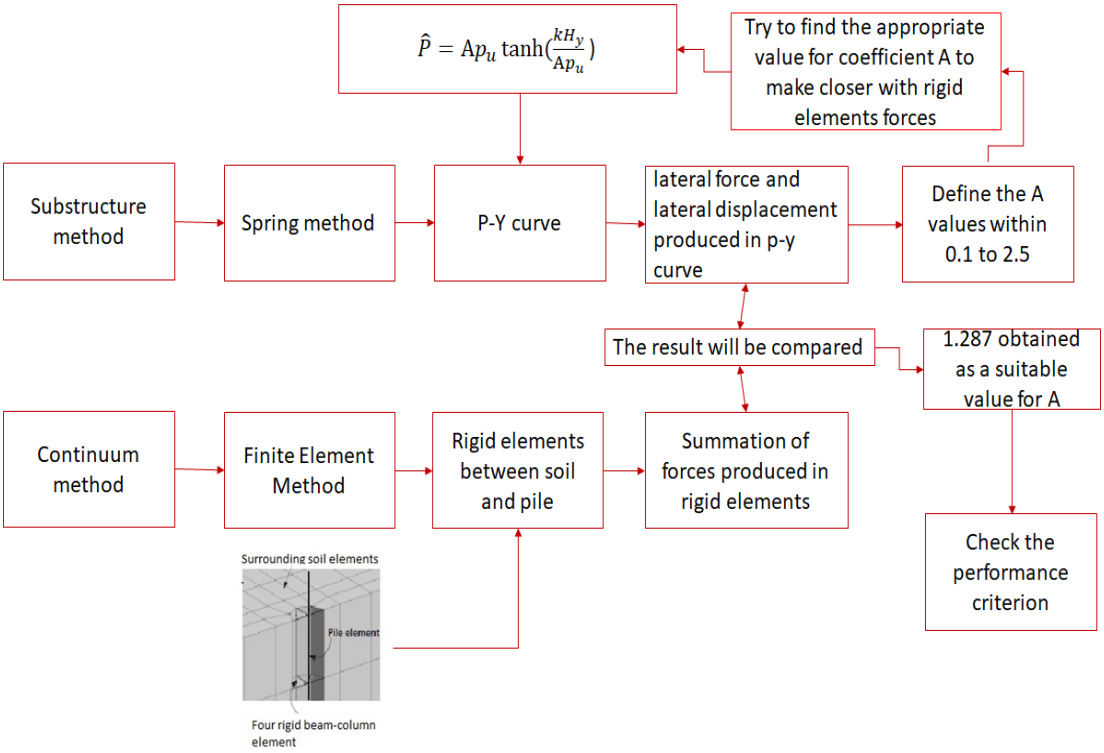

Figure 24: The cyclic procedure for obtaining A

Table 5: Record motions characteristics

No	Earthquake	Year	Station	M	Dist.(km)	PGA
Near-field ground motion's characteristics						
1	Gazli	1976	Karakyr	6.8	12.82	0.599
2	Coalinga	1983	Pleasant Valley P.P.-bldz	6.36	9.98	0.377
3	Morgan hill	1984	Andersondam(Downstream)	6.19	16.67	0.449
4	N.Palm	1986	North Palm Springs	6.06	10.57	0.669
5	Superstition	1987	Parachute Test Site	6.6	15.99	0.418
6	Superstition	1987	Niland-fire station	6.6	22	0.136
7	Erzican,Turkey	1992	Erzican	6.6	8.97	0.486
8	Loma Prieta	1989	Gilory Array #02	7.1	29.77	0.406
9	Loma Prieta	1989	Gilory array#01	7.1	25	0.966
10	Kobe	1995	KJMA	6.9	18.27	0.854
11	Northridge-01	1994	LA dam	6.69	11.79	0.576
12	Northridge-01	1994	Jansen filter plant	6.69	40	0.932
13	Chi Chi	1999	TCU065	7.62	26.67	0.831
14	Kobe	1995	KJMA	6.9	18.27	0.548
15	Chi Chi	1999	TCU065	7.62	26.67	0.557
16	Chi Chi	1999	TCU074	7.6	13.75	0.59
17	Chi Chi	1999	TCU074	7.6	13.75	0.37
18	Chi Chi	1999	TCU082	7.6	4.47	0.22
19	Chi Chi	1999	TCU128	7.6	9.08	0.14
20	Kocaeli	1999	Yarimca-EW	7.4	3.3	0.23
21	Kocaeli	1999	Sakarya-EW	7.4	3.2	0.41
Far-field ground motion's characteristics						
22	San Fernando	1971	2516 Via Tejon PV	6.6	55.2	0.025
23	San Fernando	1971	2516 Via Tejon PV	6.6	55.2	0.041
24	Tabas,Iran	1978	Ferdows	7.4	91.14	0.087
25	Tabas,Iran	1978	Ferdows	7.4	91.14	0.107
26	Imperial Valey	1979	Coachella Canal #04	6.5	50.1	0.115
27	Imperial Valey	1979	Coachella Canal #04	6.5	50.1	0.128
28	Cape	1992	Mendocino	7.01	44	0.154
29	Loma Prieta	1989	Richmond City Hall-NS	6.9	87.87	0.124
30	Loma Prieta	1989	Richmond City Hall-EW	6.9	87.87	0.105
31	Landers	1992	Baker Fire Station	7.3	87.94	0.107
32	Landers	1992	Baker Fire Station	7.3	87.94	0.107
33	Northridge-01	1994	Huntington Bch-Waikiki	6.7	69.5	0.68
34	Northridge-01	1994	Huntington Bch-Waikiki	6.7	69.5	0.068
35	Alaska	1972	Sitka observatory	7.68	55	0.096

4.1.5 Substructure result and discussion

The results of the nonlinear dynamic time histories analysis performed on the structures with STMD in both springs method and also continuum method (3D finite element method meshing) are presented in this section under different far-field and near-field record motions. For more clarity, among the data set, the series of five

seismic input vibrations by considering the low and high level of errors studied for the proposed STMD-SSI numerical example analysis selected and set out in Table 6.

Table 6: Earthquake Records used in the numerical analysis

Earthquake	Station	M	Dur.[s]	PGA[g]	situation
[1]Loma Prieta 1989	Gilory array	7.1	25	0.966	Near- fault
[2]Superstition hills 1987	Niland-fire station	6.6	22	0.136	Far-fault
[3]Northridge01 1994	Jansen filter plant	6.69	40	0.932	Near- fault
[4]Alaska 1972	Sitka observatory	7.68	55	0.096	Far-fault
[5]Cape Mendocino 1992	Mendocino	7.01	44	0.154	Far-fault

Two independent spring models are used to test the spring coefficients for soil pile structure interaction; model A, a spring model using the standard API p-y backbone curves suggested for all types, and model B, used p-y backbone curves modified as part of this research which has meticulous constant coefficient for short period structures . As discussed earlier, the modified curves are derived from the time-history analysis of the continuum models. Five major parameters are considered for evaluation p-y curves, bending moment, lateral force and head pile deflection for substructure, and also, top floor displacement and absolute acceleration for superstructure. As it mentioned in previous chapter, for finding best TMD activities during earthquake, designers need to know that how much force transmitted between two systems (structure as a main system and TMD as a supplementary damping system) called viscosity-force. Hence in this study viscosity-force which is most necessary for obtaining optimized TMD's characterizations is assessed during earthquake motion. The middle steel pile in second row and third column is the analysis target.

4.1.5.1 Lateral force and displacement of the pile

Absolute Soil ultimate resistance and pile displacement for different earthquake excitations are shown in Table 7 and, Figure 25. As it is shown in the figure, spring

models (Model A and B) act poorly in the estimation of lateral force in all excitations. The level of error in the spring Model A varies in the range from 91% to 309% and, Model B (which is derived from continuum model) within 87% to 270% with a general trend towards underestimation of the behavior observed in the continuum model. The lateral force is underestimated in all cases, whereas the lateral displacement is underestimated in some cases and overestimated in the others. For instance, in the analyses performed using Alaska record (far-field motion) spring models have underestimated the lateral force, and they overestimated lateral pile displacement. On the other hand, for Northridge and Superstition records (near-field and far-field respectively) spring models could predict lateral pile displacement reasonably well compared to the continuum model results. Therefore, it can be stated here that this is due to the type of record motion (far-field or near-field) having no impact on the p-y curve data. However, by considering the predictions obtained, it can be stated that the Model B performed better than Model A, showing to the fact that its parameters are derived from continuum method.

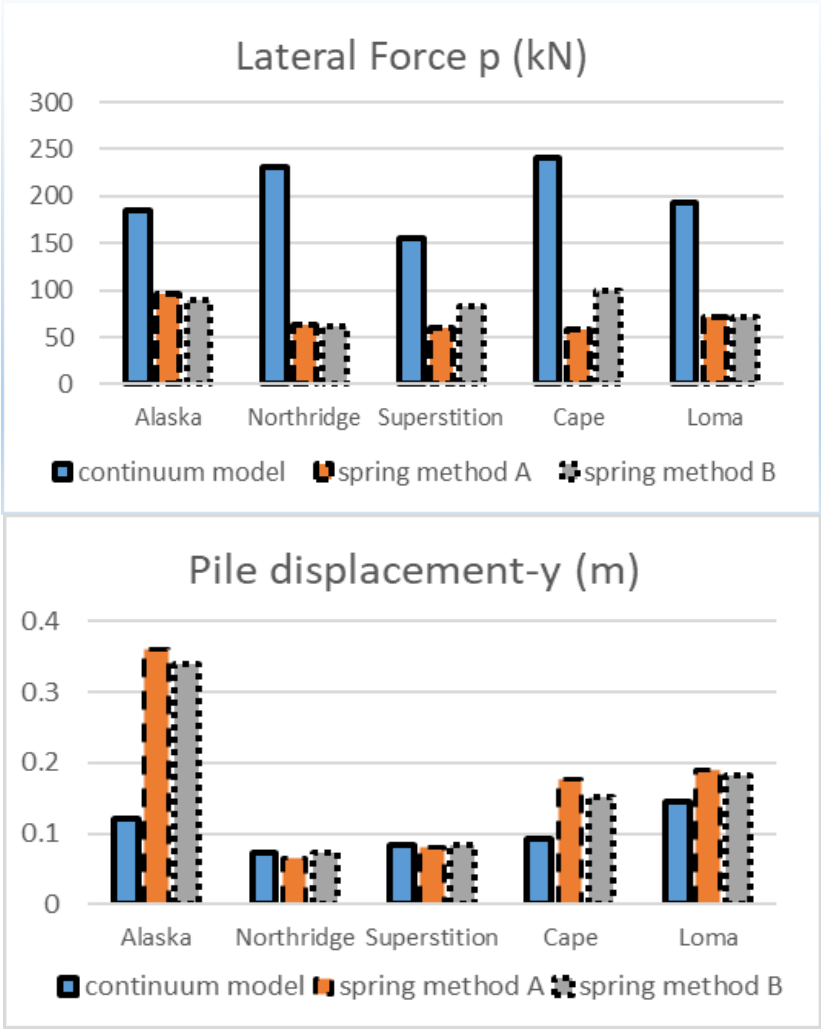

Figure 25: Lateral force and lateral displacement of pile head fluctuation during the varying excitation records

Table 7: Range of p-y deviation in case study

Earthquake	Alaska	Northridge	Superstition	Cape	Loma
Lateral Force (Model A)	91%	265%	162%	309%	169%
Lateral Force (Model B)	108%	270%	87%	142%	172%
Lateral disp. (Model A)	196%	13%	4%	91%	31%
Lateral disp. (Model B)	179%	1%	0.58%	64%	27%

4.1.5.2 Bending moment response of pile

Figure 26 presents the bending moment along the length of the pile at the time when the maximum pile head deflection is attained in the analysis of each earthquake record. In these results, the range of error is shown to be between 77% to 350% and, 20% to

78%, for model A and B respectively, with a general trend of overestimation of the maximum bending moment with respect to continuum model results. The bending moment predictions of spring models also seem to diverge significantly with pile depth. A close examination of the curves shows that spring models predicted the bending moment down to the transition zone between the first and second layer reasonably well, and with less accuracy, along the zone between second and third layer. However, the degree of error dramatically increased in the third layer, in which the soil stiffness is significantly higher compared to the upper layers. The divergence in the lateral deflection of piles and the bending moment is affected more in the third layer, which in essence acts like a fixity in the continuum model due to the high stiffness of the ground. In comparison, in the spring models, in which the subgrade modulus is generated on a similar formulation, the relationship between the lateral pile load and lateral pile deflection is similar, reflecting a similar shape of bending moment curve no matter how different the numerical value of the estimation. For Alaska record however, the shapes of the bending moment curves for the spring models are also seem to diverge significantly with depth, which is considered to be due to lower peak ground acceleration for Alaska record leading to smaller ground displacements, hence lower bending moment for Model B and continuum model.

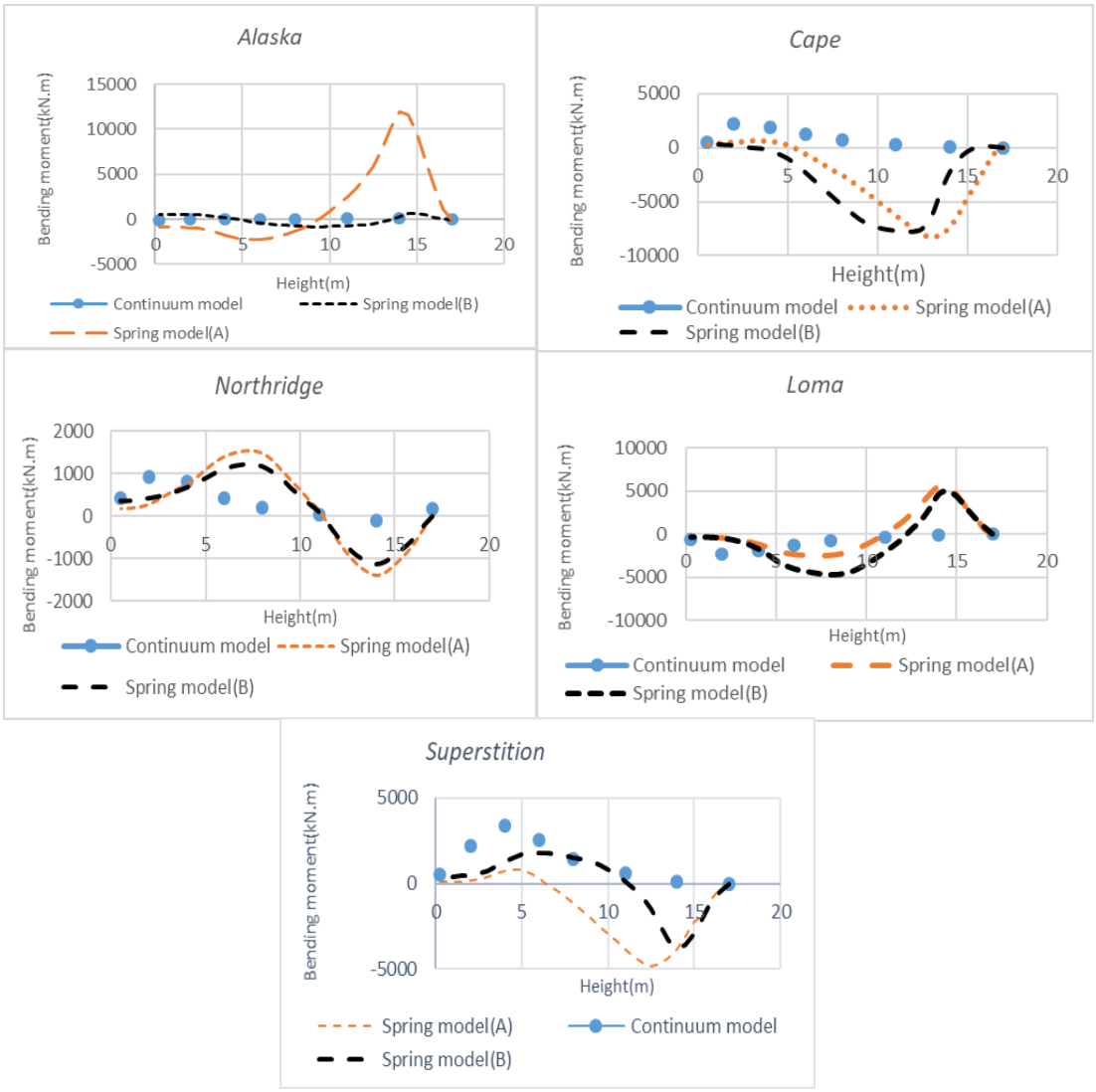

Figure 26: Bending moment graph along with the pile depth when max pile head displacement has happened for five different record motion.

4.1.5.3 Viscous damping force of STMD

Another important factor to be considered for the kind of structures used in this study is the force which is produced at the top of the structure called viscous damping force obtained by the following equation:

$$F = C\,V_r = 2\zeta_{tmd} M_{tmd} \omega_{tmd} V_r \tag{6.11}$$

$$V_r = V_s - V_{tmd} \tag{6.12}$$

where ζ_{tmd}, M_{tmd}, ω_{tmd} are damping ratio, mass, and angular frequency of TMD respectively. V_r represents relative velocity , V_s and V_{tmd} are structure's velocity and TMD's velocity respectively.

The force-time fluctuation during dynamic loading is presented in Figure 27. As previously stated, one of the main advantages of using STMD rather than the TMD is to provide variable viscous parameters during the earthquake. However, the viscous parameters depend on the dynamic attitude of the main structure, hence for some of the records STMD viscous force yields a conservative damping, and it becomes inadequate in the mitigation of oscillations from the earthquake. Although the error is reduced with the adaptation of the spring model B, the spring method in general, lacks in successfully predicting the viscous damping force leading to underestimation or overestimation of the viscous damping force. As a result of this, the STMD parameters are then poorly characterized. It can be stated that, for the models considered, STMD cannot act properly, and even though with the use of the revised p-y equation derived from continuum model (Model B), the continuum model still remains as the only way to obtain soil-pile interaction.

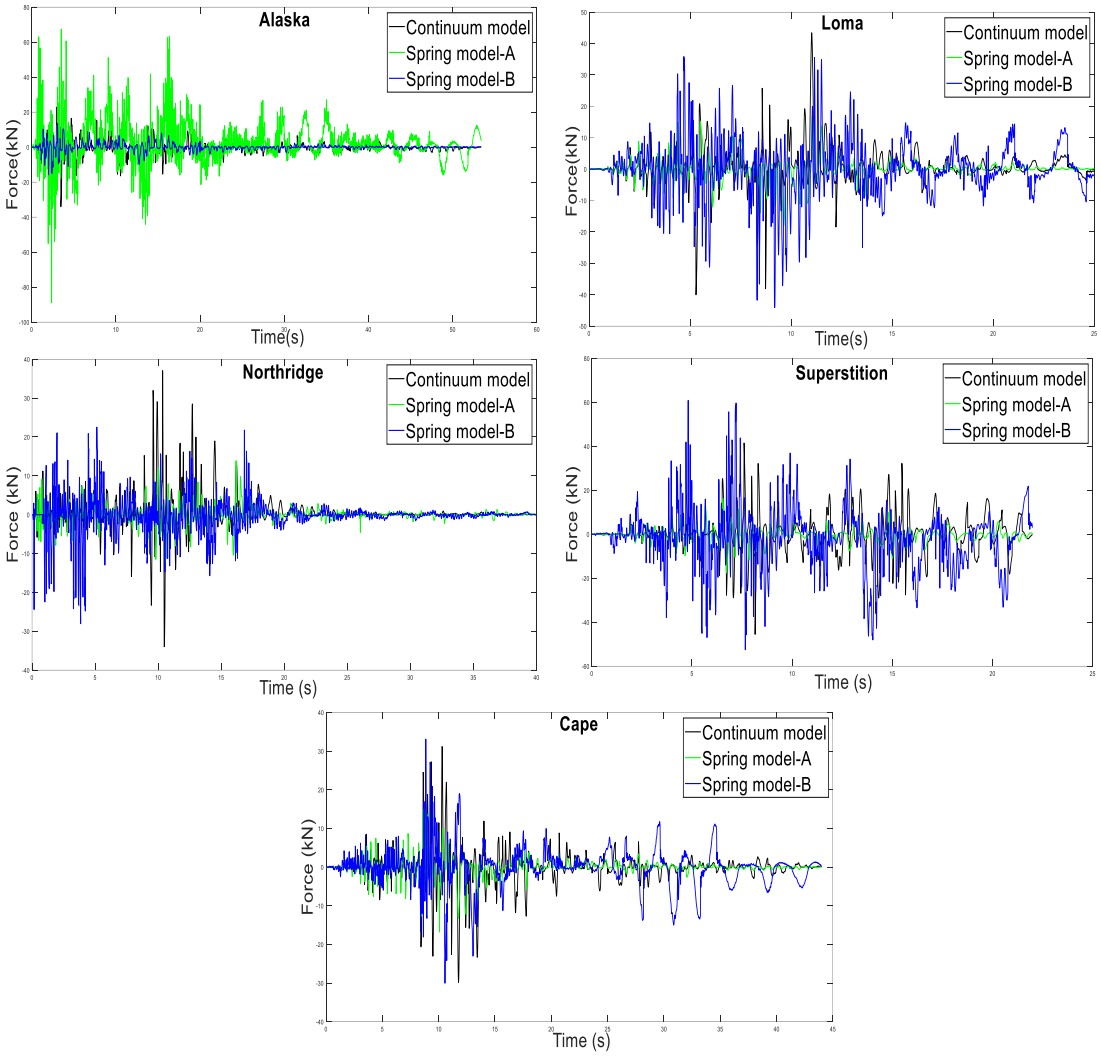

Figure 27: Force time histories in various motion records for continuum model and spring methods (A, B).

4.1.5.4 Top Displacement of structure and lateral force of pile estimation

The displacements obtained on top of the structure, are presented in Figure 28 for both spring models and also for the continuum model. The use of API curves constantly led to estimation of a lower risk level of maximum top floor displacement for most of the records, approximately between 35 to 220 percent. For the analyses performed using Alaska record, spring methods overestimated the maximum displacement by a factor of more than two, on the other hand for Northridge record, there seems to be a similar order of underestimation. This variation in the risk prediction leads to significant

uncertainties in the STMD characterization, which in turn might cause application of additional forces in the analyses, resulting increase in the total cost of the structure. In order to further analyze the results on top floor displacement, so that the whole of the displacement history can be fairly compared, two criteria are defined;

$$j_1 = \frac{peak\ displacement\ (spring\ model)}{peak\ displacement\ (continuum\ model)},$$

which is the maximum absolute displacements, and

$$j_5 = \frac{\text{RMS displacement (spring model)}}{\text{RMS displacement (continuum model)}},$$

which is the Root Mean Square(RMS) ratio of the displacement curves. The results are presented in Figure 29 which indicates that Model B clearly performed better decreasing the level of error between 2% to 58% for criteria j1 and, 15% to 40% in criteria j5 when compared to the Model A results with respect to the continuum model results. It is confirmed once again that the error of prediction in model B is less than model A.

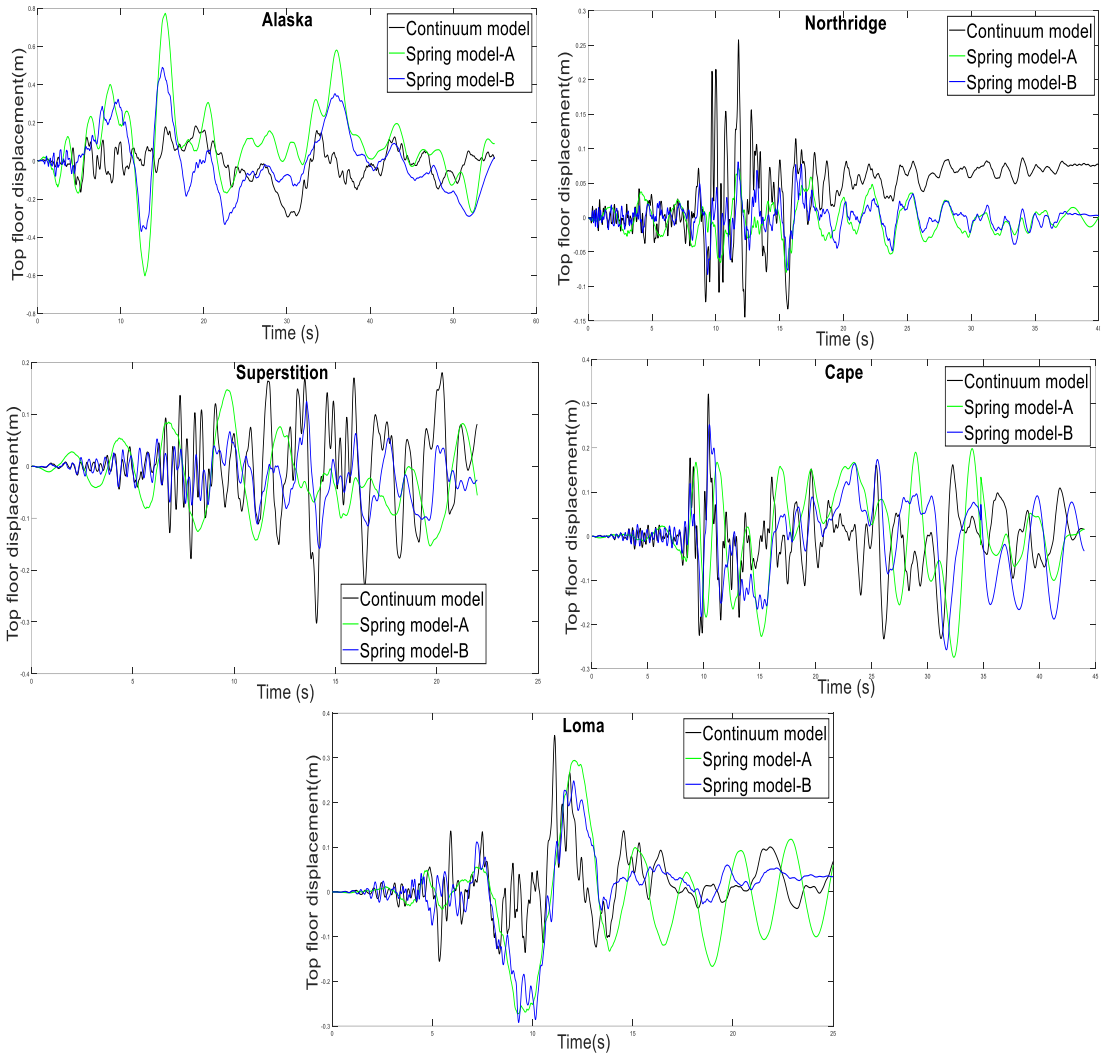

Figure 28: Controlled response of the nominal model for varying earthquake excitation.

The efficiency of Model B against Model A is also demonstrated with the lateral pile load and absolute displacement (top floor displacement and lateral pile displacement) as shown in Figure 30 and Figure 31. The lateral pile load is recorded at a depth of 0.25m from ground level. Figure 30 shows that model B yields a much better prediction on the lateral load at pile head. In addition, Model B also gives a more accurate top floor displacement as shown in Figure 31.

4.1.5.5 Acceleration response of structure

Absolute response acceleration at structure's top floor is another important factor as presented in Figure 32. For spring models it is clearly shown that there is a significant disagreement in the results, however a general trend towards overestimation of acceleration is observed. On the contrary, for Loma record, after approximately 14 seconds the spring methods underestimated the continuum model results, which might be due to the nature of the motion record for this earthquake. Also for more clarity regarding the reliability of p-y spring method, normalized acceleration response spectrum with 5% damping at three location (far-field soil, pile head, top of structure) against three different earthquake motions (far-field and near-field records) are evaluated and compared with the continuum method in Figures 33, 34 and 35. The level of error of acceleration response are increased when the analysis check point changed from soil to pile and then structure (the highest level of error occurred in structure check point), hence it can be said that for STMD structures, inertial interaction between structure and soil are most significant during the earthquake. In this figure, it can be stated that the spring and dashpot method cannot satisfy the proper response of structure especially along the period which is less than one. Remarkably the Spring model A approximately showed a similar performance in this criteria, it means for design of the important structures (such as hospitals), which has more consideration on nonstructural components, the spring method is not a reliable method.

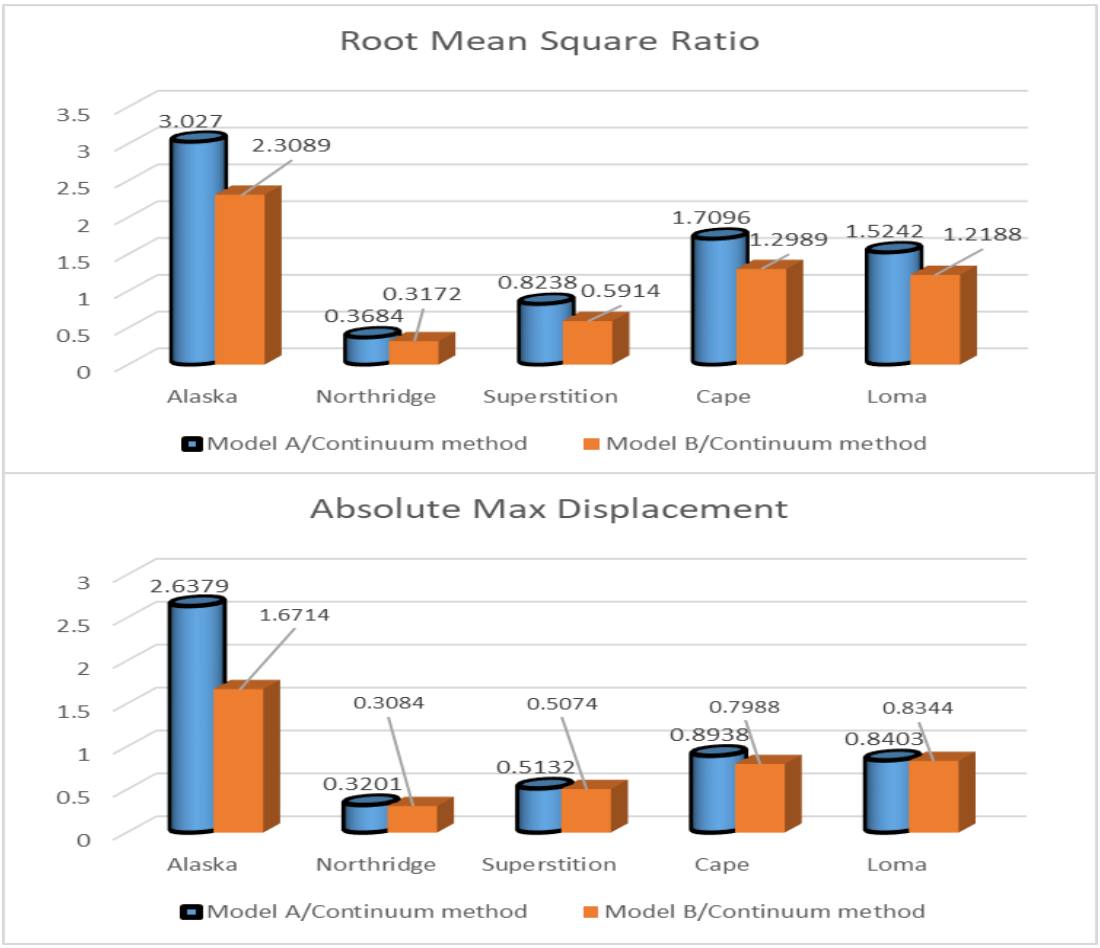

Figure 29: Absolute maximum displacement criteria (j1) and, Root mean square criteria (j2)

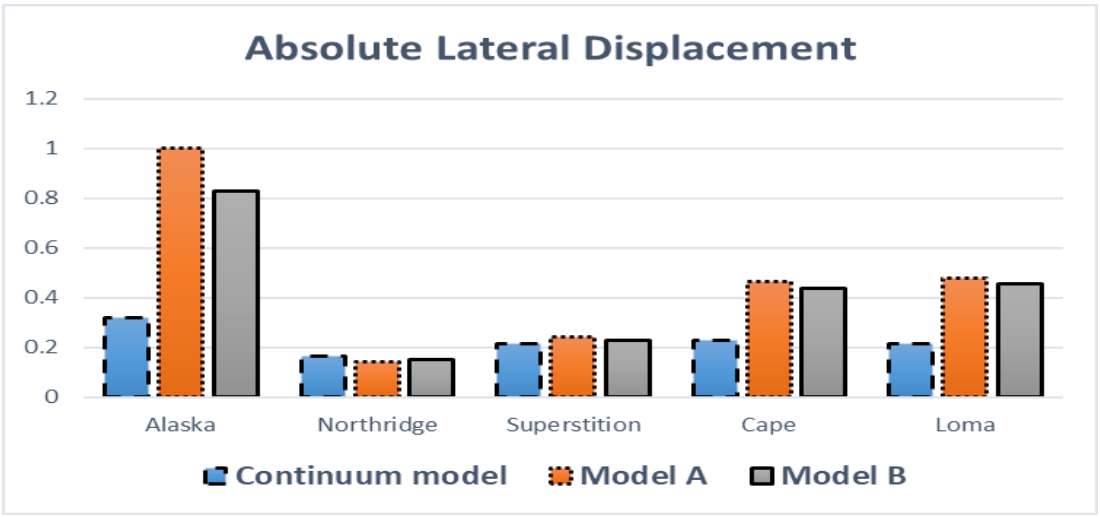

Figure 30: lateral absolute displacement for Model A, Model B and Continuum model.

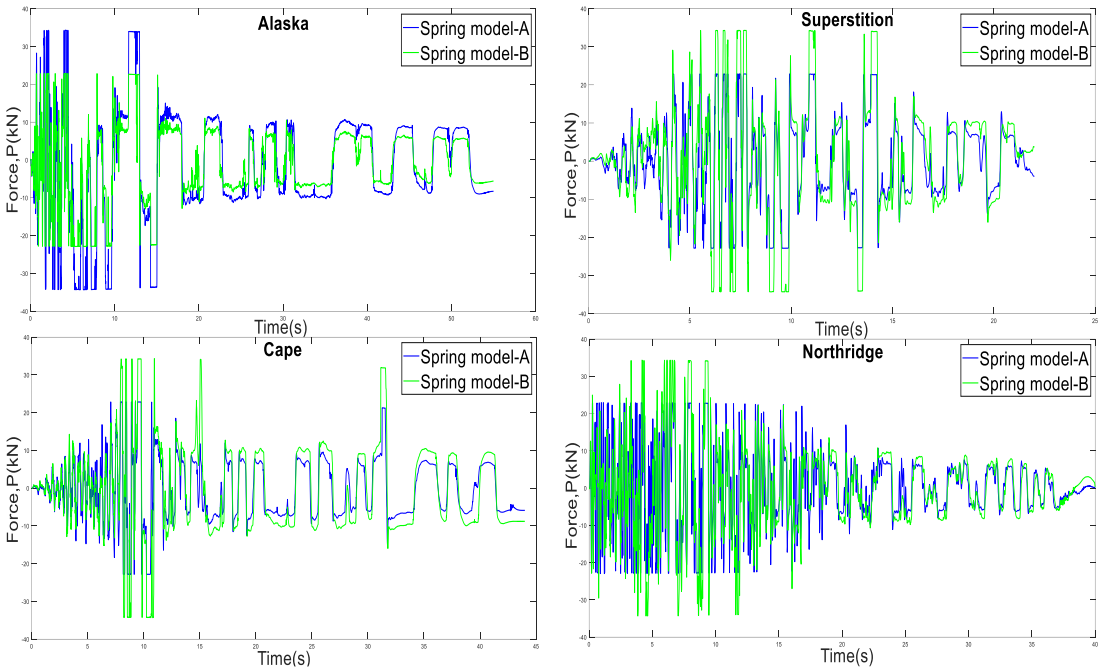

Figure 31: Lateral force time histories for pile's element at depth 0.25 m in spring model A and model B (obtained from continuum model).

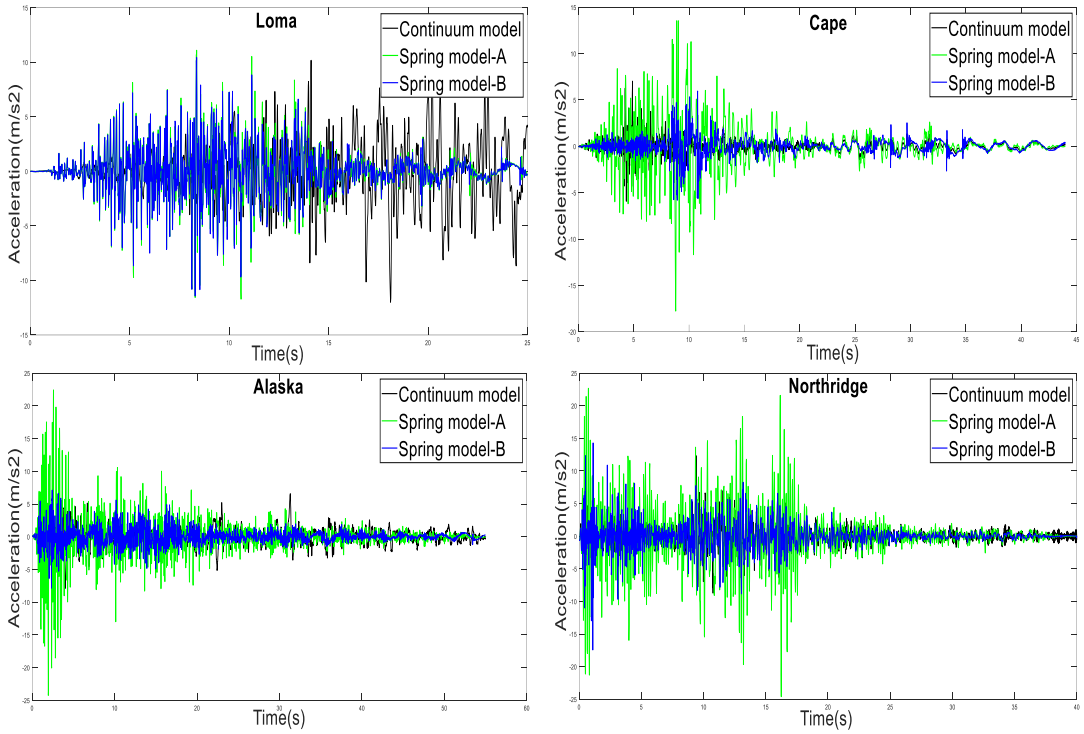

Figure 32: Comparison of absolute acceleration for model A, B and Continuum model effectiveness.

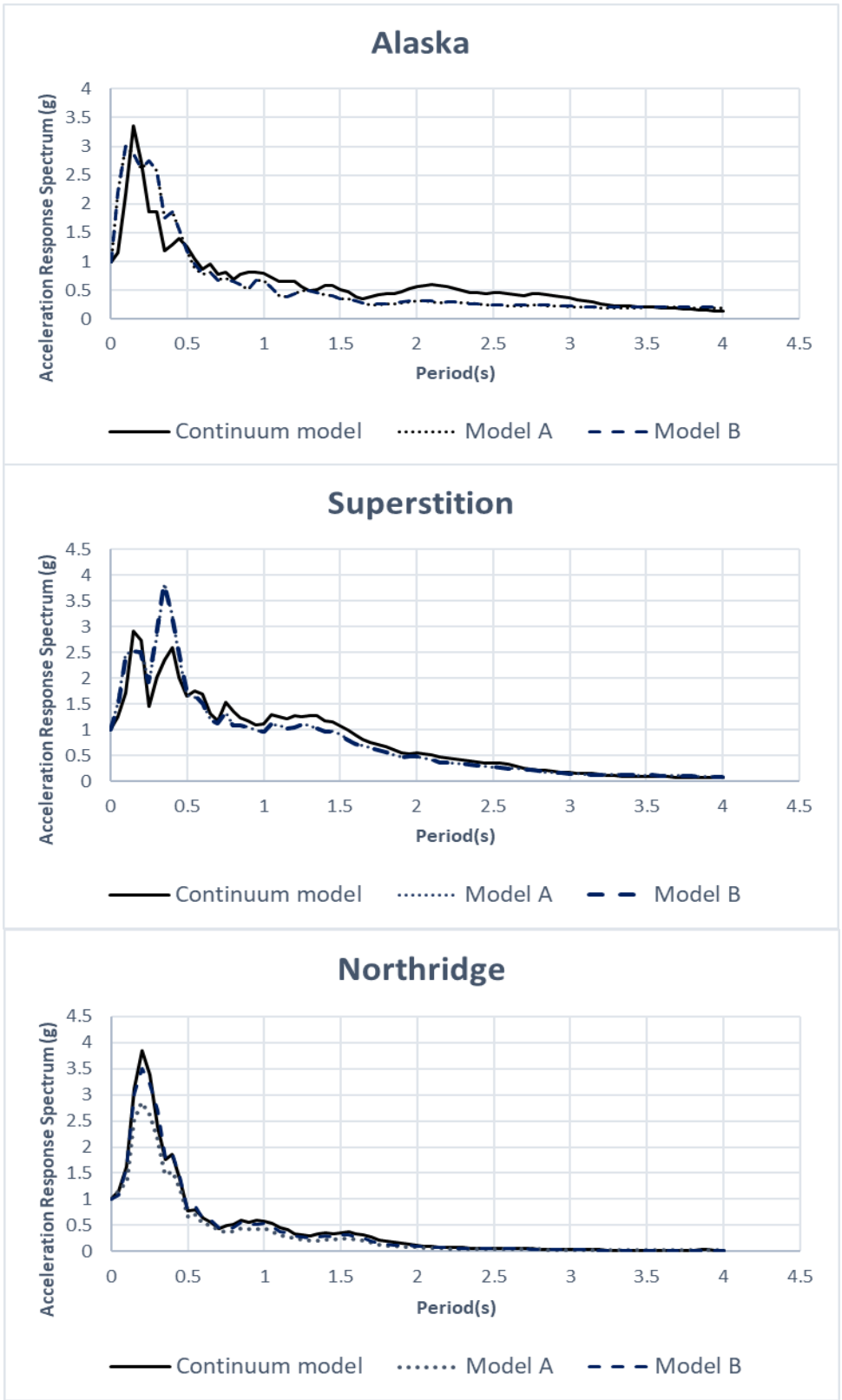

Figure 33: Normalized Acceleration response spectrum of the soil, comparing the Continuum and Spring model A, B

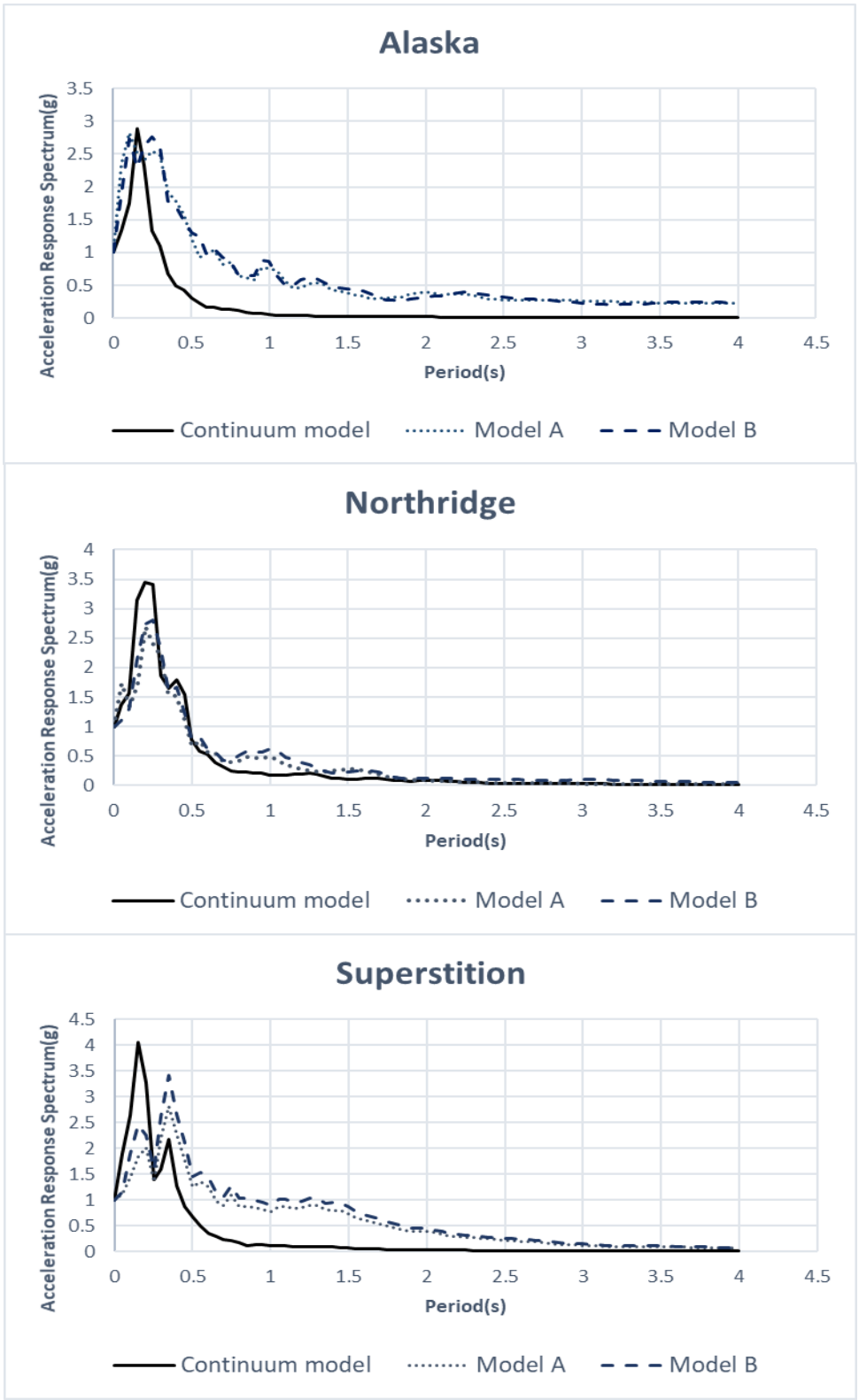

Figure 34: Normalized Acceleration response spectrum of the pile, comparing the Continuum and Spring model A, B

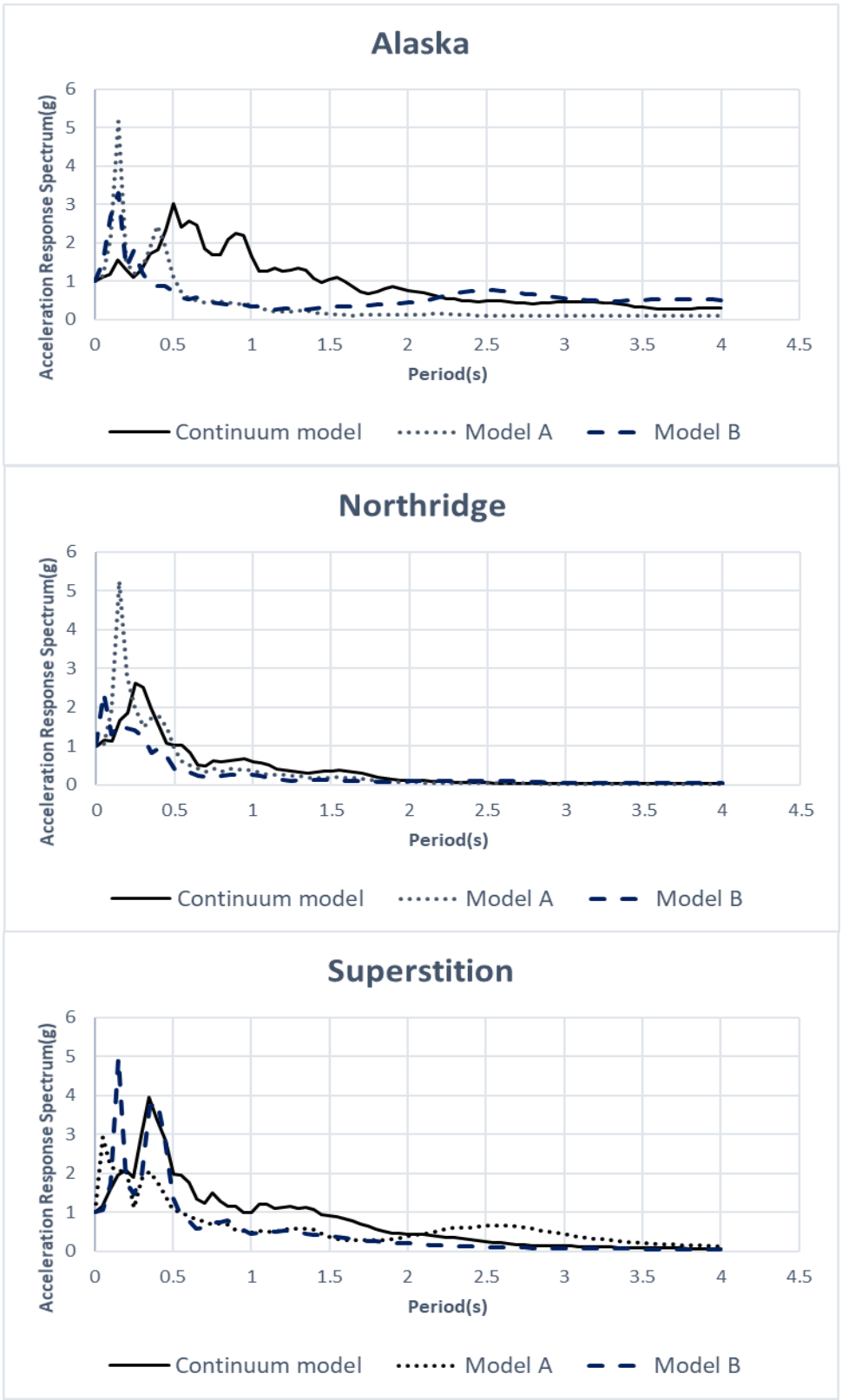

Figure 35: Normalized Acceleration response spectrum of the STMD structure, comparing the Continuum and Spring model A, B

4.2 Dynamic attitude of structure evaluation with STMD and SPSI

In this section, the effect of the SPSI-STMD Interaction (SPSSI) on a midrise steel building under far-field and near-field earthquakes is analyzed and evaluated by using nonlinear time history analysis (i e. the top analysis method for estimation structural response). Three dimensional finite element continuum method is used for simulating the superstructure, soil block, group of piles and STMD damper in one region. A precise assessment of structural performance criteria such as absolute acceleration, inter-storey drift, top displacement and base shear are evaluated. In addition, the effect of STMD on the structure with and without SPSI is also investigated to study the changes in the dynamic attitude of the superstructure.

4.2.1 Case study characterization

In this chapter, 4-storey and 7-storey special moment resisting frames in both direction (X and Y) with four bays in longitudinal and 3 bays in transverse direction (all bays length are identical and equals to 6 meter) were evaluated under seismic record motion with 5% structural damping ratio. The floor-to-floor height of both structures was taken as 3.4m. An example sketch of the 7storey model is presented in Figure 36. The columns and beams properties for both numerical examples are presented in Table 8. Both structures were equipped with STMD to evaluate structural performance criteria defined. Three principle characteristics of STMD design are Tuning ratio, Mass ratio and Damping. The STMD properties used in this study are presented in Table 9.

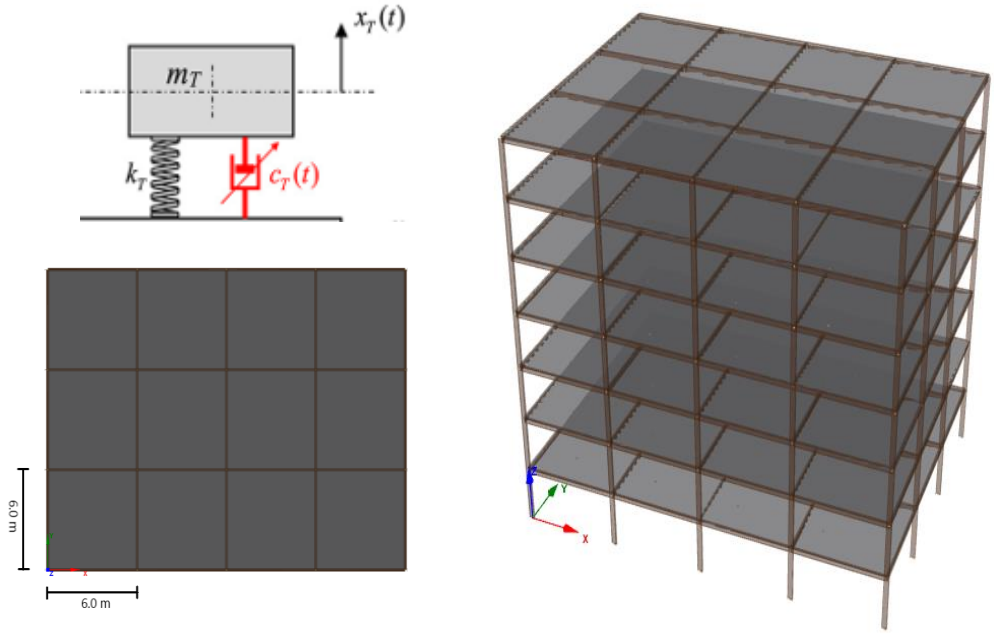

Figure 36: Example schematic of the 7 storey building

Table 8: Properties for structural elements of models used

Model	Column	Beam	Steel
4storey building	BOX400*25,BOX300*20	IPE270,IPE320	St37
7storey building	BOX450*30,BOX400*25,BOX350*20	IPE270,IPE320	St37

Table 9: STMD characterizations used in this study

STMD	Damping ratio, ζ_{STMD}	Mass ratio, μ	Frequency ratio, ω_{STMD}
4storey building	0.03 to 0.14	2%	11.03 rad/s
7storey building	0.02 to 0.18	2%	6.96 rad/s

4.2.2 Structure simulation with continuum method

In this study, all components of the model (soil, piled raft, STMD and structure) were simulated in one region by continuum method as explained before. Open System for Earthquake Engineering Simulation (Open Sees) proposed by McKenna and Fenves [131], is used to perform simulations with finite element method.

4.2.2.1 Soil block simulation

The ground model was comprised of a deep deposit of SAND simulated in three layers with increasing relative density and stiffness with depth, the top layer immediately beneath the foundation raft is a loose SAND underlain by medium dense and dense SAND layers. Drained soil response and elasto-plastic material property was chosen as the material behavior with effective stress dependent mobilization of shear stress. For simulation of behavior under dynamic loading, solid-fluid fully coupled elements were used under undrained condition.

8-node hexahedral linear isoperimetric elements with 4 degrees-of-freedom (DOF), of which three for solid displacements and one for fluid pressure are defined for simulating the soil block in accordance with the Biot's concept of porous medium. First and second runs were carried out as soil consolidation for both elastic and plastic phases of soil block, respectively.

4.2.2.2 Group of piles simulation

A 4 by 5 pile group was embedded in soil block for simulation of foundation behavior. The properties of pile group is presented in Table 3. Three dimensional beam elements were applied to simulate the piles, which are based on displacement formulation with 5 points of integration in accordance with Gauss-Legendre Quadrature formula under dynamic excitation. At the end, at same elevation, the piles node tied up with the corresponding soil node by means of four rigid beam column components for building the pile geometry in the continuum meshing. The schematic continuum method of soil block with piles group is presented in Figure 37.

Table 10: Pile material properties

Piles	Diameter d	Wall thickness t	Length L	cross-sectional area A	Young's Modulus E	Shear Modulus G	torsional moment of inertia J	second moment of area I
Pipe piles	1.2 m	5.0 cm	17 m	78.5 cm^2	27386127.9 N/m^2	10533126.1 N/m^2	0.098125 $kN\text{-}m^2$	0.049 m^4

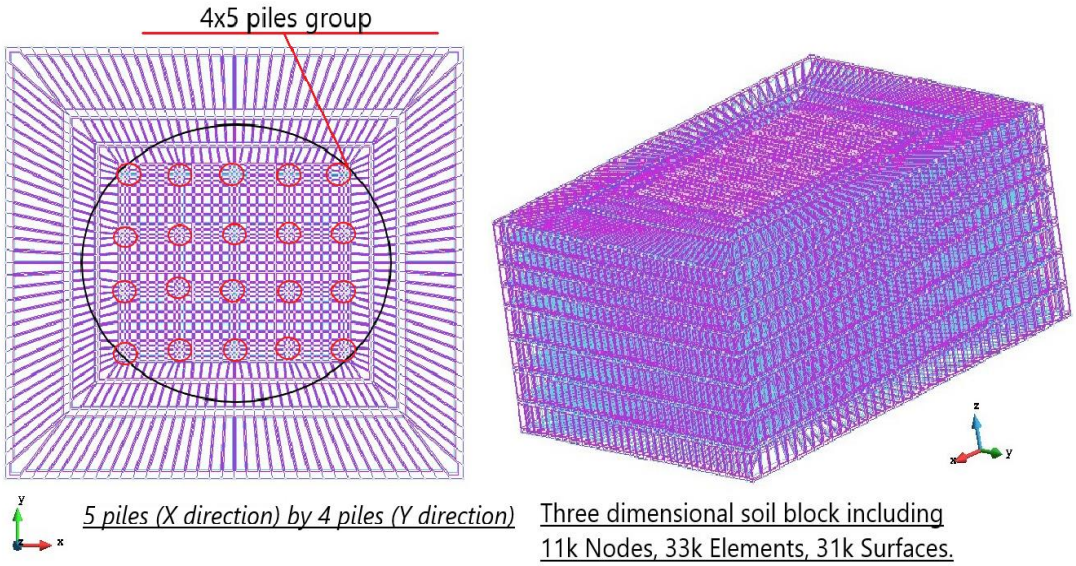

Figure 37: Soil block with embedded pile foundations

4.2.2.3 Cap of piles simulation

In this study, the axial displacement of piles were controlled by a rigid massless cap, hence all the forces associated with the soil-pile interaction were transmitted to the superstructure.

4.2.2.4 Superstructure model

Uniaxial Giuffre-Menegotto-Pinto steel material object with isotropic strain hardening was considered for column and beam materials of the superstructure [140]. In addition, in this method, Newmark time-stepping integrator object was selected for transient analysis and a Krylov Subspace Accelerated Newton Algorithm [136] was used to construct the algorithm related to the nonlinear time history analysis.

4.2.3 Applied record motions

Four acceleration seismic excitations in two categories (Far-field, Near-field) were obtained in two directional form (along X and Y) for running nonlinear time history analysis on defined structures. The general characteristics of the acceleration data, which is comprised of Northridge and Loma as Near-field earthquakes and, Superstition and Cape as Far-field earthquakes are summarized in Table 11 for reference.

Table 11: Record motions characteristics

Earthquake	Station	M	Dur.[s]	PGA[g]	Dominant frequency	situation
Loma Prieta 1989	Gilory array	7.1	25	0.966	2.77 Hz	Near- fault
Superstition hills 1987	Niland-fire station	6.6	22	0.136	3.07 Hz	Far-fault
Northridge 1994	Jansen filter plant	6.69	40	0.932	9.32 Hz	Near- fault
Cape Mendocino 1992	Mendocino	7.01	44	0.154	2.01 Hz	Far-fault

4.2.4 Results and discussion

The results indicate that the dynamic attitude of the structures was in very good correlation with the interaction between the soil-pile-STMD under the effect of the earthquake loading applied. This is clearly reflected in the storey drift, storey displacement, shear force & bending moment (base) and top floor acceleration data. Three scenarios were considered for the analyses;

First, additional damping was applied to the structures using STMD and the effect of this additional instrument on the dynamic response of the building was observed. At this stage, the SPSI was ignored by setting the foundations as a fixed support.

In the second scenario, a deep foundation soil profile was added to the uncontrolled building. Hence, the effect of SPSI on the dynamic attitude of the structure without STMD was investigated.

Finally, controlled building with STMD founded on 20 m depth in three soft soil layers (Table 12) with 17 m length group (4x5) steel pipe piles with 1.2 m diameter were modelled and the results compared for evaluation. To increase the accuracy of the analysis, transition zone 1 (between first and second layer) and transition zone 2 (between second and third layer) are additionally defined with a depth of two meters in the soil block.

Table 12: Soil layers properties

Soil/Properties	**Depth (m)**	**Shear modulus G(MPa)**	**Bulk modulus B(MPa)**	**Friction angle Ø**	**Mass density ρ(t/m³)**
Layer 1-loose sand	6	46.9	125.1	25.4	1.94
Layer 2-medium sand	8	73.7	196.8	30.3	1.99
Layer3-medium to dense	6	111.9	298.3	42.2	2.06

The results are presented for two mid-rise buildings (4 and 7-storey buildings) and all dynamic responses are compared and evaluated according to the above scenarios.

4.2.4.1 Structure response

To better illustrate the acceleration history in the soil layers, first the maximum acceleration and Root Mean Square (RMS) criterion at five locations (pile tip node, transition zone 2, transition zone 1, pile head and superstructure base node) are shown in Figure 38 (a and b) for a 7-story and 4-story building with/without STMD, respectively. As can be seen in this figure, two acceleration criteria (Max and RMS)

jumped between the transition zone 1 and the pile head in both buildings with/without STMD for all record motions, while at other locations the acceleration response increased uniformly. Consequently, the first layer where loose sand is defined as a soil block has a greater effect on the acceleration response of the structure. Considering the buildings with and without STMD, it can be concluded that although the use of STMD slightly decreases the maximum acceleration response in the first layer and the base of the structure, it does not further weaken the criterion of acceleration response in soil block, but also increases the effective acceleration value (RMS) near the ground on the structure.

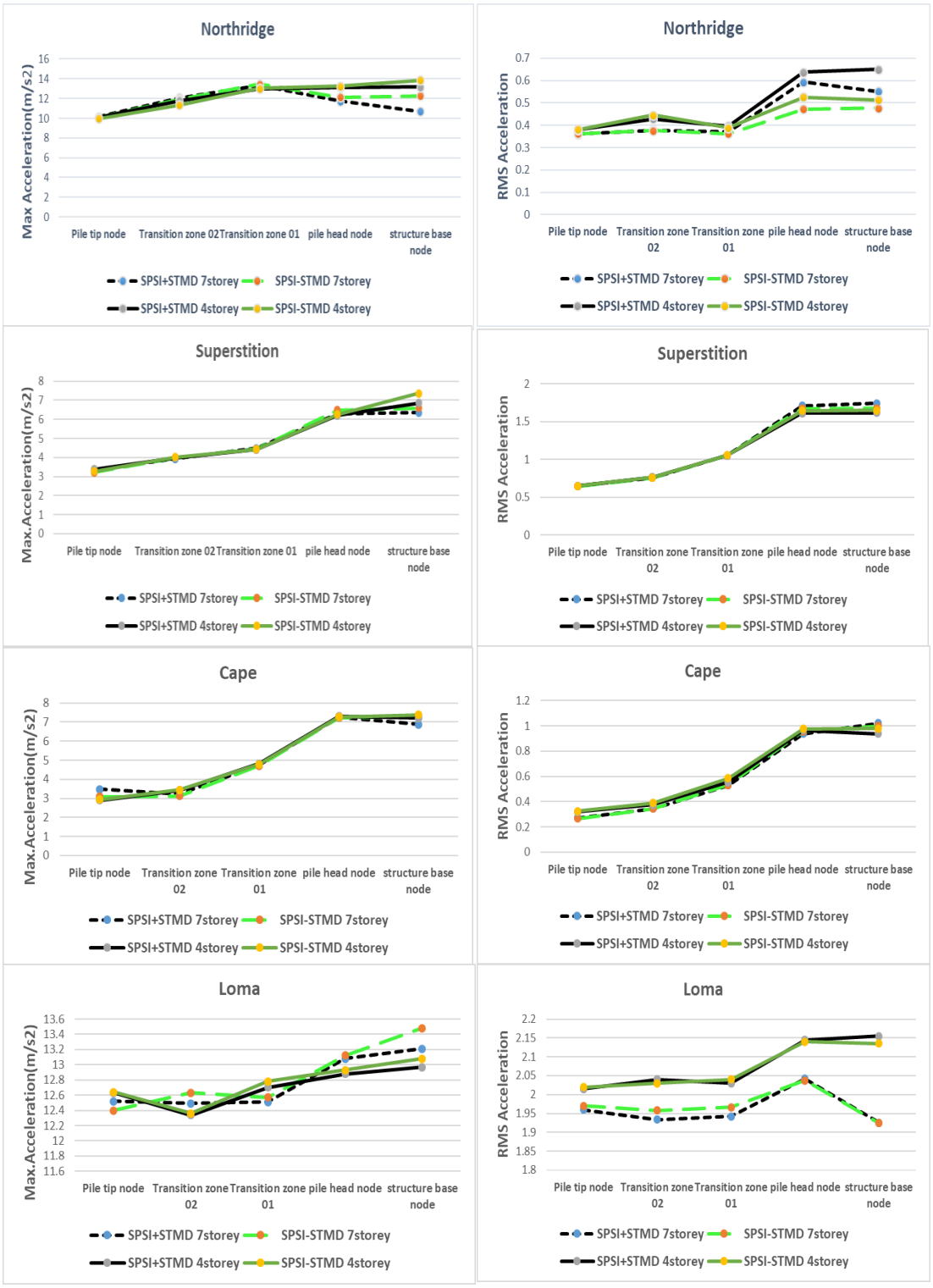

(a) (b)

Figure 38: Maximum Acceleration response (a) and RMS acceleration response (b) at five locations in soil block.

4.2.4.2 Superstructure responses

Figure 39 illustrated the Bending moment criteria on the base element of a 7-storey building with and without consideration of the STMD and SPSI under Northridge, Superstition, Cape, and Loma earthquake record motions. In all figures, the response of four cases including bare structure, structure with STMD without SPSI (fixed base controlled structure), structure with SPSI without STMD (piled raft foundation structure), and structure with STMD and SPSI (piled raft foundation controlled structure) are indicated as S, S+S, S+S-S, and S+S+S, respectively.

From Figure 39, it can be seen that when piled foundation were neglected, STMD mitigated the building bending moment criteria for the Northridge, Superstition, Cape, and Loma earthquakes by 42%, 31%, 17%, and 16%, respectively. Therefore, it can be concluded that, without SPSI, STMD had performed reasonably well in terms of bending moment reduction.

In the second case, the SPSI was added to the uncontrolled structure, therefore in this case the pile foundations were connected to the base of the uncontrolled structure. As shown in Figure 39, SPSI resulted in an increase in bending moment in the range of 59%, 160%, 65% and 50% for Northridge, Superstition, Cape and Loma earthquakes, respectively. Therefore, it can be said that SPSI had a great influence on the bending moment response of the structure.

As a third case, the STMD added to the structure by considering the SPSI. The controlled structure with STMD on a piled foundation was analyzed under seismic vibration. Figure 39 shows that structure with STMD decreased the bending moment response by about 25%, 23%, 16%, and 42% for Northridge, Superstition, Cape, and

Loma, respectively. Although STMD could greatly reduce the bending moment response while the SPSI was considered, the bending moment criteria for Northridge, Superstition, Cape, and Loma earthquakes were increased by 19%, 98%, 44%, and 6%, respectively, compared to the bare structure.

Therefore, STMD can partially cover the destructive effects of SPSI when both effects act simultaneously on the structure. That is, although the consideration of SPSI leads to a significant improvement in the bending moment response of an uncontrolled structure, the application of STMD to the structure can reduce the magnitude of the intensification. The use of STMD in any situation helps the structural behavior to mitigate the seismic vibration and has no adverse effect on the bending moment response of the structure.

The bending moment curve for a 4-storey building is shown in Figure 40. The time history of the bending moment response of the base element of the structure is shown under four separate record motions. It can be seen that STMD, without SPSI, reduced the bending moment response by 35%, 11%, 17% and 12% in comparison to the uncontrolled fixed structure for Northridge, Superstition, Loma and Cape respectively. By neglecting the pile foundations, STMD appropriately reduced the bending moment response of the structure.

In addition, STMD was able to reduce the response by 10%, 11%, 5%, and 26% when SPSI was included. Hence, the structure equipped with STMD and SPSI behaved poorly in mitigation of the bending moment response for all earthquakes. The bending moment in the structure with SPSI and without STMD increased by 42%, 65%, 82% and 73% for Northridge, Superstition, Loma and Cape earthquakes respectively. In

summary, the inclusion of STMD and SPSI increased the bending moment response by 28%, 47%, 73% and 27% in the Northridge, Superstition, Loma and Cape earthquakes, respectively.

When the responses of 4-storey and 7-storey buildings are compared, it can be seen that the bending moment response for 4-storey buildings was increased more with the inclusion of SPSI, and STMD were more effective in reducing the bending moment response with respect to the 7-storey buildings.

Time histories of the acceleration response are shown in Figure 41 for the top node of the 7-storey building under four record motions. It can be seen that when the pile foundation and soil flexibility are included, in the model without STMD, the induced seismic acceleration at the uppermost node of the structure increased sharply by 282%, 231%, 194%, and 259% for the Northridge, Superstition, Loma, and Cape earthquakes, respectively.

With STMD and SPSI, the acceleration response was increased to 189%, 190%, 175% and 172% for different earthquakes. In addition, the STMD reduced the acceleration response by only 8%, 6%, 7%, and 11% for the Northridge, Superstition, Loma, and Cape earthquakes, respectively.

Without SPSI, the STMD reduced the response by 13%, 39%, 27% and 28% compared to a fixed uncontrolled structure. Therefore, the effect of STMD in controlling the building against lateral vibration was poor in terms of peak acceleration.

In Figure 42, the acceleration time history at the top of the 4-storey building during different earthquakes is illustrated. As shown in Figure 42, STMD reduced the acceleration response by 20%, 28%, 28%, 0.13% for Northridge, Superstition, Loma and Cape earthquakes compared to the fixed bare structure when SPSI was ignored. Inclusion of SPSI, reduced STMD efficiency by 19%, 24%, 16% and 17% compared to the uncontrolled structure.

The inclusion of SPSI in the 4-storey uncontrolled building resulted in a huge increase in acceleration response by 197%, 155%, 98%, and 144%, and the inclusion of both STMD and SPSI changed the level of increase to 139%, 92%, 43%, and 109% for the Northridge, Superstition, Loma, and Cape earthquakes, respectively.

When summarising Figures 41 and 42, it is worth noting that the STMD efficiency was decreased with increasing number of storeys when SPSI was included. STMD could mitigate the acceleration response of a 4-storey building slightly better than a 7-storey building for all record motions.

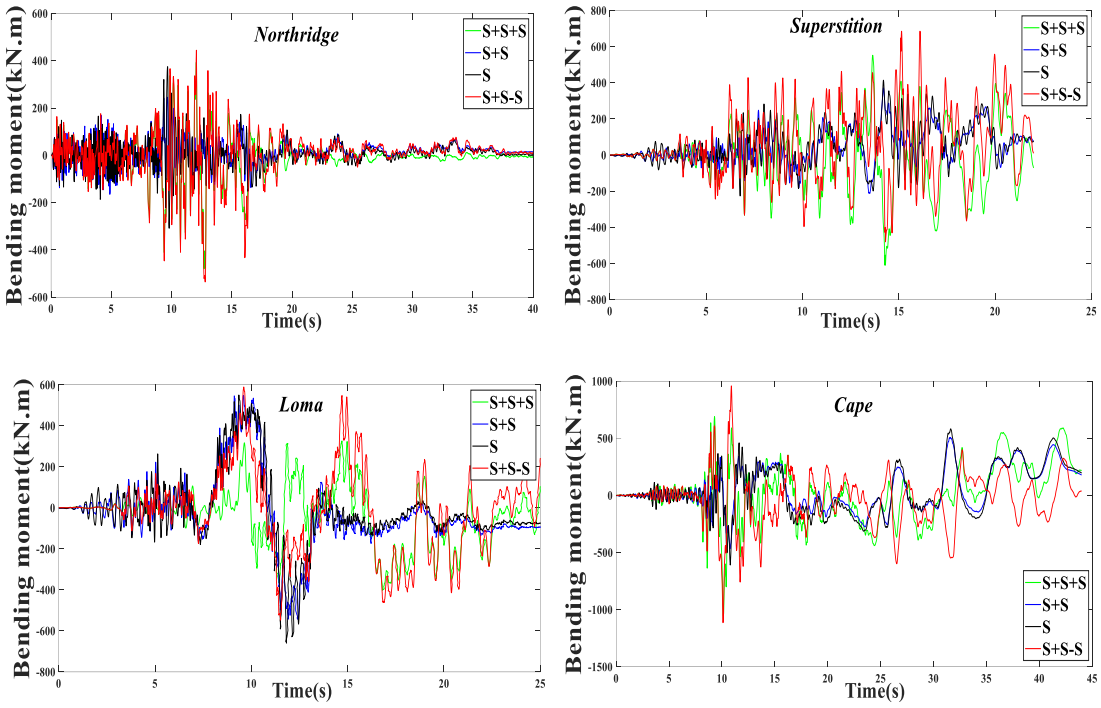

Figure 39: Bending moment response time histories of the 7storey building with respect to the near-field and far-field record motion

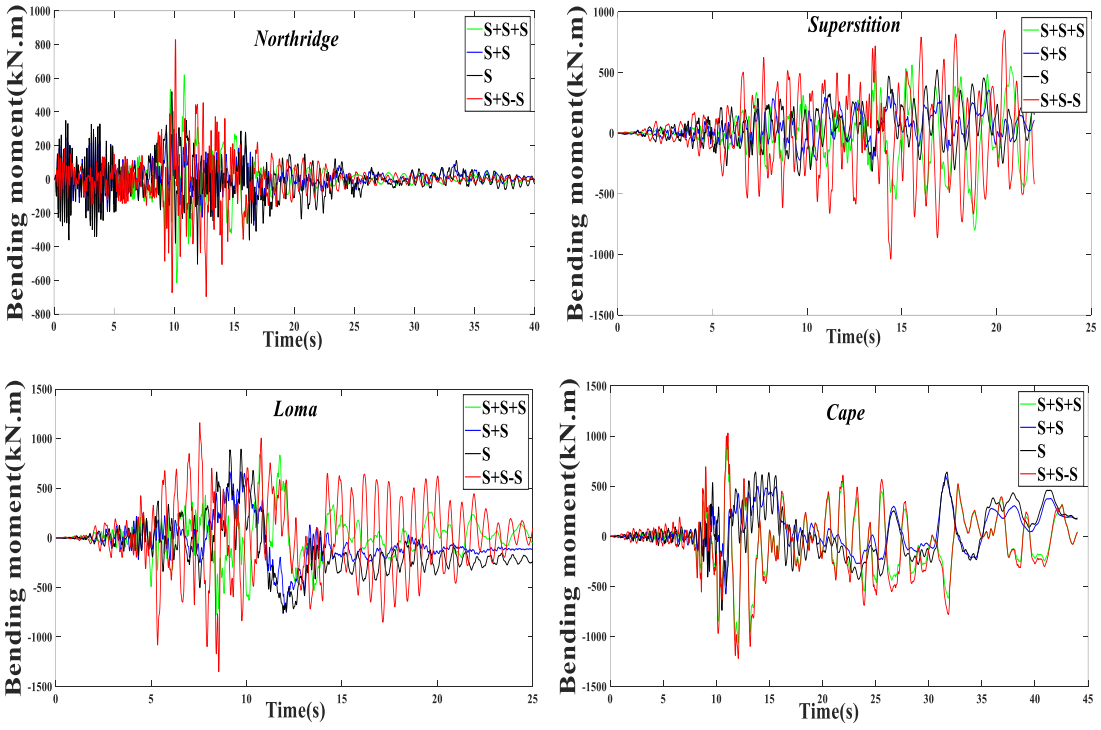

Figure 40: Bending moment response time histories of the 4storey building with respect to the near-field and far-field record motion

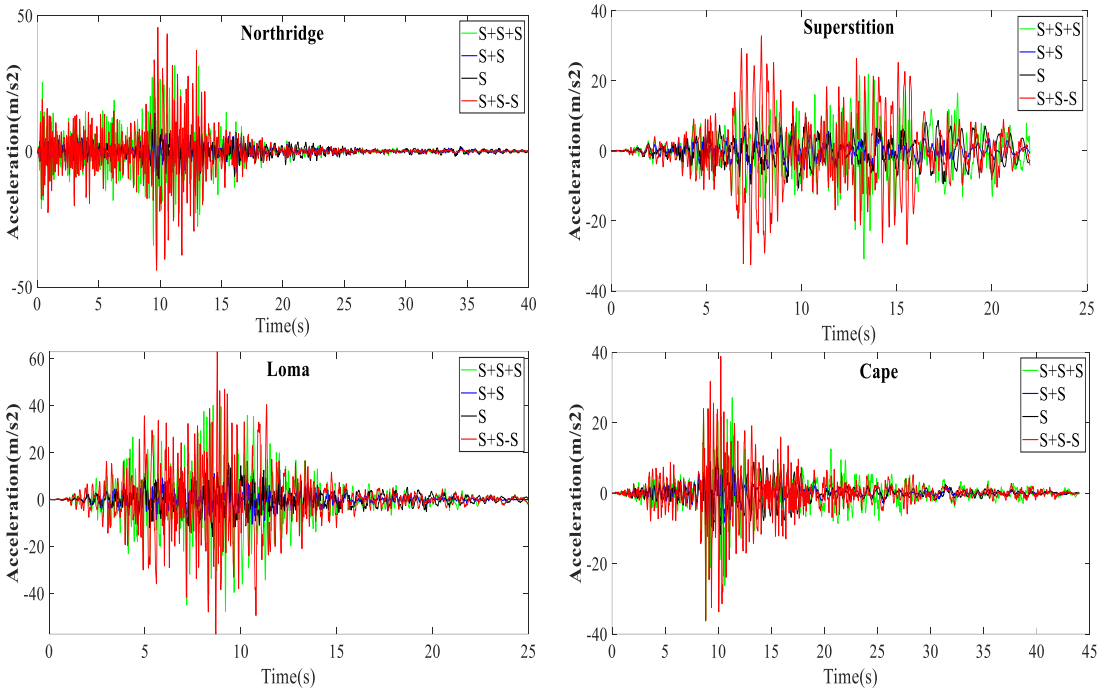

Figure 41: Acceleration response time histories of the top of the 7storey building with respect to the near-field and far-field record motion.

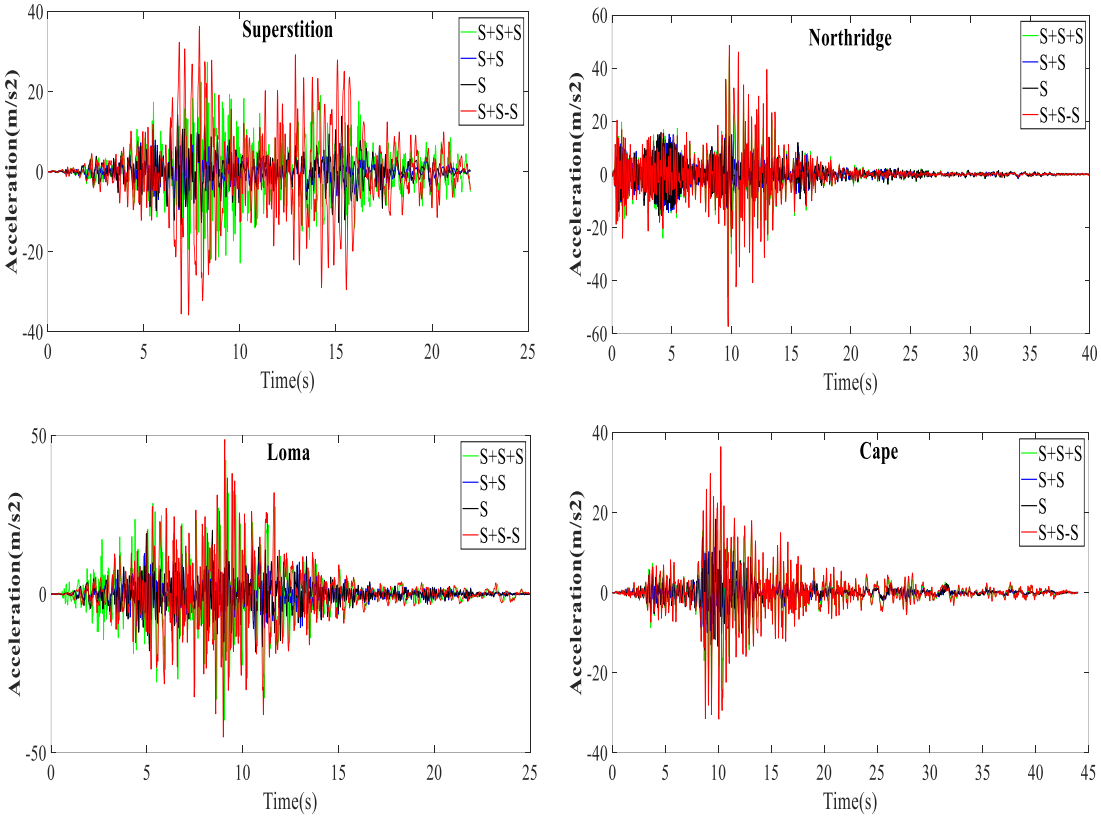

Figure 42: Acceleration response time histories of the top of the 4storey building with respect to the near-field and far-field record motion.

The other important parameter for the assessment of the effect of SPSI and STMD is the shear force response through the stories of the building. The shear force at the base node of each storey is shown in Figures 43 and 44 for 7 and 4 story buildings respectively. It is shown that the STMD on a building without SPSI could reduce the shear force at the base by 17%, 14%, 6%, and 9% for a 7-story building and 6%, 4%, 2%, and 33% for a 4-story building compared to an uncontrolled structure with a fixed base for the Northridge, Superstition, Loma, and Cape earthquakes, respectively. By including SPSI and STMD on buildings, these reduction percentages became 52%, 38%, 25%, and 50% for 7-story buildings and 34%, 6%, 14%, and 32% for 4-story buildings compared to the uncontrolled fixed base structure for the Northridge, Superstition, Loma, and Cape earthquakes, respectively. The results indicated that the soil stiffness reduces the shear force significantly.

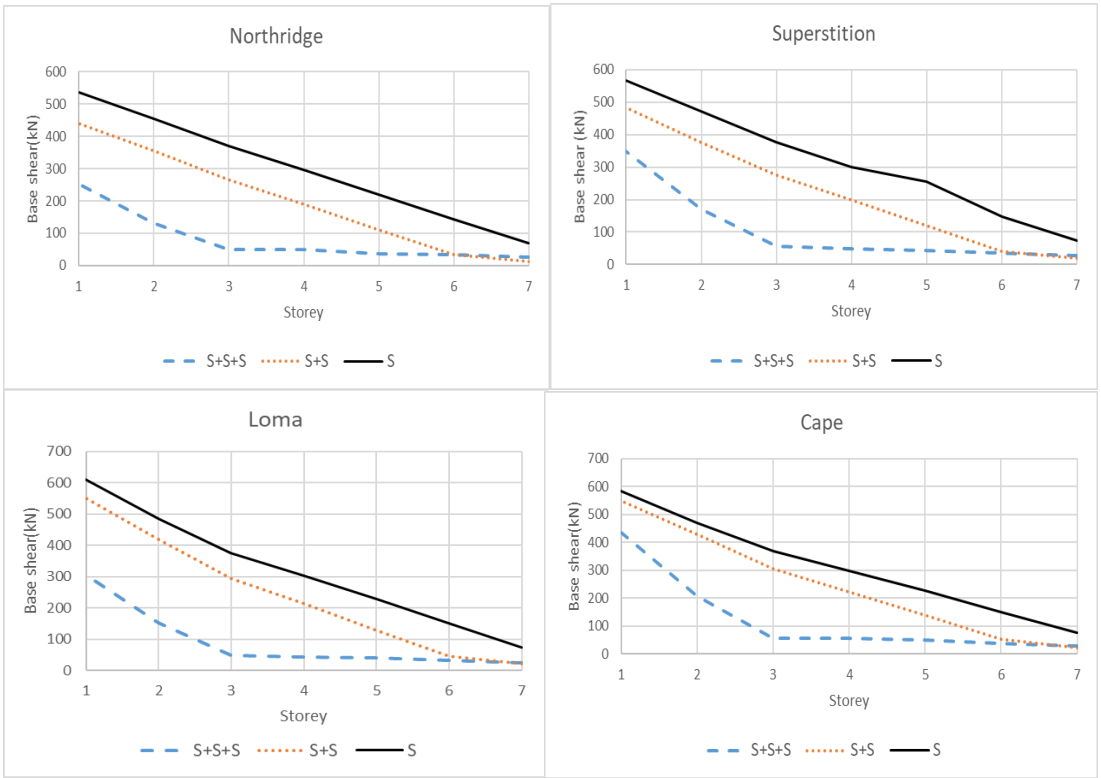

Figure 43: Shear force element response of the columns at the 7storey building.

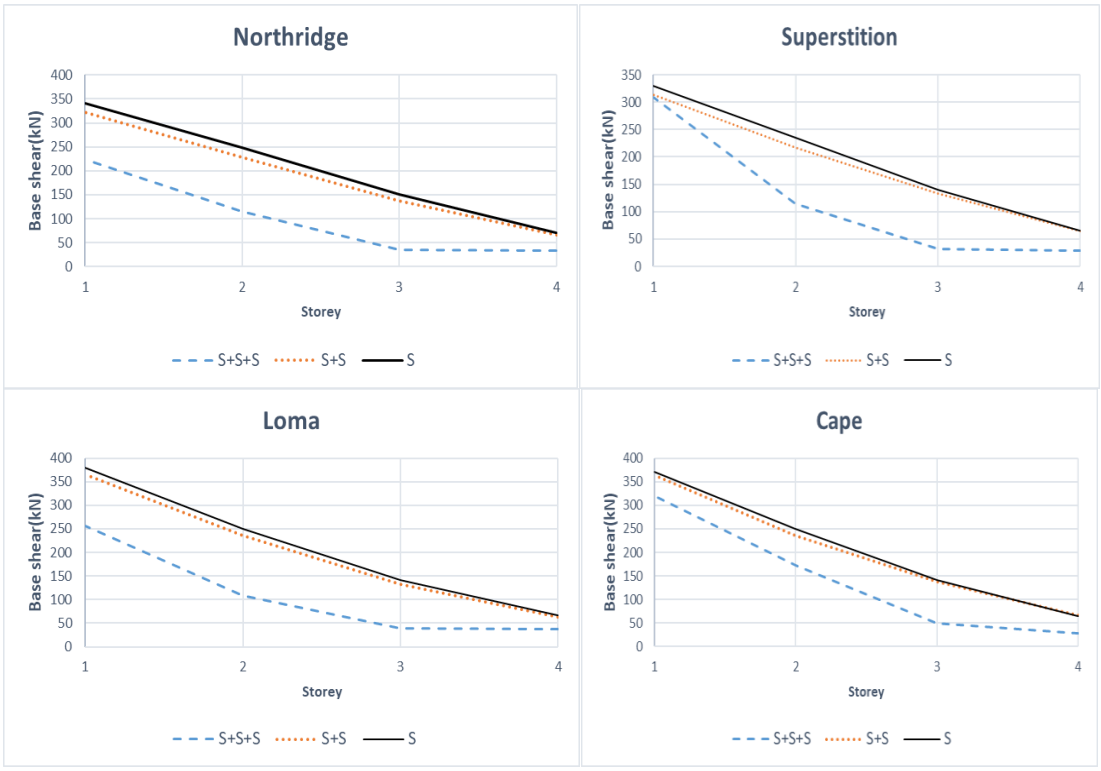

Figure 44: Shear force element response of the columns at the 4storey building.

Absolute structural displacement are shown in Figure 45 and 46 for 7- and 4-storey buildings, respectively, for each individual earthquakes. STMD reduces the building displacement in all cases, but the reduction is larger in the top floors of both buildings, while the percentages reduction are 28%, 15%, 22%, and 38% for the 7-storey building and 51%, 21%, 1.5%, and 14% for the 4-storey building for Northridge, Superstition, Loma, and Cape earthquakes, respectively. The result shows that the STMD efficiency is acceptable in both buildings. Although the STMD properly reduces the storey displacement, when both effects (STMD and SPSI) are taken into account, the storey displacement increased greatly especially for 4-storey building. The percentages are 411%, 192%, 173% and 130% related to the 7-storey building and also 382%, 529%, 247% and 251% growth in the 4-storey building for Northridge, Superstition, Loma

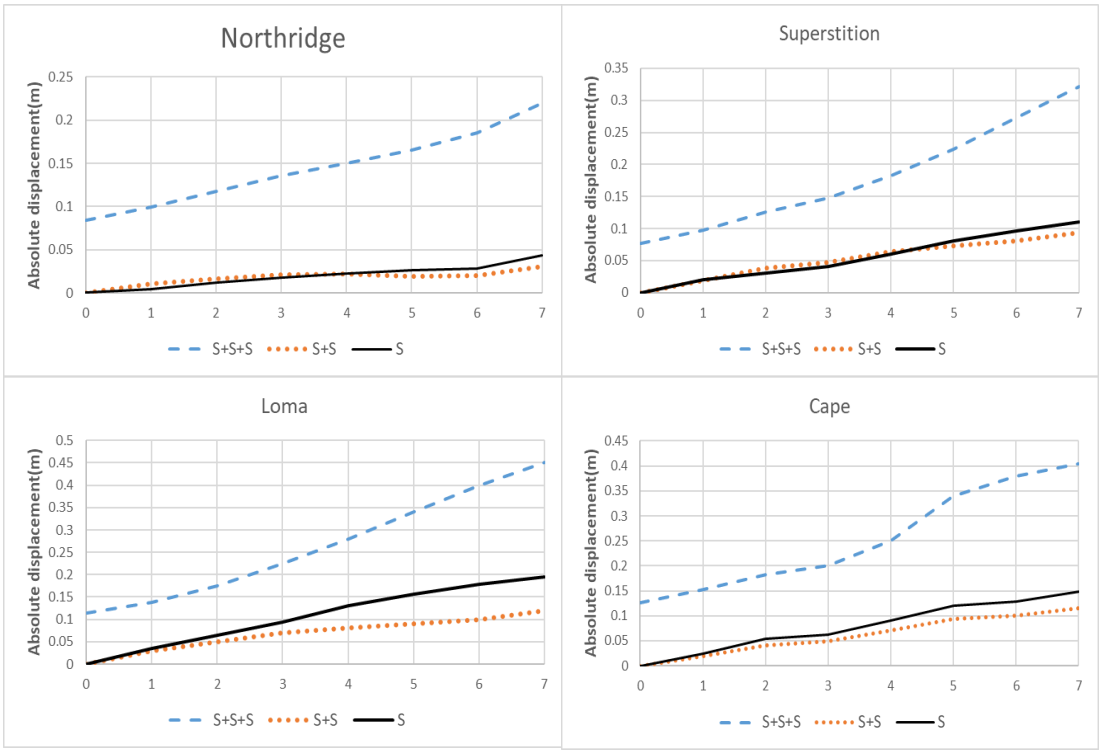

Figure 45: Storey absolute displacement for 7storey building.

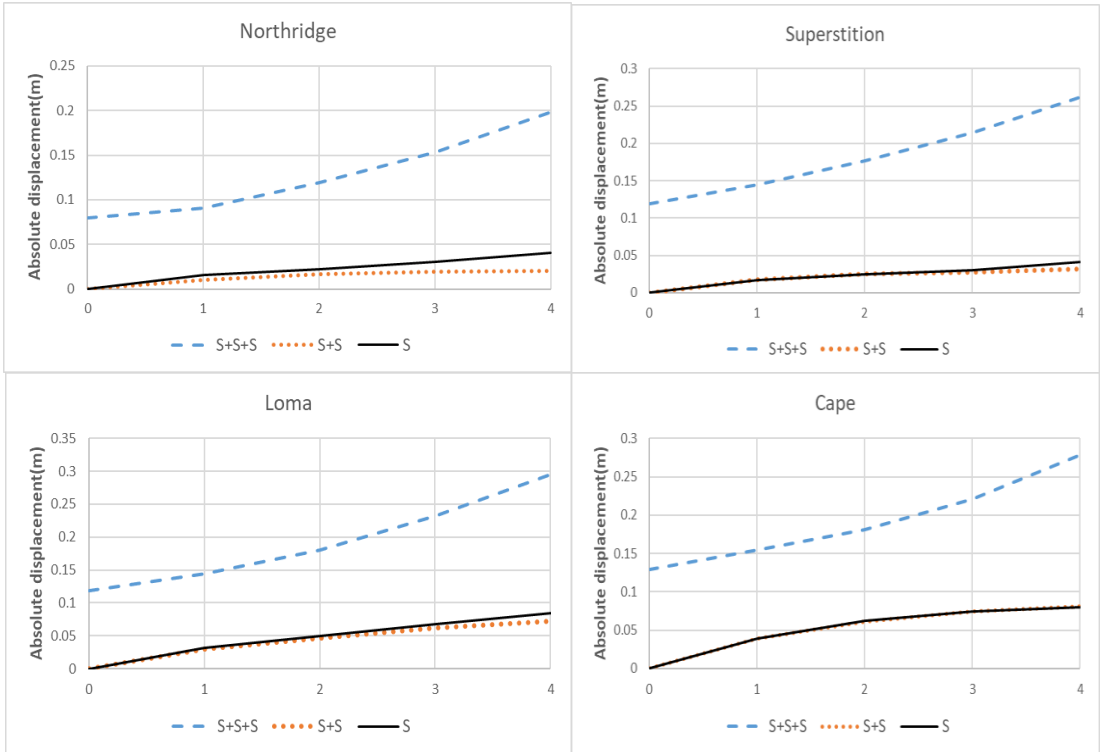

Figure 46: Storey absolute displacement for 4storey building.

and Cape earthquakes respectively. Moreover, the figure shows that the growth of structural displacement increased continuously from the base to the top of the structure when STMD and SPSI acted together.

In addition, Figure 47 for a 7-storey building and Figure 48 for a 4-storey building show the relative building displacements. With respect to the fixed base for the cases without SPSI, the building displacement at the ground level must be zero so that the relative lateral displacement is effective enough to show the changes in the storey displacement. The result shows that the simultaneous effect of STMD and SPSI on the structure can increase the top floor displacement by 216%, 122%, 88% and 72% for a 7-storey building and 189%, 243%, 86% and 109% for a 4-storey building in the Northridge, Superstition, Loma and Cape earthquakes, respectively. Therefore, the storey displacement target increases greatly when both effects are applied to the structure.

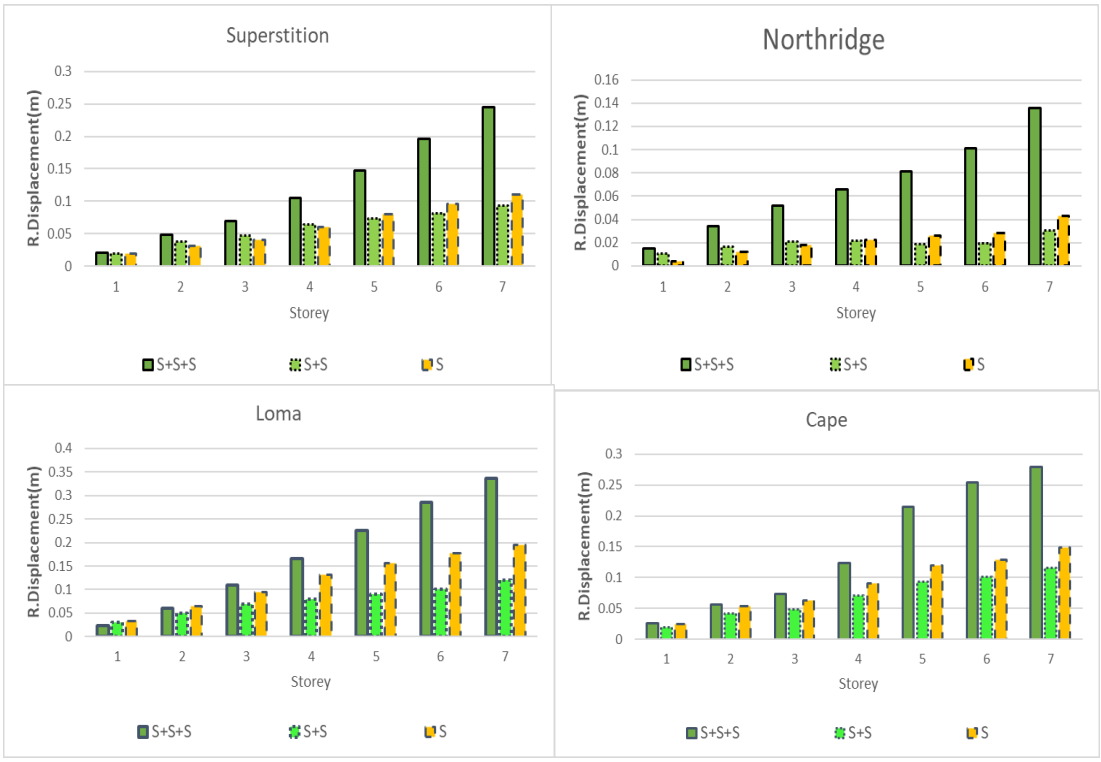

Figure 47: Relative lateral displacement for 7storey building.

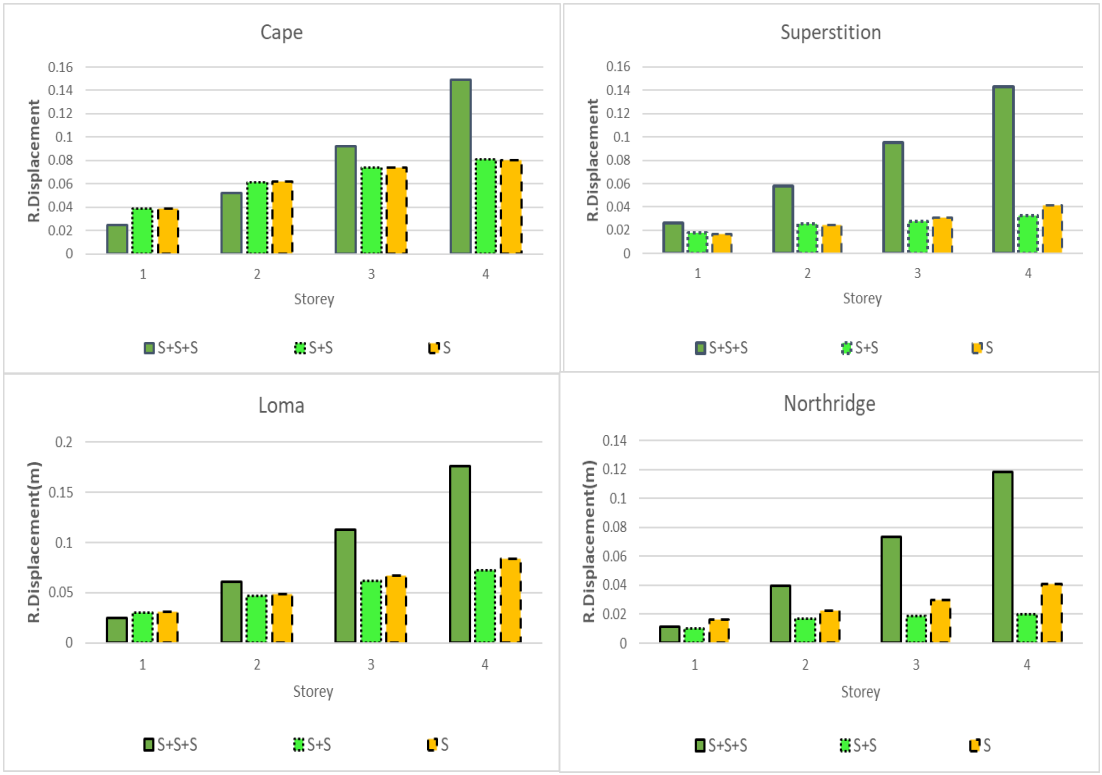

Figure 48: Relative lateral displacement for 4storey building.

Figures 49 and 50 presented the variations in story drift for a 7-story building and a 4-story building separately for the Northridge, Superstition, Loma, and Cape earthquakes. It can be seen that by including the SPSI, the drift ratio in the upper floors of the buildings is increased for all earthquakes, while the higher intensity for the Superstition and Loma records occurs mainly for the 4-story buildings. Moreover, it is observed that by equipping the buildings with STMD, the story drift ratio is reduced in all the stories as compared to the uncontrolled fixed base structure, but the percentage reduction is greater in the upper stories.

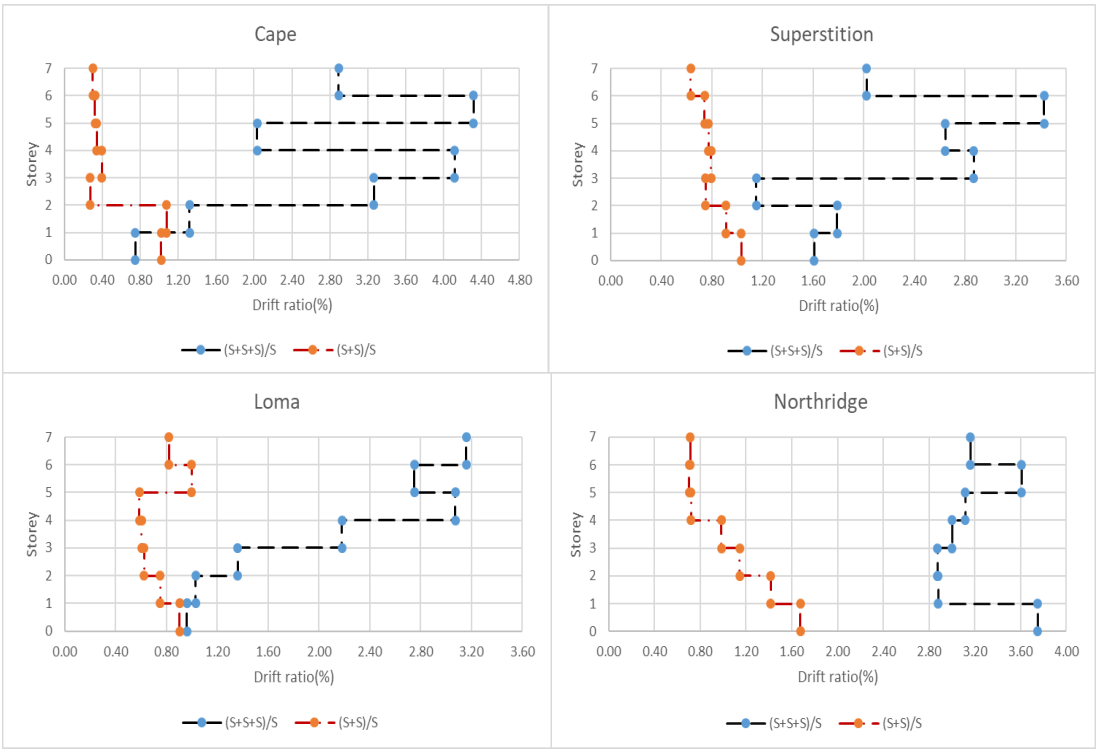

Figure 49: Maximum Storey-Drift ratio for 7storey building.

It can also be observed that the STMD efficiency is reduced by considering the SPSI effect in all records. For example, although the controlled structure reduced the drift

at the top floor to 63% of the uncontrolled structure in the Northridge earthquake, this ratio increased more than 2.0 when the SPSI effect is considered.

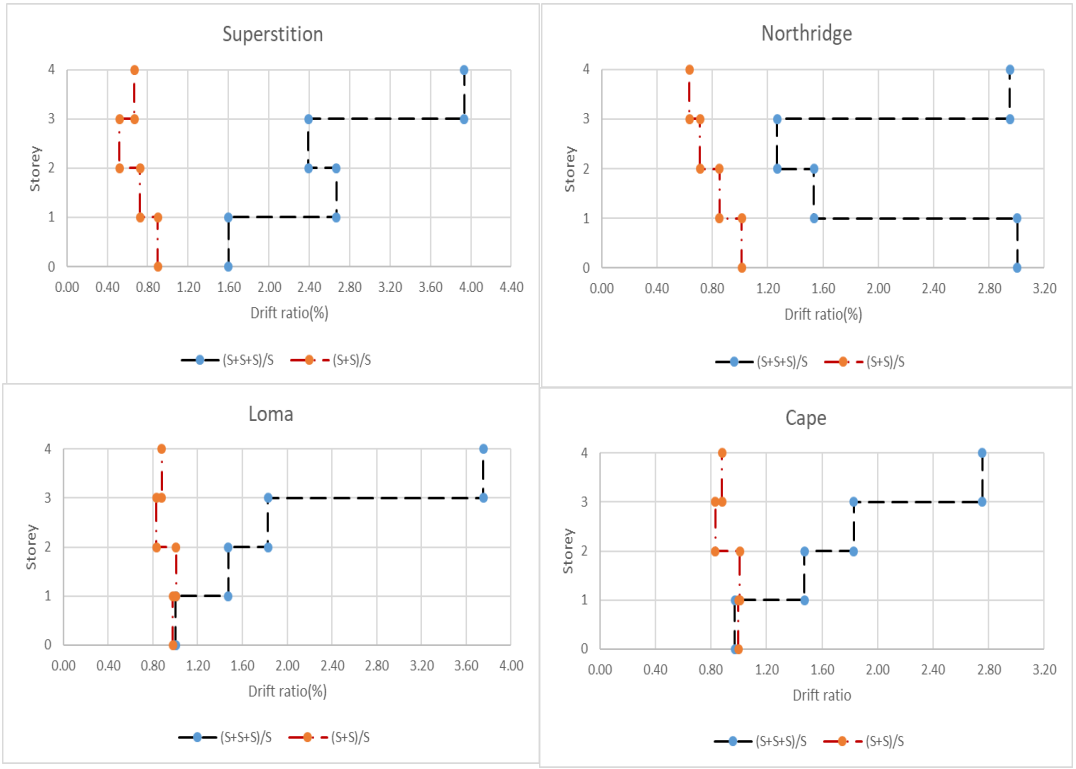

Figure 50: Maximum Storey-Drift ratio for 4storey building.

4.3 STMD performance evaluation by using substructure method

In this section, using the enhanced p-y curve which has been investigated in previous section, the efficiency of STMD with different mass ratios is evaluated and the optimal one is proposed to maintain the high performance of STMD on mid-rise buildings founded on pile foundation. the effectiveness of STMD and TMD with and without soil-pile-structure interaction is examined first and the outcome is evaluated.

In the second stage, the midrise structures fitted with STMD based on deep foundation simulated and Displacement-Driven on-off Ground-hook controller strategy are added to the vibration control device and the damping ratio is optimised with and without

respect to soil-pile interaction and STMD performance is compared . In addition, various soil layers effect on STMD performance are evaluated and the result is compared. Lastly, an optimal mass ratio is recommended to obtain the maximum performance of STMD in midrise structures founded on deep foundation.

4.3.1 Simulation of substructure (spring) method

In view of the full explanation of the substructure method in the last chapters, we will refrain from repeating the methodology here and only present the properties of the substructure simulation in the following section.

4.3.1.1 Superstructure description

The 7-storey steel structure is considered to explain the procedure of STMD damping for improving seismic mitigation of frame subjected to the six intensive record motion excitation. The record motions properties is given by Table 2. STMD is placed on top floor whereas the maximum lateral displacement will be happened with considering Soil-Pile-Structure interaction. Ultimate mass ratio, μ, is assumed by specified values (2%, 3% and, 5%), damping and stiffness of STMD have been characterized and, optimized by Grounghook Algorithm (GA) subjected to make small the maximum structure's drift as an target of this study by considering soil layers. Material properties and element details for structure is provided in Table 13 and 14 respectively.

Table 13: Structure section properties

Structure section properties		
STOREY	**COLUMNS**	**BEAMS**
First, second	BOX450x30	IPE270,IPE300
Third, fourth and fifth	BOX400x25	IPE270,IPE300
Sixth, seventh	BOX350x20	IPE270,IPE300

Table 14: Material properties

Material properties			
MATERIAL	**GRADE**	**E(GPa)**	**DENSITY(Kg/m3)**
STEEL	ST37	210	7850
CONCRETE	C25	23.34	2500

4.3.1.2 Soil block description

Mechanical properties of the soil play an essential role in the actions of structure-soil- interaction. In this analysis, for assessment of TMD and STMD proficiency separately, two layers and three layers of soil are regarded in each event. Both two cases of soil are fitted with five shaft steel piles with 1 meter and 1.2 meter subjected to the two and three layers soil in the order provided.

The 2layers soil profiles consist of medium sand (Dr=25%) with a depth of 8.0 m. about second layer, The mass density and the friction angle are 1.99 t/m3 and 30.3°, respectively. Eventually, the third layer is dense sand (Dr=35%) with a depth of 10.0 m. Also the height and thickness of pipe steel piles are 15m and 1.0m accordingly. The input soil and piles properties for the model are also shown in Figure 51. The 3layers soil profiles consist of a layer of loose sand (Dr=15%) with a depth of 5.0 m. accordingly the mass density and the internal friction angle of the soil measured 1.94 t/m3 and 25.4°. And medium sand (Dr=25%) with a depth of 8.0 m. about second layer, The mass density and the friction angle are 1.99 t/m3 and 30.3°, respectively. Eventually, the third layer is dense sand (Dr=35%) with a depth of 5.0 m. Also the

mass density and the friction angle of the third layer measured 2.06 t/m3 and 42.2°, respectively. Also the height and thickness of pipe steel piles are 15m and 1.0m accordingly. The input soil and piles properties for the model are also shown in Figure 52.

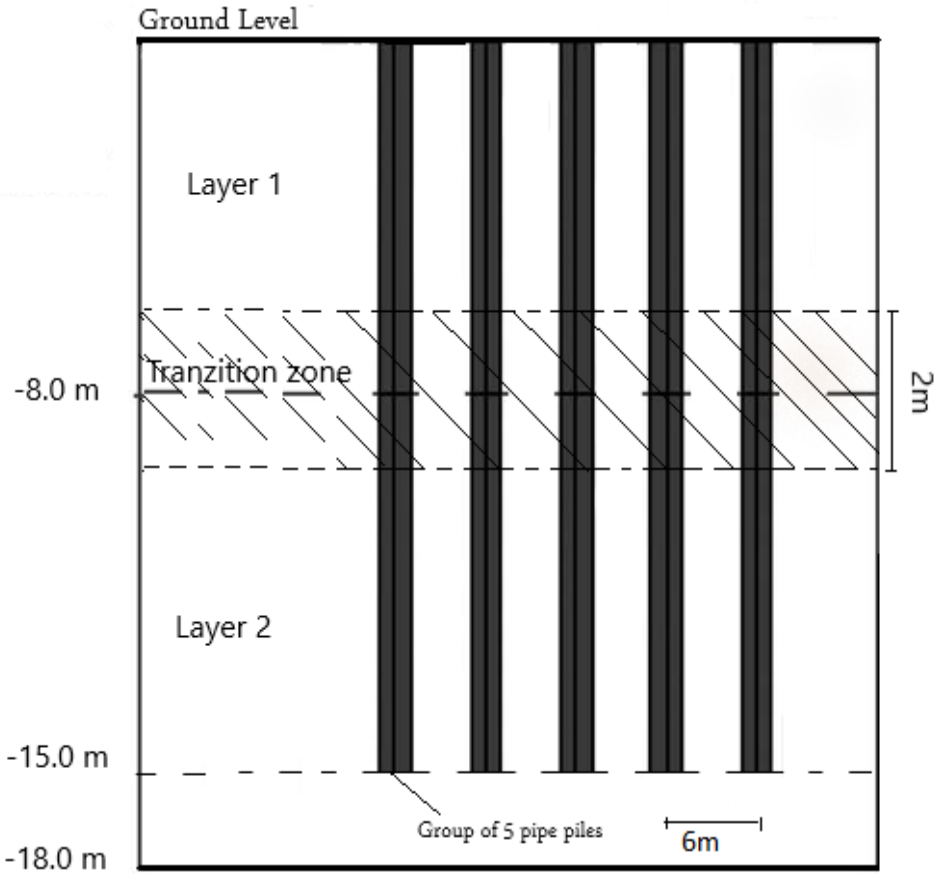

Figure 51: Two layers soil properties used in this study.

4.3.2 Result and discussion

In this study first, passive Tuned Mass Damper (TMD) and Semi Active Tuned Mass Damper (STMD) are applied for seismic control of multi degree freedom mid-rise structures with and without Soil-Pile-Structure interaction (SPSI) to evaluate the effectiveness of TMD and STMD. In the second part, the effectiveness of STMD with variable mass ratio (2%, 3% and 5% mass ratio) on top of the mid-rise structure is

investigated and evaluated by using ground-hook algorithm under nonlinear time histories analysis subjected to the six different record motions (far-field and near-field) with and without soil-pile-structure interaction. P-y curves proposed by the API recommendation (API, 2007) are used to accurately simulate the soil-pile-structure interaction. In addition, different soil layers (two and three layers) are considered to determine the effects of different soil blocks on STMD performance.

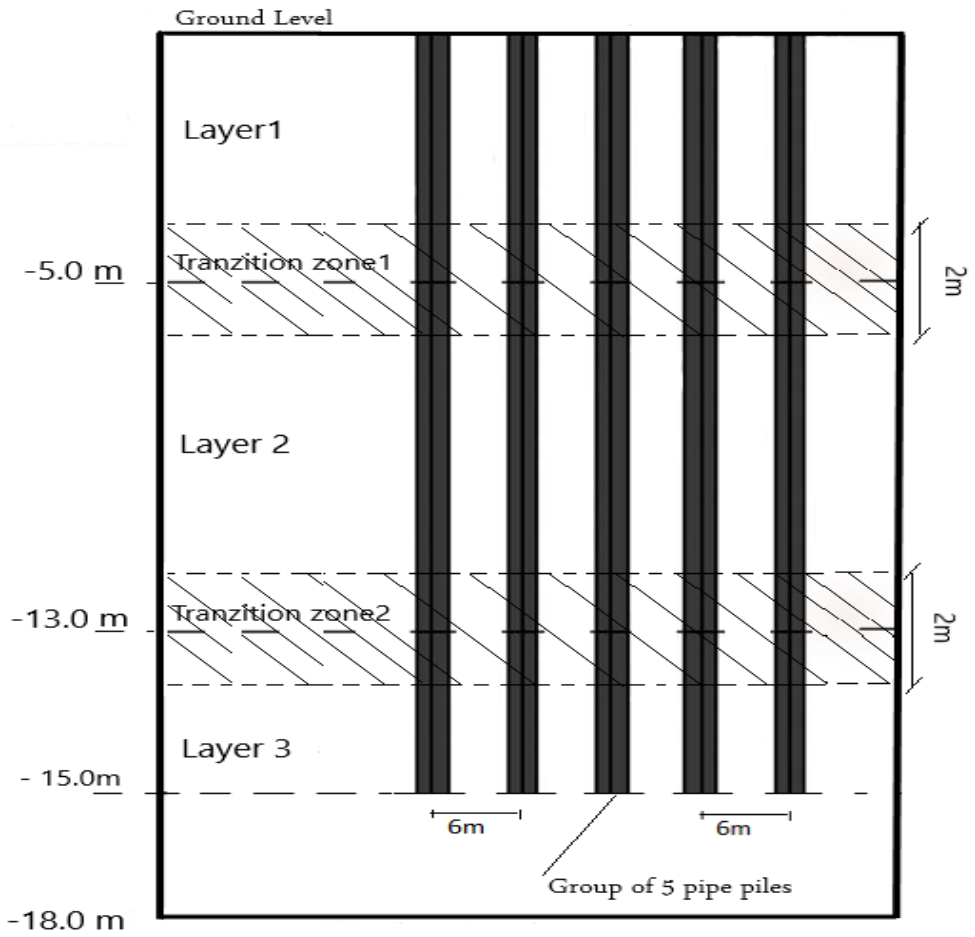

Figure 52: Three layers soil properties used in this study.

In order to assess the efficiency of the controllers (TMD and STMD), the dimensionless scales defined below in two categories (maximum and root mean square) are measured and evaluated as follows:

$$J_1, J_2, J_3, J_{13}, J_{14}, J_{15} = |\max(R_S / R_U)| \quad (4.1)$$

Where $J_1, J_2 \; and \; J_3$ define the efficiency of the controlled systems regarding the maximum dynamic response of STMD (R_S) to the uncontrolled system (R_U) with 2%, 3% and 5% mass ratio including two layers soil respectively.

Also J_{13}, J_{14}, J_{15} define the efficiency of the controlled systems regarding the maximum dynamic response of STMD (R_S) to the uncontrolled system (R_U) with 2%, 3% and 5% mass ratio including three layers soil respectively.

$$J_7, J_8, J_9, J_{19}, J_{20}, J_{21} = |\max(R_S / R_T)| \quad (4.2)$$

$J_7, J_8 \; and \; J_9$ which define the efficiency of the controlled systems regarding the maximum dynamic response of STMD (R_S) to the TMD system (R_T) with 2%, 3% and 5% mass ratio including two layers soil respectively.

Also J_{19}, J_{20}, J_{21} define the efficiency of the controlled systems regarding the maximum dynamic response of STMD (R_S) to the TMD system (R_T) with 2%, 3% and 5% mass ratio including three layers soil respectively.

$$J_4, J_5, J_6, J_{16}, J_{17}, J_{18} = RMS\left(\frac{\rho_S}{\rho_U}\right) \quad (4.3)$$

Where $J_4, J_5 \; and \; J_6$ define the efficiency of the controlled systems regarding the root mean square (RMS) dynamic response of STMD (ρ_S) to the uncontrolled system (ρ_U) with 2%, 3% and 5% mass ratio including two layers soil respectively.

Also $J_{16}, J_{17} \; and \; J_{18}$ define the efficiency of the controlled systems regarding the root mean square (RMS) dynamic response of STMD (ρ_S) to the uncontrolled system (ρ_U) with 2%, 3% and 5% mass ratio including three layers soil respectively.

$$J_{10}, J_{11}, J_{12}, J_{22}, J_{23}, J_{24} = RMS\left(\frac{\rho_S}{\rho_T}\right) \quad (4.4)$$

Where $J_{10}, J_{11}\ and\ J_{12}$ define the efficiency of the controlled systems regarding the root mean square (RMS) dynamic response of STMD (ρ_S) to the TMD system (ρ_T) with 2%, 3% and 5% mass ratio including two layers soil respectively.

Also $J_{22}, J_{23}\ and\ J_{24}$ define the efficiency of the control systems regarding the root mean square (RMS) dynamic response of STMD (ρ_S) to the TMD system (ρ_T) with 2%, 3% and 5% mass ratio including three layers soil respectively.

For better evaluation, first evaluate the efficiency of STMD and TMD for an uncontrolled structure, an STMD structure and a TMD structure without considering the soil-pile-structure interaction, as shown in Figure 53. As shown in Figure 53, the structure with the STMD reduced the maximum lateral displacement by about 20% for Superstition, 23% for Landers, 33% for Alaska, 35% for Morgan, 43% for Cape, and 53% for Northridge, and also the structure with the TMD reduced the maximum lateral displacement by 6% for Superstition, 10% for Landers, 25% for Alaska, 17% for Morgan, 30% for Cape, and 43% for Northridge. As expected, STMD performed better than TMD in the range of 4 to 25 percent more reduction, especially for earthquakes in the far-field category. It can be concluded that TMD and STMD are effective for reducing the top displacement response of structure without considering the SPSI effect.

Figure 54 shows the effectiveness of STMD and TMD in terms of displacement of the top storey of the structure in the six earthquakes, including three layers soil block. The mass ratio for both TMD and STMD is assumed to be considered as 2% of principle mode mass of structure. As Figure 54 shows, it can be found that TMD could reduce the displacement response by 15%, 2%, 9%, 12%, -12% and 1% and STMD could

reduce the displacement response by 19%, 2%, 11%, 10%, -9% and 1% in Morgan, Alaska, Northridge, Superstition, Lander and Cape earthquakes respectively. Therefore, STMD performed about the same as TMD in reducing the top displacement of the structure including the soil-pile-structure interaction.

In addition, looking at Figures 53 and 54, STMD and TMD perform well but are not as effective as their performance in the structure without considering SPSI, which results that the performance of TMD and STMD decreases when SPSI is included.

The effect of soil layers on STMD performance are investigated in Figure 55 and 56 for a two-layer and three-layer soil block, respectively. In these figures, variable mass ratios (2%, 3% and 5%) for STMD are considered to evaluate the performance level.

The efficiency of STMD with variable mass ratios, including SPSI, is shown in Figure 55. As shown in this figure, for three soil layers, STMD with a mass ratio of 2% mitigates the lateral displacement approximately between -9% and 19%, STMD with a mass ratio of 3% mitigates it between -2% and 20%, and STMD with a mass ratio of 5% mitigates it between 10% and 29%.

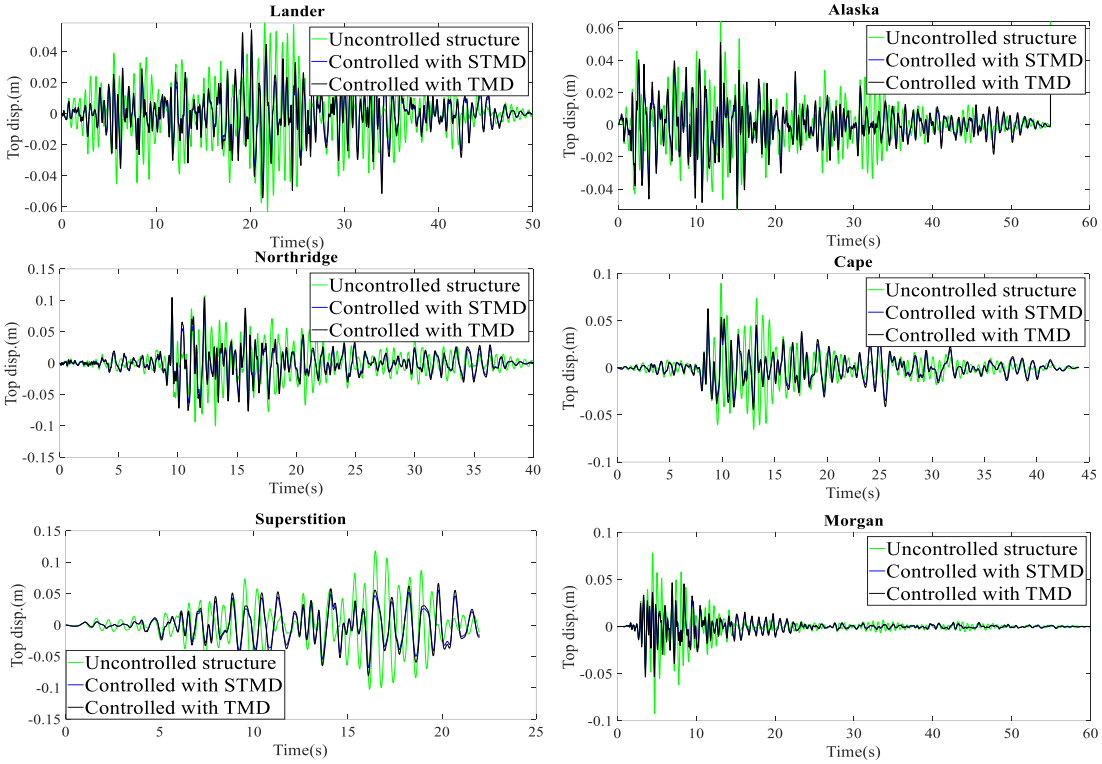

Figure 53: Responses of Uncontrolled structure, STMD structure and TMD structure ignoring SPSI.

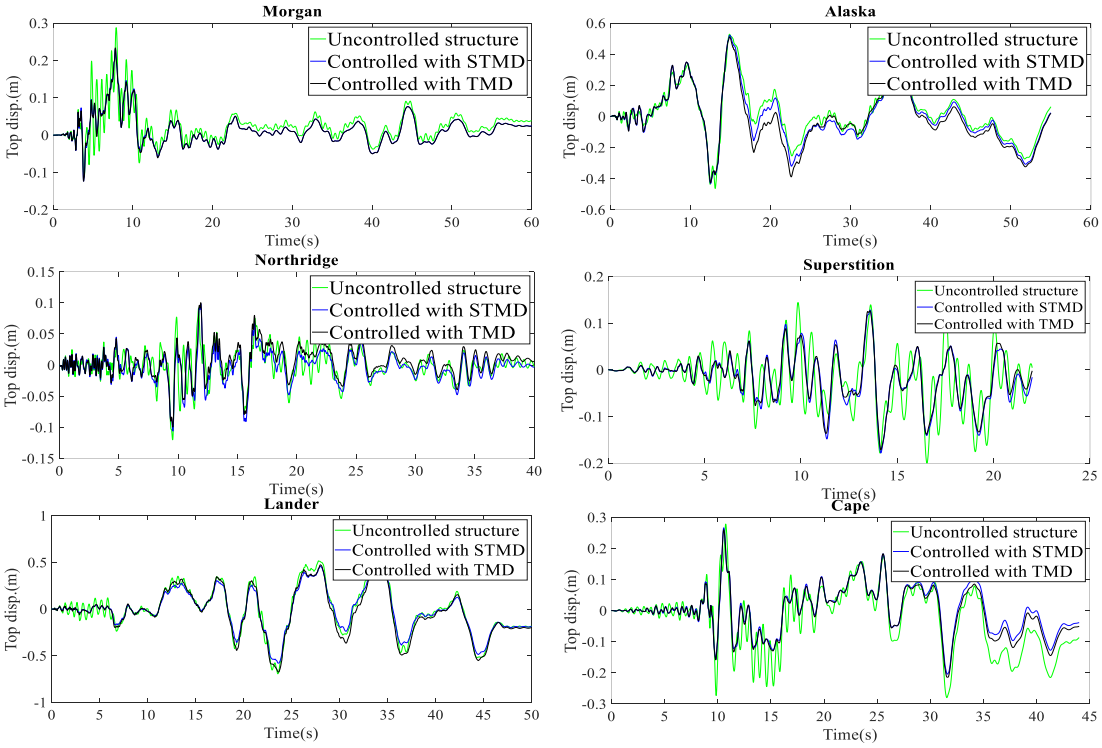

Figure 54: Responses of Uncontrolled structure, STMD structure and TMD structure considering SPSI

In a three-layer soil block, the effect of STMD with a mass ratio of 2% resulted in an increase in displacement at Landers and Cape, therefore STMD with 2% mass ratio has a negative effect. STMD with 3% mass ratio also resulted in a negative effect on the control of structure in Landers and Alaska earthquakes. Hence, it can be concluded that in this case the optimum mass ratio for STMD is 5%.

Figure 56 shows the efficiency of STMD for the structure founded on a two-layer soil, it can be seen that STMD with 2% mass ratio can reduce the response between -6% and 16%, for 3% mass ratio between 3% and 23% and for 5% mass ratio, 4% to 30%. In this case, only the STMD with 2% mass ratio has a negative effect on the system, so both 3% and 5% mass ratio can be useful. By considering the two figures (55 and 56) in a two-layer and three-layer soil block, it can be found that a mass ratio of 5% for STMD in a structure with SPSI can adequately and properly reduce the top displacement response. The nonlinear time history of acceleration for the STMD structure subjected to the six earthquakes is shown in Figure 57 and 58. Two and three layer soil block with variable mass ratio (2, 3 and 5 percent) and optimized damping ratio are evaluated in Figure 57 and 58 respectively. As can be seen in Figure 57, reduction in acceleration response for STMD with 2% mass ratio ranges from 0.14% in Northridge to 9.6% in Lander, for STMD with 3% is -8.2% in Lander to 20% in Cape, and for STMD with 5% is 4% in Alaska to 32% in Cape earthquake. STMD with 3% mass ratio has a negative effect in some earthquakes like Lander, so, in this case the optimal mass ratio can be 5% for both near-field and far-field earthquakes.

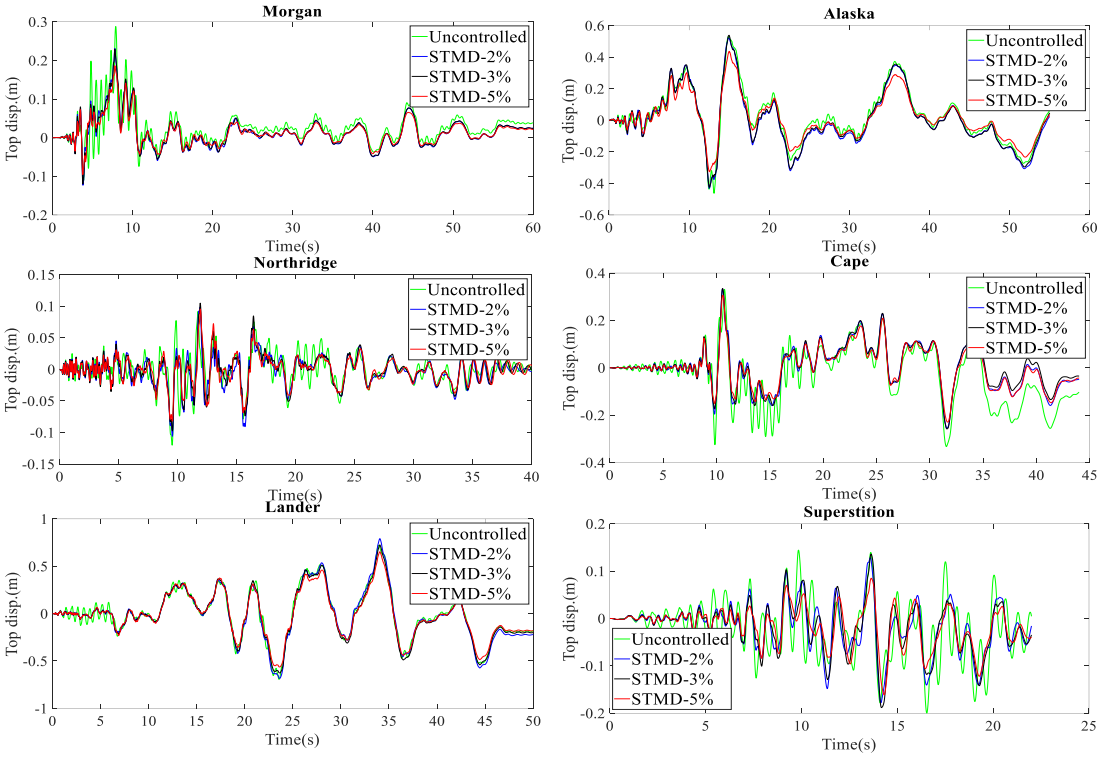

Figure 55: Responses of Uncontrolled structure and STMD structure with 2%, 3% and, 5% mass ratio founded on three layers soil.

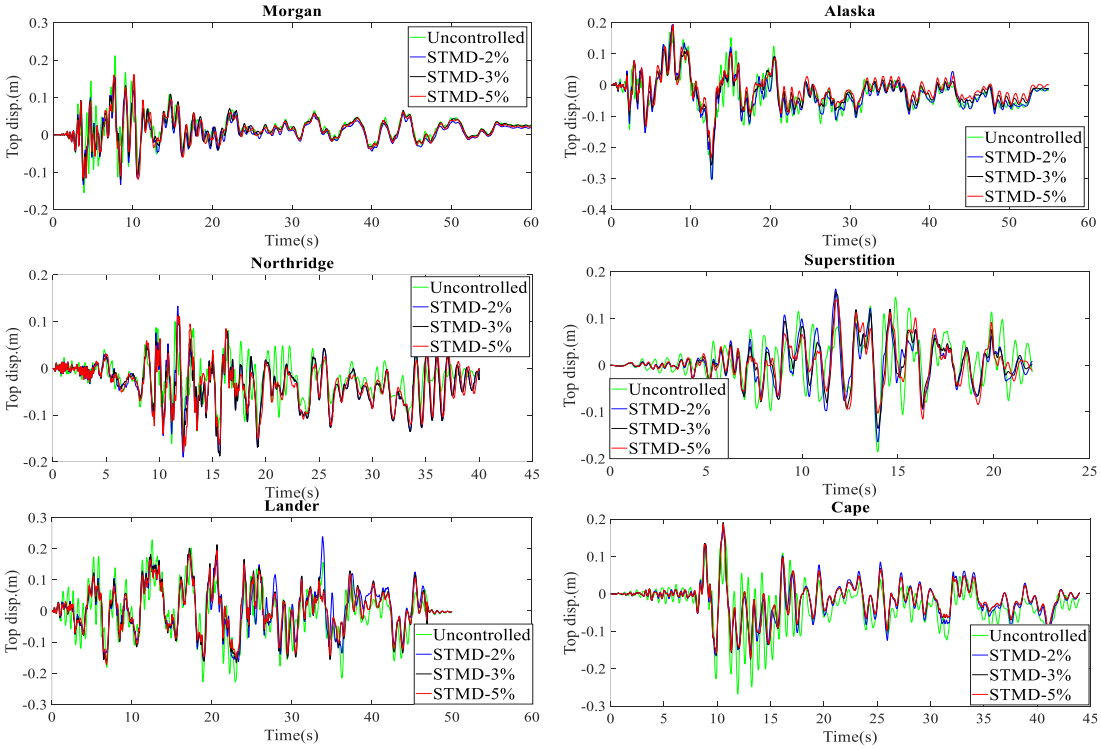

Figure 56: Responses of Uncontrolled structure and STMD structure with 2%, 3% and, 5% mass ratio founded on two layers soil.

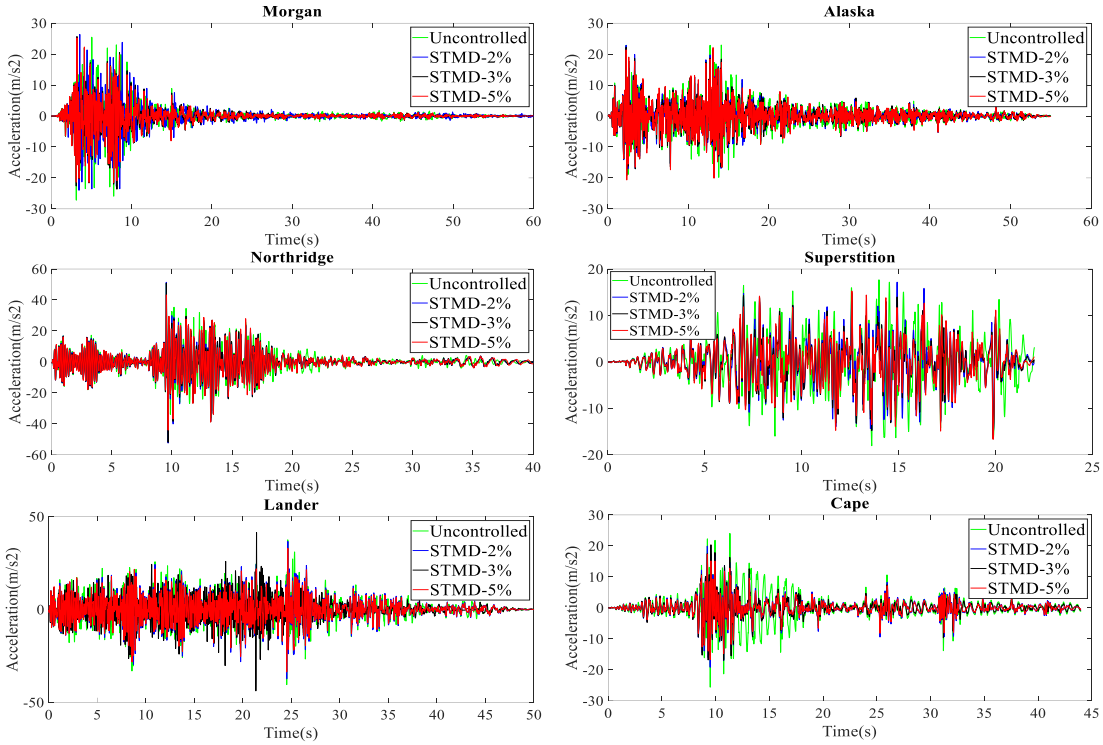

Figure 57: Acceleration response of STMD structure with 2%, 3%, and 5% mass ratio by considering two layers soil block.

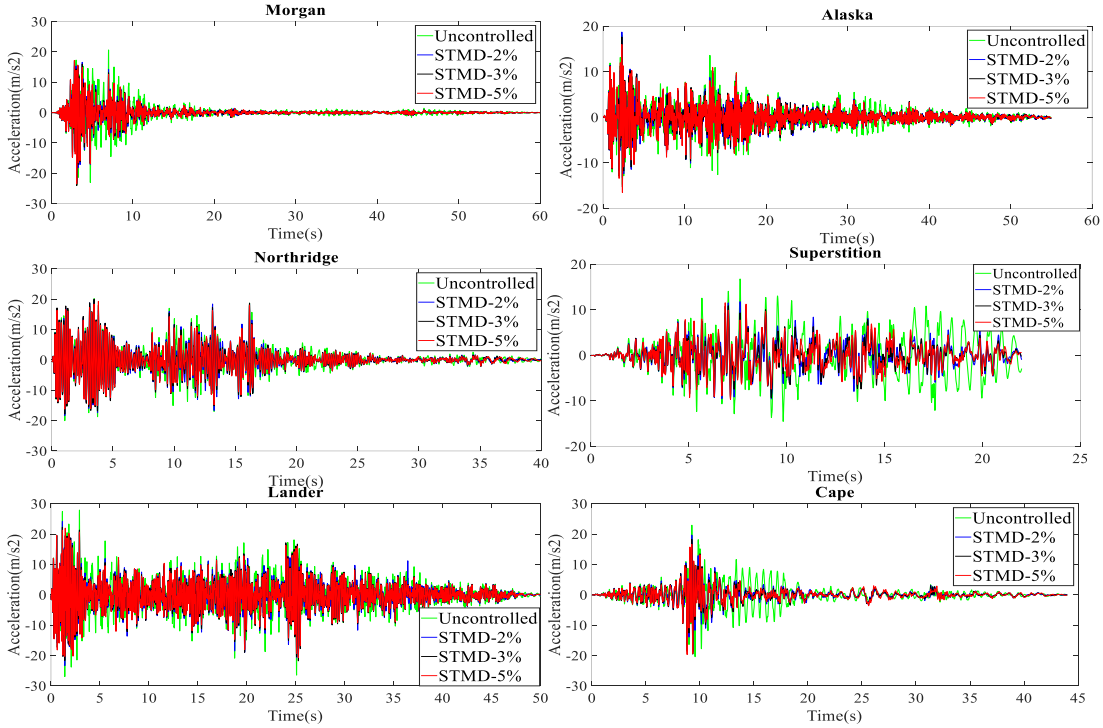

Figure 58: Acceleration response of STMD structure with 2%, 3%, and 5% mass ratio by considering three layers soil block.

For a three-layer soil block as shown in Figure 58, STMD with a mass ratio of 2% could reduce the acceleration response of the structure between -3% in Alaska to 29% in Superstition, for STMD with a mass ratio of 3% it is 0.5% in Morgan to 31% in Superstition and STMD with a mass ratio of 5% reduces between 2% in Morgan to 34% in Superstition. STMD with a mass ratio of 2% had a negative effect on reducing the Alaska response, and for a mass ratio of 3% and 5%, STMD with a mass ratio of 5% is more effective and reduces more percent than a mass ratio of 3%. Therefore, for structures founded on a three-layer soil block, the optimized indices for STMD mass ratio can be 5% for all earthquake categories. Considering the above figures, a five percent mass ratio has a higher effect level in the displacement and acceleration response of the structure compared to the other mass ratios for both a two-layer and a three-layer soil block.

Figure 59 shows the time history analysis of the bending moment of a structure with a two-layer soil block for STMD with 2%, 3% and 5% mass ratio for Alaska, Landers, Cape earthquakes as far-field earthquakes and Morgan, Northridge and Superstition as near-field earthquakes. As this figure shows, the STMD with 2% mass ratio mitigates the bending moment response in 1%, 8%, 2%, 18%, 33% and 20%, for the STMD with 3% mass ratio it is 18%, 9%, 5%, 11%, -2% and -3%, for the STMD with 5% mass ratio it is -7%, 7%, -18%, 3%, -1% and 27% in Alaska, Northridge, Superstition, Lander, Cape and Morgan earthquakes respectively. It can be inferred that the STMD with 2% mass ratio performs well in reducing the bending moment response in all earthquakes.

The bending moment response of a structure founded on a three-layer soil block is shown in Figure 60. It can be seen that an STMD with a mass ratio of 2% can reduce the response by 13%, 28%, 31%, 5%, 8% and 28%, an STMD with a mass ratio of 3% can reduce the response by 13%, 25%, 35%, 6%, 7% and 27% and an STMD with a mass ratio of 5% can reduce the response by 14%, 23%, 32%, -46%, 9% and -2% in the Alaska, Northridge, Superstition, Lander, Cape and Morgan earthquakes. Thus, it appears that STMD with a mass ratio of 2% and 3% adequately reduces the bending moment response of structures founded on a three-layer soil block. From Figures 59 and 60, it can be concluded that the optimum mass ratio for STMD is 2%, as higher percentage reduction occurred at this mass ratio of STMD in all earthquakes used in this study.

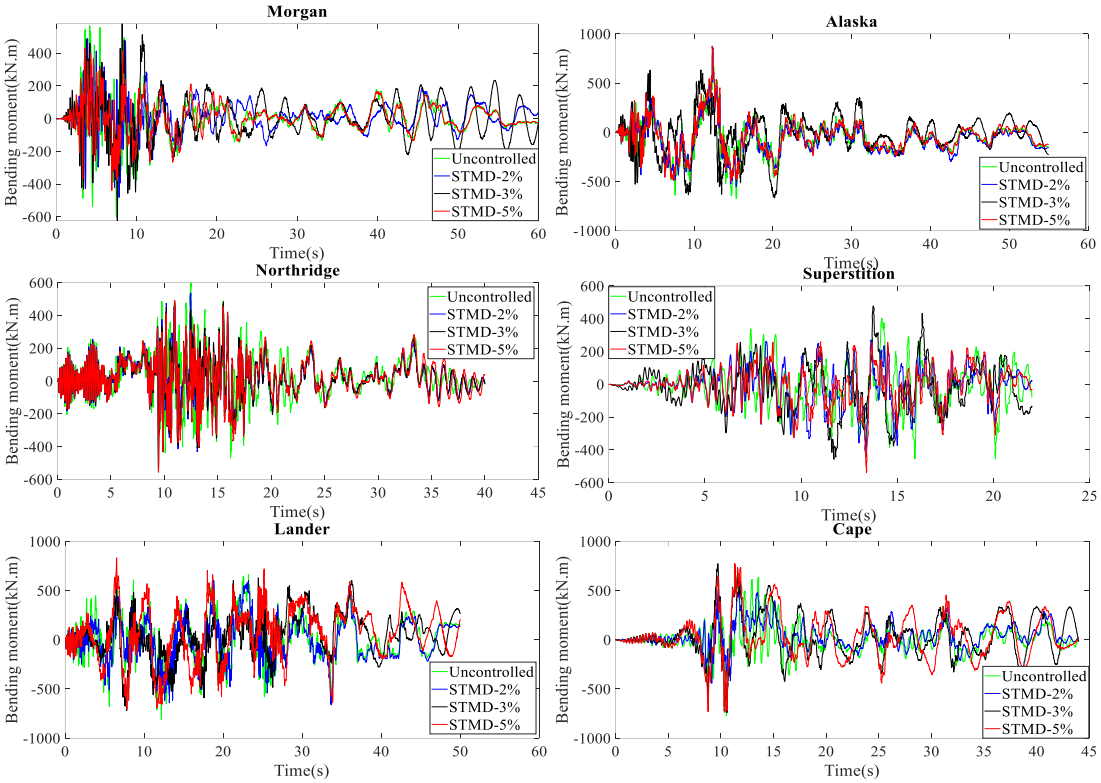

Figure 59: Bending moment response of STMD structure with 2%, 3%, and 5% mass ratio by considering two layers soil block.

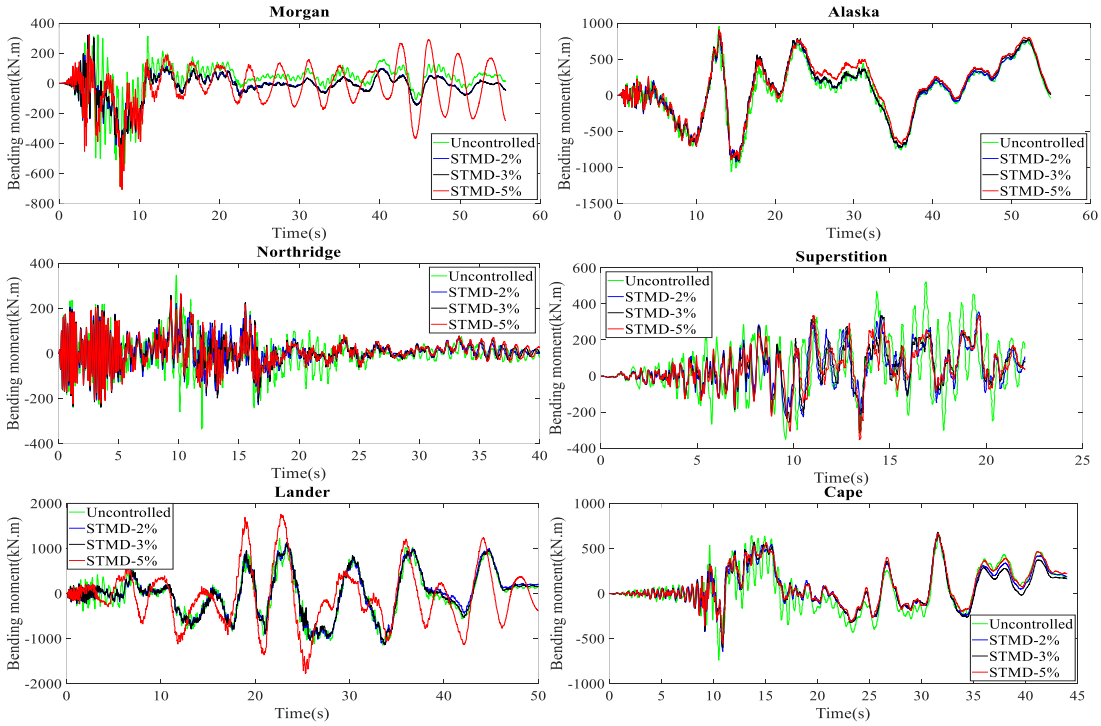

Figure 60: Bending moment response of STMD structure with 2%, 3%, and 5% mass ratio by considering three layers soil block.

Evaluation of the operation indices of the SATMD controllers regarding to the uncontrolled system and TMD system, in the Alaska, Landers, Cape as a far-field earthquakes and, Morgan, Northridge and, Superstition as near-field earthquakes are presented in Table 5, 6 and 7. The mass ratio of the TMD is considered 2, 3 and 5% of modal mass of the first mode corresponding to the STMD and the frequency ratio of the TMD is equivalent to the natural frequency of the principle vibrational mode of the structure.

Peak structural response and root mean square (RMS) response of base shear, acceleration and displacement are presented in Table 5, 6 and 7 respectively.

The maximum and Root Mean Square (RMS) base shear response of the structure with SPSI for the TMD performance with 2% mass ratio and also the STMD performance with variable mass ratio (2, 3 and 5%) are shown in Table 15 for six defined earthquake record motions in this study. The results in this table show that for both the two-layer and three-layer soil block, the STMD with all mass ratios adequately attenuates the maximum base shear response, and the STMD with 5% mass ratio performs better than others compared to the uncontrolled system. Moreover, the STMD with 3% mass ratio has a better effect on the RMS base shear response of the structure during the earthquake period compared to the uncontrolled system. The table shows that for a two-layer soil block, the STMD with 2% and 3% better than the TMD reduces the maximum base shear response of the structure, and for a three-layer soil block, only the STMD with 5% mass ratio has a better effect. Moreover, the indices on RMS, show that STMD with 5% mass ratio can reduce the base shear response better during the earthquake period.

Table 15: Base Shear performance indices of STMD

Indices/Records	Morgan	Northridge	Superstition	Landers	Cape	Alaska
J1	0.91	0.88	0.85	0.71	0.74	1.01
J2	0.91	0.88	0.81	0.86	0.77	1.00
J3	0.91	0.89	0.75	0.52	0.79	0.98
J4	0.83	1.25	0.81	0.80	0.62	0.84
J5	0.82	0.91	0.77	0.78	0.67	0.89
J6	0.81	0.92	0.74	0.79	0.71	0.95
J7	0.98	1.00	1.00	0.76	1.02	1.02
J8	0.99	1.01	0.92	1.00	1.02	0.98
J9	0.98	0.99	0.87	0.56	1.00	0.98
J10	1.00	1.34	1.03	1.03	0.99	1.01
J11	1.00	0.98	0.97	1.01	1.00	1.02
J12	0.99	0.98	0.92	0.96	1.00	1.02
J13	0.71	0.82	0.77	0.79	0.77	0.76
J14	0.75	0.82	0.82	0.78	0.79	0.78
J15	0.77	0.80	0.72	0.67	0.79	0.85
J16	0.58	0.87	0.62	0.72	0.66	0.82
J17	0.56	0.86	0.62	0.70	0.63	0.85
J18	0.58	0.86	0.62	0.72	0.62	0.91
J19	0.99	1.03	1.05	1.12	1.02	0.94
J20	1.00	1.03	1.06	1.02	1.00	0.93
J21	0.97	1.00	0.96	0.89	0.98	0.93
J22	0.99	1.00	1.08	1.01	1.00	0.99
J23	0.98	1.02	1.03	1.01	1.00	1.00
J24	0.97	1.04	1.00	0.98	0.97	0.99

Table 16 shows the efficiency criterion of STMD with variable mass ratios and TMD for the maximum and root mean square acceleration response of the structure including SPSI. From the table, it can be seen that STMD with mass ratio of 5% act better than 2 and 3% mass ratio. This is the case while TMD and STMD with all mass ratios could not properly satisfy the RMS criterion of acceleration response in both two and three layer soil blocks. Moreover, by considering in this table, it can be found that STMD is better than TMD in reducing the maximum acceleration of the structure in both two and three layers, but in terms of RMS acceleration response, it can be said that TMD is better in reducing the response during the earthquake period. It also seems that STMD with mass ratio of 2 and 3% act poorly in terms of maximum and RMS acceleration response in all defined earthquake record motions.

Table 16: Acceleration performance indices of STMD

Indices/Records	Morgan	Northridge	Superstition	Landers	Cape	Alaska
J1	0.97	0.99	0.95	0.91	0.78	0.99
J2	0.95	0.99	0.91	1.08	0.80	0.97
J3	0.93	0.86	0.90	0.84	0.70	0.96
J4	1.36	1.4	1.01	1.07	1.1	1.30
J5	1.25	1.3	0.98	0.94	1.1	1.2
J6	1.20	1.01	0.98	0.97	1.00	1.00
J7	1.05	0.99	1.06	0.85	0.96	1.02
J8	1.00	0.98	0.93	0.94	1.08	1.00
J9	0.96	1.00	0.91	0.65	1.00	0.98
J10	0.96	1.39	1.01	1.00	1.01	1.01
J11	1.01	1.00	0.97	0.93	1.01	1.03
J12	1.00	0.99	0.98	0.92	0.93	1.03
J13	0.98	0.98	0.71	0.87	0.86	1.03
J14	1.00	0.99	0.70	0.80	0.86	0.95
J15	0.99	0.96	0.66	0.78	0.85	0.90
J16	1.03	1.05	1.24	1.33	1.05	1.11
J17	1.02	1.06	1.19	1.29	1.00	1.13
J18	1.02	1.01	1.13	1.35	0.99	1.15
J19	1.00	0.92	0.93	0.98	1.01	0.99
J20	1.00	0.93	0.91	0.96	0.99	0.97
J21	0.96	0.93	0.89	0.95	1.00	0.97
J22	0.99	1.03	1.04	1.01	1.00	1.00
J23	0.99	1.02	1.03	1.00	1.00	0.99
J24	1.00	1.01	1.01	0.98	1.00	1.00

The maximum and root mean square displacement criterion is shown in Table 17 for the structure on the two- and three-layer soil block at six earthquake record motions. The table shows that STMD with mass ratio of 3% and 5% reduce the maximum displacement response of the structure well for all record motions, but STMD with mass ratio of 5% work better in the cases with two-layer and three-layer soil block. As for the response indices of RMS, only STMD with mass ratio of 5% performed acceptably to reduce the displacement during the earthquake period in the two cases with two and three soil layers. Looking at the table on STMD efficiency versus TMD indices, it can be seen that in all cases (maximum and RMS) STMD with all mass ratios, especially with mass ratio of 5%, could mitigate the displacement response more. From the consideration of Tables 15, 16 and 17, it can be concluded that STMD

with mass ratio of 2% cannot be useful in some cases and poorly mitigate the response of the structure, while STMD with 3% and 5% can be useful in any response of the structure, therefore, depending on the design objective, the choice of 3% or 5% must be considered.

Table 17: Displacement performance indices of STMD

Indices/Records		Morgan	Northridge	Superstition	Landers	Cape	Alaska
J1		0.74	1.06	0.89	1.05	0.69	0.87
J2		0.74	1.05	0.85	0.94	0.72	0.85
J3		0.77	1.00	0.76	0.86	0.69	0.78
J4		0.88	1.19	0.92	1.38	0.79	0.99
J5		0.97	1.16	0.89	1.38	0.74	0.98
J6		0.95	1.01	0.87	1.02	0.72	0.95
J7		0.92	0.99	1.03	1.27	1.01	1.01
J8		1.04	0.95	1.01	1.19	1.00	1.04
J9		1.01	0.91	0.95	0.99	0.95	0.98
J10		0.94	1.04	1.01	1.02	1.00	1.02
J11		1.03	1.00	0.95	1.01	0.91	1.02
J12		0.98	1.04	0.92	0.76	0.87	1.02
J13		0.81	0.89	0.89	1.09	0.99	0.99
J14		0.79	0.88	0.94	1.00	1.00	1.01
J15		0.66	0.80	0.82	0.89	0.92	0.86
J16		0.83	0.96	0.86	1.03	0.89	1.02
J17		0.83	0.95	0.85	0.99	0.87	1.01
J18		0.85	0.98	0.88	0.54	0.90	1.01
J19		0.98	1.05	1.03	1.16	1.02	1.01
J20		0.99	0.97	0.98	1.07	1.00	0.97
J21		0.93	0.97	0.99	0.52	1.00	0.95
J22		1.00	0.96	1.03	1.05	0.96	0.97
J23		0.99	0.98	1.03	1.01	0.95	0.97
J24		0.98	0.98	0.95	0.54	0.94	0.98

Moreover, STMD act better in far-field earthquake in terms of TMD to control the base shear response of the system, and for about acceleration response, they act close for both near-field and far-field earthquakes and for displacement response, they act suitable in far-field earthquake rather than near-field earthquake category.

4.4 Summary

First, in this chapter the accuracy of the standard API backbone curves developed for the spring method is analyzed for seismic soil-pile-structure interaction analysis of short period (T<1s) structures (5 storey structure to represent midrise buildings) equipped with Semi Tuned Mass Damper (STMD). In order to achieve this, two parts of soil-pile-structure interface (inertial and kinematic interaction) are analyzed by both continuum and spring methods (A, B) with reliable nonlinear time history analysis. Both stages for vibration analysis (site response analysis and dynamic analysis of the piles) of spring methodology are synthesized in just one stage to obtain more accurate result. Spring method characterizations are assigned by using the API recommendation. The five-story STMD structure of full-scale models on group piles is simulated by the continuum approach and the spring method is used by the general API backbone curves to describe non-linear spring parameters. An enhanced p-y curve equation for soft sandy soil is also presented and the results compared.

The analyses indicated that, the Model A and B results show approximately a range of deviation of 1% to 196% compared to the continuum model results for the assessment of pile head displacements and, range of 87% to 310% for the lateral force. Whereas for the prediction of maximum bending moments the Models A and B indicated significantly different ranges of deviation from the continuum model results, with Model A yielding a range of 77% to 350% and Model B yielding a range of 20% to 78%.

In sands, the maximum bending moment was typically underestimated by Model A and B, however, Model B results (such as lateral force and lateral displacement in

piles, acceleration response and top floor displacement) have provided better estimations with respect to the continuum model results.

It is important to note that, in contrast to the traditional assumption that ignoring SSI usually leads to consider more conservative design for structures, for the studied short period structure equipped with STMD on pile foundations that is not the case. In actual fact, the results of this study indicated that important design information such as viscosity force, top floor displacement and acceleration are all underestimated when SSI is omitted in the analyses.

In structures which are equipped by STMD, the suitable prediction of viscosity force is essential for finding design characterization range of STMD. Although it is suggested as far as possible using the continuum method for STMD structures, the modified API curve equation in this study provides an efficient alternative for short period structures founded on sand with similar properties.

The results have shown that, whilst the use of modified p-y curves for specific structures is a suitable efficient approach for modelling, the spring method may still has weakness in reflecting the actual soil-pile-structure interaction when compared to the more comprehensive continuum method results. In this study this demonstrated for short period structures with STMD on pile foundations under dynamic loading.

Then, in this chapter the seismic behavior of mid-rise steel buildings equipped with STMD were analyzed considering SPSI using three dimensional finite element analysis. The effect of ground stratification and the change in ground shear strength

and stiffness were incorporated in the analysis models. The nonlinear time history analysis was performed under near and far field earthquake excitations.

The results showed that, without SPSI, STMD effectiveness is increased, which might lead to optimistic designs, especially when structural acceleration and displacements are considered. SPSI leads to a significant change in the dynamic behavior of the superstructure, most likely to an onerous design compared to the case of the fixed base design. The increase in structural response due to SPSI is also observed to be independent of the earthquake data used (near-field or far-field).

STMD use has led to a reduction in the base shear when SPSI is considered due to beneficial effect of passive force mobilized around the pile foundations. SPSI inclusion affected STMD structure more than the structure without STMD, as indicated by the whole set of watch parameters defined in the FEM model.

The results show that the acceleration of the structure can be greatly altered in soil layers with low stiffness, and also in terms of inertial interaction, it appears that the use of STMD does not play a major role in mitigating the response of the structure in a pile foundation, so the presence or absence of STMD on the structure does not alter the response of the structure in the soil block.

It can be seen that the effect of SPSI is much more pronounced for the dynamic responses of the 7-storey building than for the 4-storey building, but still both have an undesirable and significant drawback of SPSI effects on the dynamic responses of the structure. Inclusion of SPSI in the analysis model was shown to be crucial for two

reasons; 1- to identify whether the control device is needed at all, and, 2- if found to be necessary, to estimate the optimal characteristics of the STMD.

Finally in this chapter, STMD are applied on the top floor of the structure to mitigate the seismic vibration of the structure including Soil-Pile-Structure Interaction (SPSI), and the efficiency of STMD considering the SPSI effect is evaluated. For this purpose, STMD with variable damping ratio optimized by Groundhook Algorithm controller and variable mass ratios of 2%, 3% and 5% are used to investigate the high proficiency of STMD. Two cases, a two-layer and a three-layer soil block with a group of 20 pipe piles, are considered to determine the exact effect of SPSI on the dynamic behavior of the structure. Nonlinear time history analysis using six record motion (three in the far field and three in the near field) is applied to the seismic control of the structure using the spring method (p-y curves).

The result shows that STMD is useful for seismic control of structures founded on deep foundations but not as much as structures with fixed support, while STMD reduces the vibration response of fixed structures within 20% to 50% by varying input excitations and controls the response of SPSI structures within 4% to 30%.

The result showed that the effect of soil-pile-structure interaction on the controlled system can be reduced by finding a suitable mass ratio and the same STMD parameters such as stiffness and damping frequency used in fixed support.

It seems that by reducing the soil stiffness, the efficiency of the controlled system decreases. As the results of this study show, in almost all cases, the STMD has higher efficiency when three soil layers are considered compared to two layers.

Moreover, for some control objectives, such as displacement and base shear responses, STMDs have a strong effect on attenuating the peak responses compared to TMDs.

Even considering the performance criterion, it can be concluded that the appropriate mass ratio for STMDs completely depends on the design objective. For example, although STMDs with 2 and 3 percent mass ratio are suitable for the base shear control objective, the 5 percent mass ratio seems reasonable for the displacement control of the system and the 2 percent mass ratio for the acceleration control of the system showed a better ratio in almost all cases.

Overall, it can be said that the 3 and 5 percent mass ratios are the most suitable for the control system of the structure because, as it is shown in the figures, the mentioned mass ratio leads STMD to act well or at least without any disadvantage and behaves neutrally.

It is necessary to mention that structures with STMD controller founded on deep foundation are not sensitive to input earthquake records and both categories (far-field and near-field) with varying seismic parameters, except for a few performance criteria of the controlled structure, may affect the response of the structure in different ways considering the results of three near-field and three far-field input excitations.

Chapter 5

CONCLUSION AND FURTHER RECOMMENDATIONS

5.1 Summary

In order to consider the high operation of STMD to mitigate the dynamic structural response, the soil-pile-structure interaction must be accurately estimated. The substructure method, in which a system is separated into two subsystems: the superstructure, which mainly contains the building and STMD controls, and the foundations to the building supports, that contain the pile group foundation and soil surrounding field, is most frequently applied to model the response of seismic systems. The soil-structure interaction (SSI) is accounted for by substituting the foundation volume with a constant dynamic stiffness matrix informed by sets of linear and nonlinear springs and dashpots that simulate the soil field. The method is widely used both in practice and in research, but the validity of the approach for STMD structures has never been investigated.

In this work, an attempt has been made to fill this important gap by comparing the results of this regularly used basic practical method with those of a more accurate technique, namely continuum modeling. This is to contribute to the improvement of the numerical simulation of SSI, which is used in engineering practice for system design. On the basis of the existing state of practice at Caltrans, the substructure approach is presented in five phases. The basic data for the analysis of the substructure approach are obtained by studying continuum models of different short-time systems

subjected to different natural earthquake shaking. Comprehensive models of the foundation soil, pile foundation, STMD control, and superstructure were created. The investigation of the substructure approach started with a look at the p-y backbone curves proposed by API recommendations.

The accuracy of the substructure method depends on the accuracy of these backbone curves. For this purpose, a five-storey building equipped with Semi Tuned Mass Damper (STMD) is simulated and the result is evaluated. The study indicated that the use of API recommendation in simulating dynamic analysis on laterally loaded group piles leads to significant errors, ranging from 1 to 196% in the estimation of pile head displacements and from 77 to 350% in the estimation of maximum lateral force.

It has also been shown that the results are different and are not in a satisfactory range. For example, when the substructure approach was used to simulate the maximum bending moments at the pile cap during the earthquakes, the results were overestimated by factors of approximately 2.

On the other hand, it is shown that the continuum modeling technique successfully reproduces the seismic response of soil-pile interaction. In summary, the investigation of this study are as follows:

- The dissertation is one of the few studies with full-scale nonlinear continuum simulation of STMD systems on deep foundations have been developed for analysis under dynamic excitations produced by earthquake.
- The work also recommended the updated p-y curve equation proposed by the API recommendation for short period structures equipped with STMD devices.

The presented capabilities of the continuum modeling method validate the significance of comprehensive analysis with great accuracy of dynamic SSI, regarding to increase earthquake protection, decrease unjustified costs, and improve the flexibility of the constructed environment. Since that the continuing advances in full scale modeling of structural and geotechnical materials, large-scale continuum models and computational tools may gradually become a great and much more trustworthy approach for appropriate modeling of earthquakes SPSI in civil industrial. Vibration control devices applying an additional mechanism for improving seismic structural operation. In order to find high efficiency of these devices, a minimum control power is required to reach the favorite performance purposes. Regarding to this end, this study has evaluated the reliability of STMD building for assessing strategy of design and simulation in future. Therefore, these systems can be considered for further studies to investigate their benefits and also further improvement in experimental validation and design methods, eventually leading to practical designs which include the Soil-Pile interaction.

5.2 Remaining challenges

There is no predictable general approach to improving spring modeling and, in particular, the general approach to the substructure method for seismic SSI analysis of all types of systems. As mentioned in this thesis, previous studies aimed at improving the substructure approach which is not be practical for all types of structures. Considering that the efficiency of damping devices directly depends directly to the structural attitude under dynamic analysis, the substructure method needs to be improved and specialized for all types of buildings, especially for structures with additional dampers. Future research must also be focused on enhancing the continuum modeling approach regarding to the simulation procedure and computational effort

demanded. For example, more inclusive constitutive simulations can be realized in the practical numerical codes for continuum modeling and applicable for seismic analysis of structures to gain more realistic assessments of the inertial and kinematic interactions through the structure and the supporting soil, especially for structures with damping devices.

REFERENCES

[1] A.C. and R. R., Building configuration and seismic design, John Wiley. (1982).

[2] J.F. Challa, V. R. M., and Hall, Earthquake collapse analysis of steel frames, Earthq. Eng. Struct. Dyn. 23(11), 11 (1994).

[3] Y.X. Gu, G.Z. Zhao, H.W. Zhang, Z. Kang, R. V. Grandhi, Buckling design optimization of complex built-up structures with shape and size variables, Struct Multidiscip.Optim.19(2000)183–191. https://doi.org/10.1007/s001580050101.

[4] A.J. Aref, W.Y. Jung, Advanced composite panels for seismic and vibration mitigation of existing structures, J. Eng. Mater. Technol. Trans. ASME. 128 (2006) 618–632. https://doi.org/10.1115/1.2345455.

[5] P.D. Moncarz, B.M. McDonald, R.D. Caligiuri, Earthquake failures of welded building connections, Int. J. Solids Struct. 38 (2001) 2025–2032. https://doi.org/10.1016/S0020-7683(00)00150-5.

[6] J. Wu, G. Chen, M. Lou, Seismic effectiveness of tuned mass dampers considering soil-structure interaction, Earthq. Eng. Struct. Dyn. 28 (1999) 1219–12, https://doi.org/10.1002/(SICI)1096-9845(199911)28:11<1219::AID-EQE861>3.0.CO;2-G.

[7] D. Demetriou, N. Nikitas, K.D. Tsavdaridis, Semi active tuned mass dampers of buildings: A simple control option, Am. J. Eng. Appl. Sci. 8 (2015) 620–632.

https://doi.org/10.3844/ajeassp.2015.620.632.

[8] A. Rahmani, M. Taiebat, W.D.L. Finn, C.E. Ventura, Evaluation of p-y springs for nonlinear static and seismic soil-pile interaction analysis under lateral loading, Soil Dyn. Earthq. Eng. 115 (2018) 438–447. https://doi.org/10.1016/j.soildyn.2018.07.049.

[9] Api Standards : International Usage, (2019).

[10] S.C. Dutta, K. Bhattacharya, R. Roy, Response of low-rise buildings under seismic ground excitation incorporating soil-structure interaction, Soil Dyn. Earthq. Eng. 24 (2004) 893–914. https://doi.org/10.1016/j.soildyn.2004.07.001.

[11] K. Galal, M. Naimi, Effect of soil conditions on the response of reinforced concrete tall structures to near-fault earthquakes, Struct. Des. Tall Spec. Build. 17 (2008) 541–562. https://doi.org/10.1002/tal.365.

[12] A.S. Veletsos, J.W. Meek, Dynamic behaviour of building-foundation systems, Earthq Eng. \& Struct. Dyn. 3 (1974) 121–138. https://doi.org/ https://doi.org/10.1002/eqe.4290030203.

[13] F. Edition, API Specification, (2009) 1–12.

[14] D. Hrovat, F. Barak, M. Rabins, Semi-active versus passive or active tuned mass dampers for structural control, J. Eng. Mech. 109 (1983) 691–705. https://doi.org/10.1061/(ASCE)0733-9399(1983)109:3(691).

[15] T. Pinkaew, Y. Fujino, Effectiveness of semi-active tuned mass dampers under harmonic excitation, Eng. Struct. 23 (2001) 850–856. https://doi.org/10.1016/S0141-0296(00)00091-2.

[16] M. Abe, Semi-active tuned mass dampers for seismic protection of civil structures, Earthq. Eng. Struct. Dyn. 25 (1996) 743–749. https://doi.org/10.1002/(SICI)1096-9845(199607)25:7<743::AID-EQE579>3.0.CO;2-S.

[17] S. Elias, V. Matsagar, T.K. Datta, Distributed Multiple Tuned Mass Dampers for Wind Response Control of Chimney with Flexible Foundation, Procedia Eng. 199 (2017) 1641–1646. https://doi.org/10.1016/j.proeng.2017.09.087.

[18] F. Ferreira, C. Moutinho, Á. Cunha, E. Caetano, Use of semi-active tuned mass dampers to control footbridges subjected to synchronous lateral excitation, J. Sound Vib. 446 (2019) 176–194. https://doi.org/10.1016/j.jsv.2019.01.026.

[19] P. Silva Lobo, J. Almeida, L. Guerreiro, Semi-active Damping Device Based on Superelastic Shape Memory Alloys, Structures. 3 (2015) 1–12. https://doi.org/10.1016/j.istruc.2015.06.006.

[20] M. Khatibinia, H. Gholami, S.F. Labbafi, DAMPERS CONSIDERING SOIL – STRUCTURE INTERACTION c r v i h o e f c f, 6 (2016) 595–610.

[21] R.N. Jabary, S.P.G. Madabhushi, Structure-soil-structure interaction effects on structures retrofitted with tuned mass dampers, Soil Dyn. Earthq. Eng. 100

(2017) 301–315. https://doi.org/10.1016/j.soildyn.2017.05.017.

[22] S.M. Nigdeli, G. Bekdaş, Optimum tuned mass damper design in frequency domain for structures, KSCE J. Civ. Eng. 21 (2017) 912–922. https://doi.org/10.1007/s12205-016-0829-2.

[23] J. Salvi, F. Pioldi, E. Rizzi, Optimum Tuned Mass Dampers under seismic Soil-Structure Interaction, Soil Dyn. Earthq. Eng. 114 (2018) 576–597. https://doi.org/10.1016/j.soildyn.2018.07.014.

[24] S. Bakhshinezhad, M. Mohebbi, Multi-Objective Optimal Design of Satmd Including Soil-Structure Interaction Using Nsga-Ii, 10 (2020) 391–409.

[25] S. Gaur, S. Elias, T. Höbbel, V.A. Matsagar, K. Thiele, Tuned mass dampers in wind response control of wind turbine with soil-structure interaction, Soil Dyn. Earthq. Eng. 132 (2020). https://doi.org/10.1016/j.soildyn.2020.106071.

[26] M. Lou, W. Wang, Study on soil-pile-structure-TMD interaction system by shaking table model test, Earthq. Eng. Eng. Vib. 3 (2004) 127–137. https://doi.org/10.1007/bf02668858.

[27] J. E. Luco; M. D. Trifunac; H. L. Wong, On the apparent change in dynamic behavior of a nine-story reinforced concrete building, Bull. Seismol. Soc. Am. 77 (6): 19 (1987).

[28] R. Saha, S.C. Dutta, S. Haldar, S. Kumar, Effect of soil-pile raft-structure

interaction on elastic and inelastic seismic behaviour, Structures. 26 (2020) 378–395. https://doi.org/10.1016/j.istruc.2020.04.022.

[29] P. Li, J. Yang, Z. Lu, Shaking table test and theoretical analysis of the pile–soil–structure interaction at a liquefiable site, Struct. Des. Tall Spec. Build. 27 (2018) 1–16. https://doi.org/10.1002/tal.1513.

[30] O.S. Ali, M. Mahamid, Effect of Soil-Foundation Interaction on the Dynamic Response of a Four-Cylinder Compressor Foundation, Pract. Period. Struct. Des. Constr. 23 (2018) 1–13. https://doi.org/10.1061/(ASCE)SC.1943-5576.0000380.

[31] S. Liu, Z. Lu, P. Li, W. Zhang, E. Taciroglu, Effectiveness of particle tuned mass damper devices for pile-supported multi-story frames under seismic excitations, Struct. Control Heal. Monit. 27 (2020). https://doi.org/10.1002/stc.2627.

[32] P. Raychowdhury, P. Singh, Effect of nonlinear soil-structure interaction on seismic response of low-rise SMRF buildings, Earthq. Eng. Eng. Vib. 11 (2012) 541–551. https://doi.org/10.1007/s11803-012-0140-2.

[33] S. Naserkhaki, F.N.A.A. Aziz, H. Pourmohammad, Earthquake induced pounding between adjacent buildings considering soil-structure interaction, J. Earthq. Eng. Eng. Vib. 11 (2012) 343–358. https://doi.org/10.1007/s11803-012-0126-0.

[34] N. Sharma, K. Dasgupta, A. Dey, Natural period of reinforced concrete building frames on pile foundation considering seismic soil-structure interaction effects, Structures. 27 (2020) 1594–1612. https://doi.org/10.1016/j.istruc.2020.07.010.

[35] S. Elias, Effect of SSI on vibration control of structures with tuned vibration absorbers, Shock Vib. 2019 (2019). https://doi.org/10.1155/2019/7463031.

[36] S. Liu, Z. Lu, P. Li, S. Ding, F. Wan, Shaking table test and numerical simulation of eddy-current tuned mass damper for structural seismic control considering soil-structure interaction, Eng. Struct. 212 (2020) 110531. https://doi.org/10.1016/j.engstruct.2020.110531.

[37] X. Zhao, S. Wang, D. Du, W. Liu, Simplified analysis of frame structures with viscoelastic dampers considering the effect of soil-structure interaction, Earthq. Eng. Eng. Vib. 16 (2017) 199–217. https://doi.org/10.1007/s11803-017-0377-x.

[38] J. Yang, Z. Lu, P. Li, Large-scale shaking table test on tall buildings with viscous dampers considering pile-soil-structure interaction, Eng. Struct. 220 (2020). https://doi.org/10.1016/j.engstruct.2020.110960.

[39] A. Rahmani, M. Taiebat, W.D.L. Finn, C.E. Ventura, Evaluation of p-y springs for nonlinear static and seismic soil-pile interaction analysis under lateral loading, Soil Dyn. Earthq. Eng. 115 (2018) 438–447. https://doi.org/10.1016/j.soildyn.2018.07.049.

[40] T. Liu, M. Wang, Experimental research on the development of residual strain in seasonal frozen soil under freezing-thawing and impact type traffic loads, Earthq. Eng. Eng. Vib. (2020). https://doi.org/10.1007/s11803-021-2001-3.

[41] C.R. McGann, P. Arduino, P. Mackenzie-Helnwein, Applicability of conventional p-y relations to the analysis of piles in laterally spreading soil, J. Geotech. Geoenvironmental Eng. 137 (2011) 557–567. https://doi.org/10.1061/(ASCE)GT.1943-5606.0000468.

[42] N. GM, Theoretically based on laterally loaded pile analysis, in: Proc. Third Int. Conf. Numer. Methods Offshore Piling, 1986: pp. 361–86.

[43] P.H. Ashour M, Pilling P, Norris G, Development of strain wedge model program for pile group interference and pile cap contribution effects, Tech. Rep. 96-4. rep. 96-4 (1996).

[44] A.M. Elmeliegy, Y.F. Rashed, Efficient Preconditioned Soil-Foundation-Structure Interaction Approach to Compute Tall-Building Time Periods, Pract. Period. Struct. Des. Constr. 24 (2019) 1–13. https://doi.org/10.1061/(ASCE)SC.1943-5576.0000422.

[45] A. Rahmani, Three-dimensional nonlin. ear analysis of dynamic soil-pile-structure interaction for bridge systems under earthquake shakings, The University of British Columbia, 2014.

[46] A. Rahmani, M. Taiebat, W. Finn, C. Ventura, Determination of Dynamic py

Curves for Pile Foundations Under Seismic Loading, World Conf. Earthq. Eng. (2012). http://www.iitk.ac.in/nicee/wcee/article/WCEE2012_5228.pdf.

[47] A. Tyapin, The frequency-dependent elements in the code SASSI: A bridge between civil engineers and the soil-structure interaction specialists, Nucl. Eng. Des. 237 (2007) 1300–1306. https://doi.org/10.1016/j.nucengdes.2006.09.031.

[48] H.S. Kim, J.W. Kang, Semi-active fuzzy control of a wind-excited tall building using multi-objective genetic algorithm, Eng. Struct. 41 (2012) 242–257. https://doi.org/10.1016/j.engstruct.2012.03.038.

[49] F. Behnamfar, M. Nooraei, M. Talebi, Amirkabir Journal of Civil Engineering A 3-stage Method for Selection of Ground Motions for Dynamic Time History Analysis, Civ. Eng. 49 (2017) 39–41. https://doi.org/10.22060/ceej.2016.603.

[50] M. Bayat, L. V. Andersen, L.B. Ibsen, P-Y-Ẏ Curves for Dynamic Analysis of Offshore Wind Turbine Monopile Foundations, Soil Dyn. Earthq. Eng. 90 (2016) 38–51. https://doi.org/10.1016/j.soildyn.2016.08.015.

[51] B.J. Turner, S.J. Brandenberg, J.P. Stewart, Influence of kinematic SSI on foundation input motions for bridges on deep foundations, (2017) 1–228.

[52] S. Elias, V. Matsagar, T.K. Datta, Distributed Tuned Mass Dampers for Multi-Mode Control of Benchmark Building under Seismic Excitations, J. Earthq. Eng. 23 (2019) 1137–1172. https://doi.org/10.1080/13632469.2017.1351407.

[53] C.C. Lin, L.Y. Lu, G.L. Lin, T.W. Yang, Vibration control of seismic structures using semi-active friction multiple tuned mass dampers, Eng. Struct. 32 (2010) 3404–3417. https://doi.org/10.1016/j.engstruct.2010.07.014.

[54] B. Zhao, D. Wu, Z. Lu, Shaking table test and numerical simulation of the vibration control performance of a tuned mass damper on a transmission tower, Struct. Infrastruct. Eng. (2020). https://doi.org/10.1080/15732479.2020.1800755.

[55] A. Farshidianfar, S. Soheili, Ant colony optimization of tuned mass dampers for earthquake oscillations of high-rise structures including soil-structure interaction, Soil Dyn. Earthq. Eng. 51 (2013) 14–22. https://doi.org/10.1016/j.soildyn.2013.04.002.

[56] M. Mohebbi, S. Moradpour, Y. Ghanbarpour, Improving the Seismic Behavior of Nonlinear Steel Structures Using Optimal Mtmds, Int. J. Optim. Civ. Eng. 4 (2014) 137–150.

[57] J.P. Den Hartog, Mechanical Vibrations, third ed, McGraw-Hill, New York, 1947.

[58] H.Frahm, Devicefordampingvibrationofbodies, U.S.Patent. 989,958,19 (1925).

[59] Z. Zhang, T. Balendra, Passive control of bilinear hysteretic structures by tuned mass damper for narrow band seismic motions, Eng. Struct. 54 (2013) 103–111. https://doi.org/10.1016/j.engstruct.2013.03.044.

[60] M. Chey, Parametric control of structures using a tuned mass damper system under earthquake excitations, Dep. Civ. Eng. (2000).

[61] T.T. Chang, James CH and Soong, Structural control using active tuned mass dampers, J. Eng. Mech. Div. 106 (1980) 1091–1098.

[62] M. Abdel-Rohman, Optimal design of active TMD for buildings control, Build. Environ. 19 (1984) 191–195. https://doi.org/10.1016/0360-1323(84)90026-X.

[63] E. Nazarimofrad, S.M. Zahrai, Fuzzy control of asymmetric plan buildings with active tuned mass damper considering soil-structure interaction, Soil Dyn. Earthq. Eng. 115 (2018) 838–852. https://doi.org/10.1016/j.soildyn.2017.09.020.

[64] H. Shariatmadar, H.M. Razavi, Seismic control response of structures using an ATMD with fuzzy logic controller and PSO method, Struct. Eng. Mech. 51 (2014) 547–564. https://doi.org/10.12989/sem.2014.51.4.547.

[65] M. Domaneschi, L. Martinelli, Optimal passive and semi-active control of a wind excited suspension bridge, Struct. Infrastruct. Eng. 9 (2013) 242–259. https://doi.org/10.1080/15732479.2010.542467.

[66] M. Setareh, Application of semi-active tuned mass dampers to base-excited systems, Earthq. Eng. Struct. Dyn. 30 (2001) 449–462. https://doi.org/10.1002/eqe.19.

[67] M.T. Koo JH, Setareh M, In search of suitable control methods for semi-active tuned vibration absorbers, J Vib Control. 10 (2004) 163–74.

[68] F. Ricciardelli, A. Occhiuzzi, P. Clemente, Semi-active tuned mass damper control strategy for wind-excited structures, J. Wind Eng. Ind. Aerodyn. 88 (2000) 57–74. https://doi.org/10.1016/S0167-6105(00)00024-6.

[69] M.P. Lytle, R. S., Hom, P. W., & Mokwa, Information To Users Umi, Dissertation. Ph.D. Thes (1998) 274.

[70] U. Aldemir, Optimal control of structures with semiactive-tuned mass dampers, J. Sound Vib. 266 (2003) 847–874. https://doi.org/10.1016/S0022-460X(03)00191-3.

[71] K. Mulligan, Experimental and Analytical Studies of Semi-Active and Passive Structural Control of Buildings, (2007).

[72] J. D. Hartog, Mechanical Vibration, 1956.

[73] D. De Domenico, G. Ricciardi, Optimal design and seismic performance of tuned mass damper inerter (TMDI) for structures with nonlinear base isolation systems, Earthq. Eng. Struct. Dyn. 47 (2018) 2539–2560. https://doi.org/10.1002/eqe.3098.

[74] S. Elias, V. Matsagar, Effectiveness of tuned mass dampers in seismic response control of isolated bridges including soil-structure interaction, Lat. Am. J.

Solids Struct. 14 (2017) 2324–2341. https://doi.org/10.1590/1679-78253893.

[75] W.D. Crandall, Stephen H and Mark, Random vibration in mechanical systems, Acad. Press. (2014).

[76] K. Ioi, T. and Ikeda, On the dynamic vibration damped absorber of the vibration system, Bull. JSME. 21(151) (1978) 64–71.

[77] S.E. Randall, D.M. Halsted, D.L. Taylor, Optimum vibration absorbers for linear damped systems, J. Mech. Des. Trans. ASME. 103 (1981) 908–913. https://doi.org/10.1115/1.3255005.

[78] A.G. Thompson, Optimum tuning and damping of a dynamic vibration absorber applied to a force excited and damped primary system, J. Sound Vib. 77 (1981) 403–415. https://doi.org/10.1016/S0022-460X(81)80176-9.

[79] A. Farshidianfar, S. Soheili, Optimization of Tmd Parameters for Earthquake Vibrations of Tall Buildings Including Soil Structure Interaction, Int. J. Optim. Civ. Eng. Int. J. Optim. Civ. Eng. 3 (2013) 409–429.

[80] N. Hoang, P. Warnitchai, Design of multiple tuned mass dampers by using a numerical optimizer, Earthq. Eng. Struct. Dyn. 34 (2005) 125–144. https://doi.org/10.1002/eqe.413.

[81] Y.-C.H. Arthur E. Bryson, Optimization, Estimation, and Control, 1st Editio, Routledge, 1975. https://doi.org/https://doi.org/10.1201/9781315137667.

[82] Warburton G., Optimum absorber parameters for various combinations of response and excitation parameters, Earthq Eng Struct Dyn. 10 (1982) 381–401.

[83] R. Greco, G.C. Marano, Optimum design of tuned mass dampers by displacement and energy perspectives, Soil Dyn. Earthq. Eng. 49 (2013) 243–253. https://doi.org/10.1016/j.soildyn.2013.02.013.

[84] A.M. Reggio A, Optimal energy-based seismic design of non-conventional Tuned Mass Damper (TMD) implemented via inter-story isolation., Earthq Eng Struct Dyn. 44 (2015) 1623–42.

[85] Y.J. Liu, S. Tong, C.L.P. Chen, D.J. Li, Adaptive NN Control Using Integral Barrier Lyapunov Functionals for Uncertain Nonlinear Block-Triangular Constraint Systems, IEEE Trans. Cybern. 47 (2017) 3747–3757. https://doi.org/10.1109/TCYB.2016.2581173.

[86] P. Brezas, M.C. Smith, W. Hoult, A clipped-optimal control algorithm for semi-active vehicle suspensions: Theory and experimental evaluation, Automatica. 53 (2015) 188–194. https://doi.org/10.1016/j.automatica.2014.12.026.

[87] L.D. Viet, N.B. Nghi, N.N. Hieu, D.T. Hung, N.N. Linh, L.X. Hung, On a combination of ground-hook controllers for semi-active tuned mass dampers, J. Mech. Sci. Technol. 28 (2014) 2059–2064. https://doi.org/10.1007/s12206-014-0109-3.

[88] J. Lysmer, Roger L. Kuhlemeyer, Finite Dynamic Model For Infinite Media, J.

Eng. Mech. Div. 95 (1969) 859–878.

[89] G. Lysmer, J.;Wass, Shear waves in plane infinite structures., J. Eng. Mech. ASCE. 98 (1972) 85–105.

[90] I.K. White, W.; Valliappan, S.; Lee, Unified boundary for finite dynamic models, J. Eng. Mech. ASCE. 103 (1977) 949–964.

[91] H.. Liao, Z.P.; Wong, A transmitting boundary for the numerical simulation of elastic wave propagation., Oil Dyn. Earthq. Eng. 3 (1984).

[92] F.Q. Zienkiewicz, O.C.; Bielak, J.; Shen, Earthquake input definition and the transmitting boundary condition, Adv. Comput. Non-Linear Mech. (1988) 109–138.

[93] M.F. Deeks, A.J.; Randolph, Axisymmetric Time-domain Transmitting Boundaries, J. Eng. Mech. ASCE. 120 (1994) 25–42.

[94] J.H. Lee, Nonlinear soil-structure interaction analysis in poroelastic soil using mid-point integrated finite elements and perfectly matched discrete layers, Soil Dyn. Earthq. Eng. 108 (2018) 160–176. https://doi.org/10.1016/j.soildyn.2018.01.043.

[95] J.L. Coleman, C. Bolisetti, A.S. Whittaker, Time-domain soil-structure interaction analysis of nuclear facilities, Nucl. Eng. Des. 298 (2016) 264–270. https://doi.org/10.1016/j.nucengdes.2015.08.015.

[96] J.M. Solberg, Q. Hossain, G. Mseis, Nonlinear time-domain soil-structure interaction analysis of embedded reactor structures subjected to earthquake loads, Nucl. Eng. Des. 304 (2016) 100–124. https://doi.org/10.1016/j.nucengdes.2016.04.026.

[97] J.A. Abell, N. Orbović, D.B. McCallen, B. Jeremic, Earthquake soil-structure interaction of nuclear power plants, differences in response to 3-D, 3 × 1-D, and 1-D excitations, Earthq. Eng. Struct. Dyn. 47 (2018) 1478–1495. https://doi.org/10.1002/eqe.3026.

[98] P.E.B. QUINAY, T. ICHIMURA, M. HORI, M.L.L. WIJERATHNE, A. NISHIDA, Seismic Structural Response Analysis Considering Fault-Structure System: Application to Nuclear Power Plant Structures, Prog. Nucl. Sci. Technol. 2 (2011) 516–523. https://doi.org/10.15669/pnst.2.516.

[99] M. Miyamura, T.; Tanaka, S.; Hori, Large-Scale Seismic Response Analysis of a Super-High-Rise-Building Fully Considering the Soil–Structure Interaction Using a High-Fidelity 3D Solid Element Model., J. Earthq. Tsunami. 10 (2016) 1–21.

[100] A. Pecker, R. Paolucci, C. Chatzigogos, A.A. Correia, R. Figini, The role of non-linear dynamic soil-foundation interaction on the seismic response of structures, Bull. Earthq. Eng. 12 (2014) 1157–1176. https://doi.org/10.1007/s10518-013-9457-0.

[101] M. Davoodi, M. Sagjadi, P. Goljahani, M. Kamalian, Effects of Near-Field and

Far-Field Earthquakes on Seismic Response of SDOF System Considering Soil Structure Interaction, 15th World Conf. Earthq. Eng. (2012).

[102] J.E. Luco, Impedance functions for a rigid foundation on a layered medium, Nucl. Eng. Des. 31 (1974) 204–217. https://doi.org/10.1016/0029-5493(75)90142-9.

[103] J. Enrique Luco, Vibrations of a rigid disc on a layered viscoelastic medium, Nucl. Eng. Des. 36 (1976) 325–340. https://doi.org/10.1016/0029-5493(76)90026-1.

[104] G. Gazetas, I. Anastasopoulos, O. Adamidis, T. Kontoroupi, Nonlinear rocking stiffness of foundations, Soil Dyn. Earthq. Eng. 47 (2013) 83–91. https://doi.org/10.1016/j.soildyn.2012.12.011.

[105] S.Y. Kwon, M. Yoo, Study on the dynamic soil-pile-structure interactive behavior in liquefiable sand by 3D numerical simulation, Appl. Sci. 10 (2020) 1–22. https://doi.org/10.3390/APP10082723.

[106] S. Carbonari, M. Morici, F. Dezi, G. Leoni, A lumped parameter model for time-domain inertial soil-structure interaction analysis of structures on pile foundations, Earthq. Eng. Struct. Dyn. 47 (2018) 2147–2171. https://doi.org/10.1002/eqe.3060.

[107] P. Bucinskas, L.V. Andersen, Dynamic response of vehicle–bridge–soil system using lumped-parameter models for structure–soil interaction, Comput. Struct.

238 (2020) 106270. https://doi.org/10.1016/j.compstruc.2020.106270.

[108] J.J. Maslenikov, O. R. and Chen, J. C. and Johnson, Uncertainty in soil-structure interaction analysis arising from differences in analytical techniques, Osti_6869711. (1982).

[109] F.S. Matlock H, Simulation of lateral pile behavior under earthquake motion, The University of Texas at Austin, 1978.

[110] M.H. El Naggar, K.J. Bentley, Dynamic analysis for laterally loaded piles and dynamic p-y curves, Can. Geotech. J. 37 (2000) 1166–1183. https://doi.org/10.1139/cgj-37-6-1166.

[111] Gohl B, Response of pile foundations to simulated earthquake loading, University of British Columbia, 1991.

[112] R.W. Boulanger, C.J. Curras, B.L. Kutter, D.W. Wilson, A. Abghari, Seismic soil-pile-structure interaction experiments and analysis, J. Geotech. Geoenvironmental Eng. ASCS, 125((1999).

[113] M. Ertugrul Taciroglu; ChangSoon Rha; and John W. Wallace, A Robust Macroelement Model for Soil–Pile Interaction under Cyclic Loads, J. Geotech. Geoenvironmental Eng. Volume 132 (n.d.).

[114] H. Meyer, P., Holmquist, D. and Matlock, Computer predictions for axially-loaded piles with nonlinear supports, (1975).

[115] Y. Kim, S. Jeong, Analysis of soil resistance on laterally loaded piles based on 3D soil-pile interaction, Comput. Geotech. 38 (2011) 248–257. https://doi.org/10.1016/j.compgeo.2010.12.001.

[116] M.T. Yoo, J.I. Choi, J.T. Han, M.M. Kim, Dynamic P-Y curves for dry sand from centrifuge tests, J. Earthq. Eng. 17 (2013) 1082–1102. https://doi.org/10.1080/13632469.2013.801377.

[117] A. Rahmani, M. Taiebat, W.D. Liam Finn, C.E. Ventura, Evaluation of substructuring method for seismic soil-structure interaction analysis of bridges, SoilDyn.Earthq.Eng.90(2016)112–127. https://doi.org/10.1016/j.soildyn.2016.08.013.

[118] S. Dash, M. Rouholamin, D. Lombardi, S. Bhattacharya, A practical method for construction of p-y curves for liquefiable soils, Soil Dyn. Earthq. Eng. 97 (2017) 478–481. https://doi.org/10.1016/j.soildyn.2017.03.002.

[119] K.I. Al-Hulwah, R. Kashani, Floor vibration control using three-degree-of-freedom tuned mass dampers, Am. Soc. Mech. Eng. Des. Eng. Div. 117 (2004) 509–515. https://doi.org/10.1115/IMECE2004-60106.

[120] A.A. Bramlette McClelland ; and John A. Focht Jr., Soil Modulus for Laterally Loaded Piles, Trans. Am. Soc. Civ. Eng. 123 (1958).

[121] H. Matlock, S. Foo, Simulation of lateral pile behavior under earthquake motion, 1978.

[122] M. Allotey, N. and El Naggar, Generalized dynamic Winkler model for nonlinear soil-structure interaction analyses, Can. Geotech. J. (2008) 560–573.

[123] F. Kausel, E., Whitman, R., Morray, J. and Elsabee, The spring method for embedded foundations, Nucl. Eng. Des. (1978) 377–392.

[124] A. Shamsabadi, Seismi soil-foundation-structure-interaction (SFSI): practical bridge seismic foundation specifications design and analysis, USA, 2013.

[125] AASHTO, AASHTO LRFD bridge, 2012. https://search.proquest.com/docview/1732672743?accountid=14504%0Ahttp://godot.lib.sfu.ca/GODOT/hold_tab.cgi?url_ver=Z39.88-2004&rft_val_fmt=info:ofi/fmt:kev:mtx:dissertation&genre=dissertations+%26+theses&sid=ProQ:ProQuest+Dissertations+%26+Theses+A%26I&a.

[126] G.R. Lam, I. P., Law, H. K. and Martin, Bridge foundations: Modeling large pile groups and caissons for seismic design, US Multidisciplinar Center for Earthquake Engineering Research., 2007.

[127] S. Fan, K., Gazetas, G., Kaynia, A., Kausel, E. and Ahmad, Kinematic seismic response of single piles and pile groups, J. Geotech. Eng. 117 (1991) 1860–1879.

[128] G. Makris, N., Badoni, D., Delis, E. and Gazetas, Prediction of observed bridge response with soil-pile-structure interaction, J. Struct. Eng. 120 (1994) 2922–3011.

[129] A. Dassault Systèmes, CATIA, (2005).

[130] A. Inc, ANSYS FLUENT theory guide, (2013).

[131] G. McKenna, F. and Fenves, The OpenSees command language manual, (2001). http://opensees.berkeley.edu.

[132] E. Yang, Z., Elgamal, A. and Parra, Computational model for cyclic mobility and associated shear deformation, J. Geotech. Geoenvironmental Eng. (2003) 1119–1127.

[133] J. Prevost, Plasticity theory for soil stress-strain behavior, J. Eng. Mech. Div. 104(5), 11 (1978).

[134] V.N. Burlayenko, T. Sadowski, Free vibrations and static analysis of functionally graded sandwich plates with three-dimensional finite elements, Meccanica. 55 (2020) 815–832. https://doi.org/10.1007/s11012-019-01001-7.

[135] J. B. Mander; M. J. N. Priestley; and R. Park, Observed Stress-Strain Behavior of Confined Concrete, J. Struct. Eng. 114 (1988).

[136] M.H. Scott, G.L. Fenves, Krylov Subspace Accelerated Newton Algorithm: Application to Dynamic Progressive Collapse Simulation of Frames, J. Struct. Eng. 136 (2010) 473–480. https://doi.org/10.1061/(asce)st.1943-541x.0000143.

[137] J.M. Rosset, E. Kausel, Dynamic Soil-Structure Interaction, in: Proceedings of the Second International Conference on Numerical Methods in Geomechanics, Blacksburg, Virginia, 1976: pp. 3–19.

[138] M. Seidalinov, G. and Taiebat, Bounding surface SANICLAY plasticity model for cyclic clay behavior, Int. J. Numer. Anal. Methods Geomech. 38 (2014) 702–724.

[139] M. Chako, Analysis of dynamic soil-pile structure interaction, University of California, Davis, 1995.

[140] F.C. Filippou, E.P. Popov, V.V. Bertero, Effects of bond deteroriation on hysteretic behavior of renforce concrete joint (EERC 83-19), Earthq. Eng. Res. Center, Univ. California, Berkeley. (1983) 212.

APPENDIX

SHAPE FUNCTION

A.1 Shape function

The finite element method requires subdivision of the field region into sub-regions or subdomains and approximation of the solution in each sub-region by a trial function. Then functional minimization or a weighted residual procedure is employed to determine the parameters of the interpolation function satisfying boundary conditions for the field problem.

The shape function is the function which interpolates the solution between the discrete values obtained at the mesh nodes. Therefore, appropriate functions have to be used and low order polynomials are typically chosen as shape functions. In this study, the brick element are used in finite element model. Brick (solid) element is a three-dimensional finite element with both local and global coordinates. It is characterized by linear shape functions in each of the x, y, and z directions. It is also called a trilinear hexahedron. The linear brick element has modulus of elasticity E and Poisson's ratio v. Isoparametric interpolation within the element volume is defined in terms of the natural coordinates (ζ, η, ξ) each spanning the range from -1 to +1, as presented in Figure 61 [134].

$$\sum_i^8 N = \frac{1}{8}(1-\xi_i)(1-\eta_i)(1-\zeta_i), \quad for\ i = 1 \ldots .8 \tag{A.1}$$

$$\sum_i^{20} N = -(2+\xi_i+\eta_i+\zeta_i)\sum_i^8 N, \quad for\ i = 1 \ldots .8 \tag{A.2}$$

$$\sum_i^{20} N = 2(1+\xi_i)\sum_i^8 N, \ for\ i = 9,11,13,15 \tag{A.3}$$

$$\sum_i^{20} N = 2(1+\eta_i)\sum_i^8 N, \quad for\ i = 10,12,14,16 \tag{A.4}$$

$$\sum_i^{20} N = 2(1+\zeta_i)\sum_i^8 N \quad for\ i = 17 \ldots 20 \tag{A.5}$$

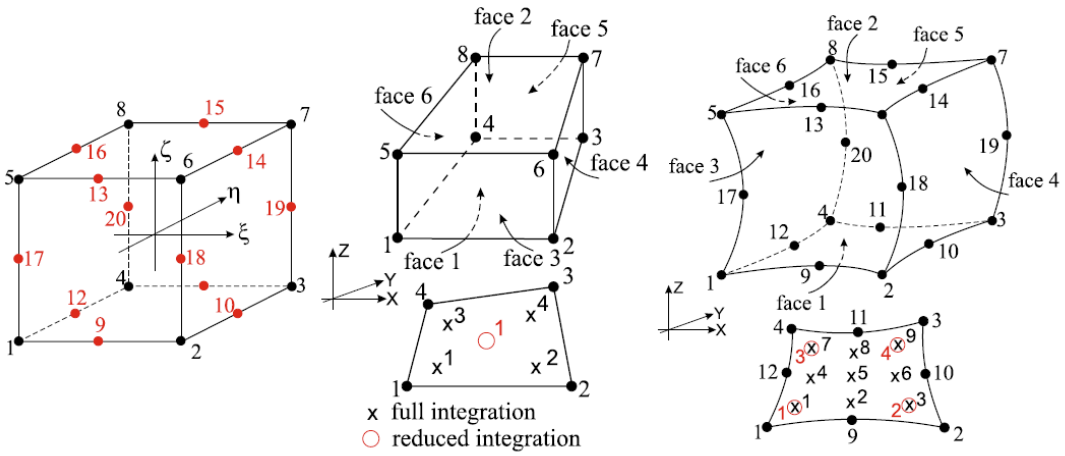

Figure 61: Isoperimetric 3-D brick finite elements [134]

The method of deriving shape functions for Lagrange-or serendipity-type two-dimensional rectangular elements can be easily extended to hexahedral elements in three dimensions. The shape functions for these elements are derived in exactly the same manner for the corresponding rectangular elements. For example, the element shape functions for the linear eight-noded Lagrangian element are obtained by taking the product of the corresponding linear interpolation functions in the x, y, and z directions, respectively. Thus, for node 1 for the linear Lagrange element shown in Figure 62,

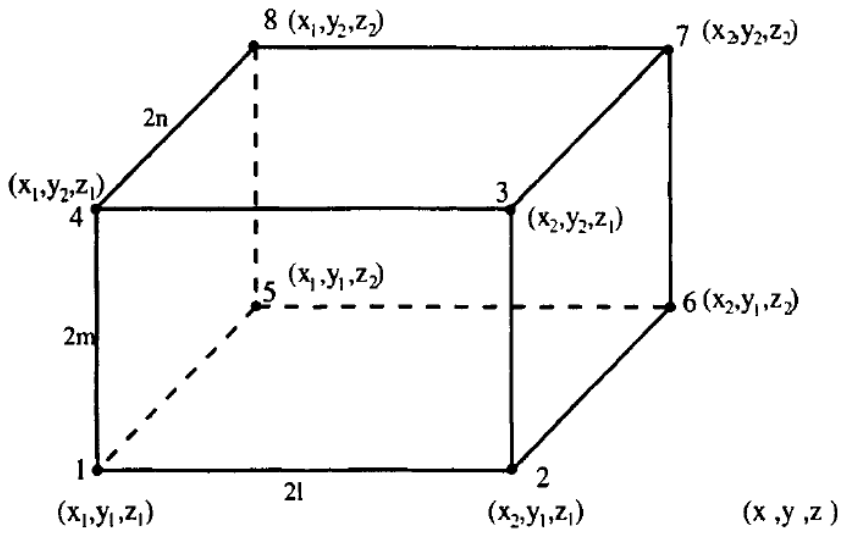

Figure 62: Linear Lagrange Element with Node Numbering and Coordinates

$$\zeta_1 = \zeta_{x1}\zeta_{y1}\zeta_{z1} \tag{A.6}$$

$$\zeta_{x1} = \frac{x-x_2}{x_1-x_2} \tag{A.7}$$

$$\zeta_{y1} = \frac{y-y_2}{y_1-y_2} \tag{A.8}$$

Substituting x_1 = - I and x_2 = +l, y_1= - m and Y_2 = +m, Z_1 = - n and Z_2 = +n, and introducing non-dimensional parameters or natural coordinates ζ= x/l, η=y/m, and λ=z/n, the shape function for node 1 is obtained as:

$$\zeta_1 = \frac{(1-\zeta)(1-\eta)(1-\lambda)}{8} \tag{A.9}$$

Similarly, the shape functions for the other nodes can also be obtained. For high-order elements, Lagrange-type elements involve a very large number of nodes and therefore are used only in special cases. The more commonly used ones are the Serendipity elements. The procedure for obtaining these follow the method described earlier for two-dimensional elements and will not be repeated here. For the reader's convenience, the shape functions for the serendipity-type hexahedral elements for first through third order are given next:

Linear elements:

$$\zeta_i = \frac{1}{8}(1+\zeta_i\zeta)(1+\eta_i\eta)(1+\lambda_i\lambda), \zeta_i = \pm 1, \eta_i = \pm 1, \lambda_i = \pm 1 \quad \text{(A.10)}$$

Quadratic elements: for the corner nodes

$$\zeta_i = \frac{1}{8}(1+\zeta_i\zeta)(1+\eta_i\eta)(1+\lambda_i\lambda)(\zeta_i\zeta+\eta_i\eta+\lambda_i\lambda-2) \quad \text{(A.11)}$$

And for the mid-side nodes

$$\zeta_i = \frac{1}{4}(1+\zeta^2)(1+\eta_i\eta)(1+\lambda_i\lambda), \eta_i = \pm 1, \lambda_i = \pm 1, \zeta_i = 0 \quad \text{(A.12)}$$

Cubic elements: for the corner nodes:

$$\zeta_i = \frac{1}{64}(1+\zeta_i\zeta)(1+\eta_i\eta)(1+\lambda_i\lambda)\left[9\left(\zeta^2+\eta^2+\lambda^2\right)-19\right],\ \zeta_i = \pm 1 \quad \text{(A.13)}$$

And for the mid-side nodes:

$$\zeta_i = \frac{9}{64}\left(1+\zeta^2\right)(1+9\zeta_i\zeta)(1+\eta_i\eta)(1+\lambda_i\lambda),\ \eta_i = \pm 1,\ \ \lambda_i = \pm 1,\ \zeta_i = \pm\frac{1}{3} \quad \text{(A.14)}$$

In order to help understand the nature of the shape function and computational aspects of interpolation, the shape function are given for each degree of freedom determined by the shape order and type of an element (Figure 63). The characteristics of element modeling can be examined through the graphical representation. They include the inter element continuity related to compatibility of the shape function between adjacent elements.

Hence the shape function of brick elements which are used in this study are depicted by using VisualFEA software. Figure 64 and 65 shows the shape function of eight and four quadrilateral elements with values of the function and its derivatives at the middle position of element respectively. Also, the shape function of the quadrilateral elements at four integration points is shown in Figure 66. Finally, the contour and shading shape function of quadrilateral elements are shown in Figures 67 and 68 respectively.

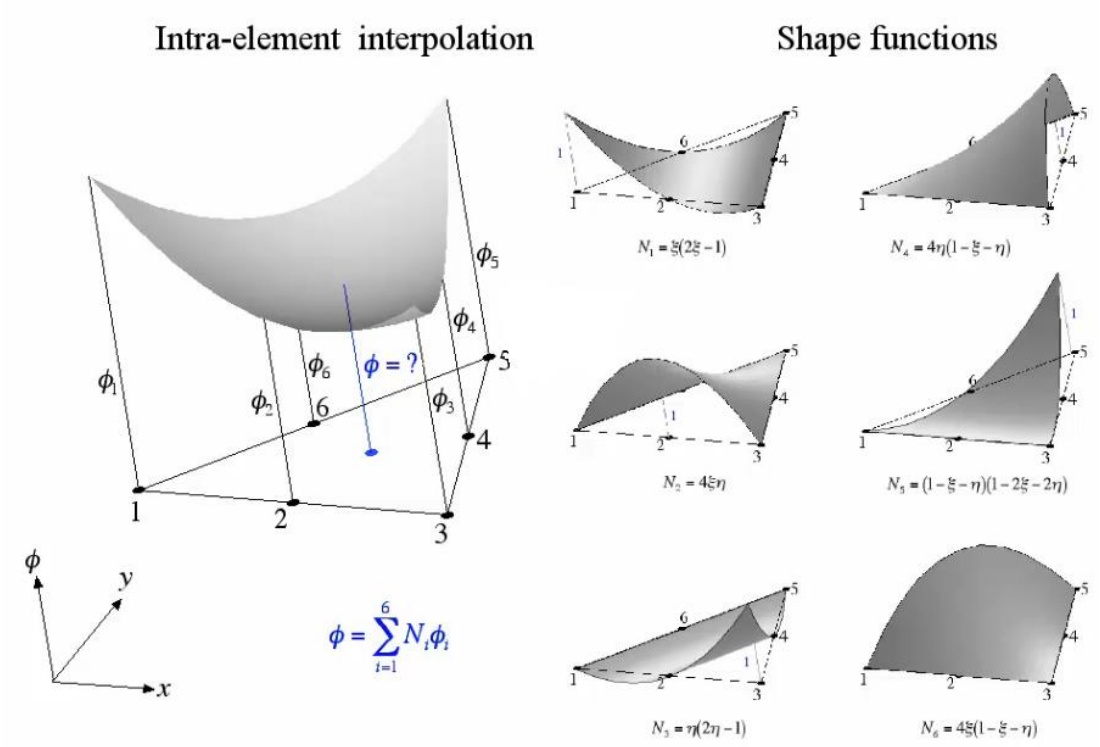

Figure 63: Shape function computational nature

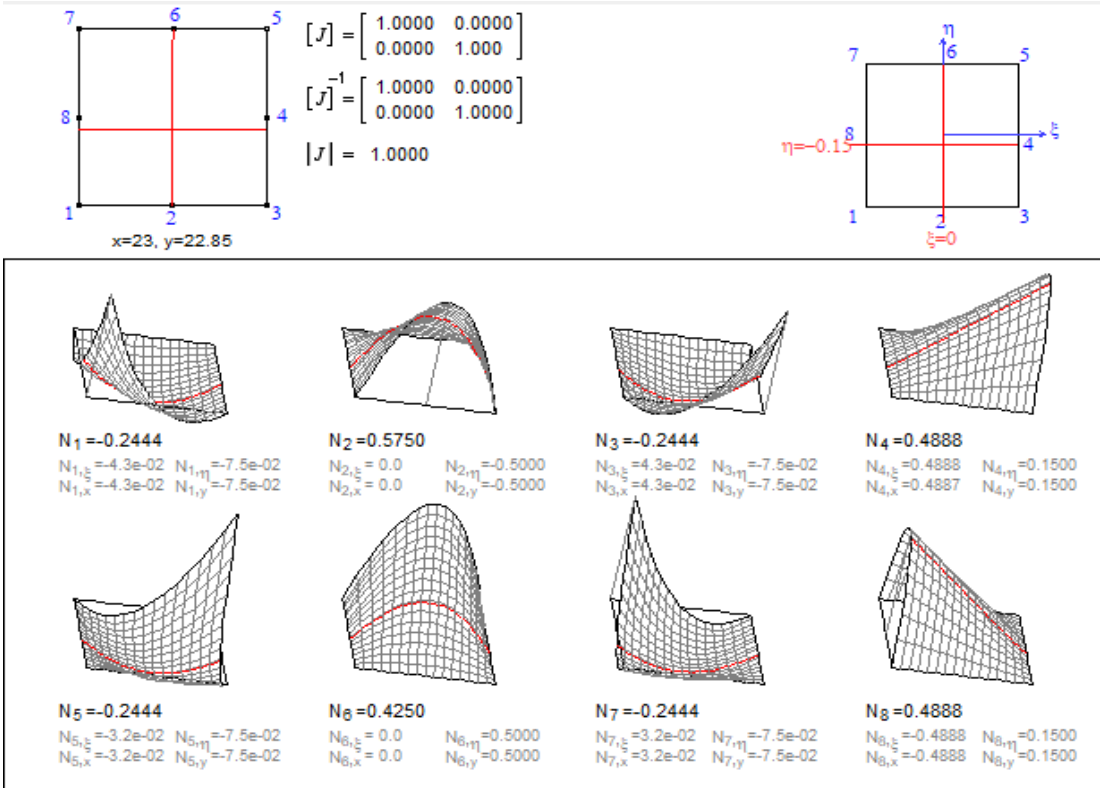

Figure 64: Eight nodes quadrilateral element shape function

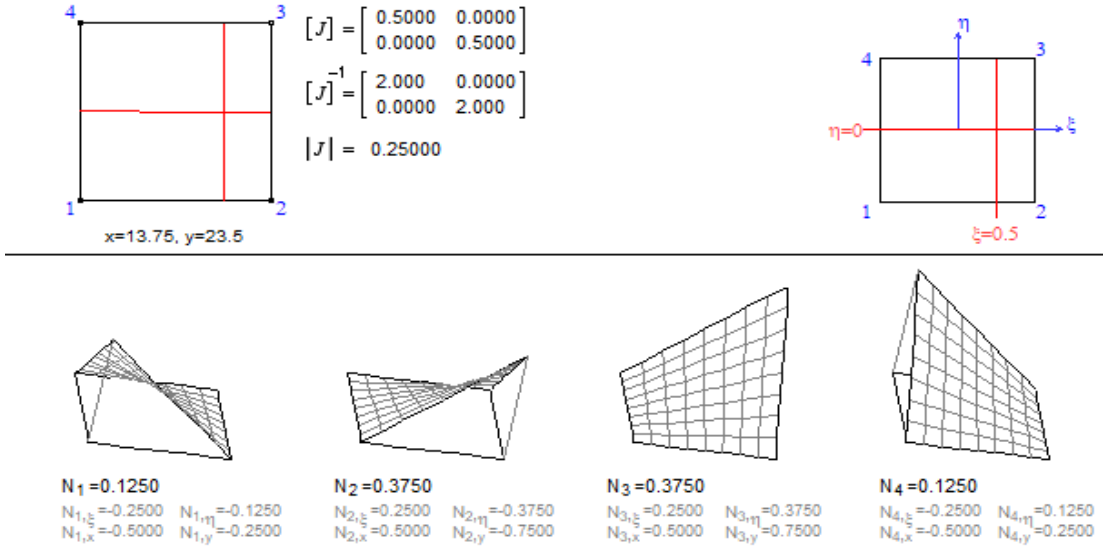

Figure 65: Four nodes quadrilateral element shape function

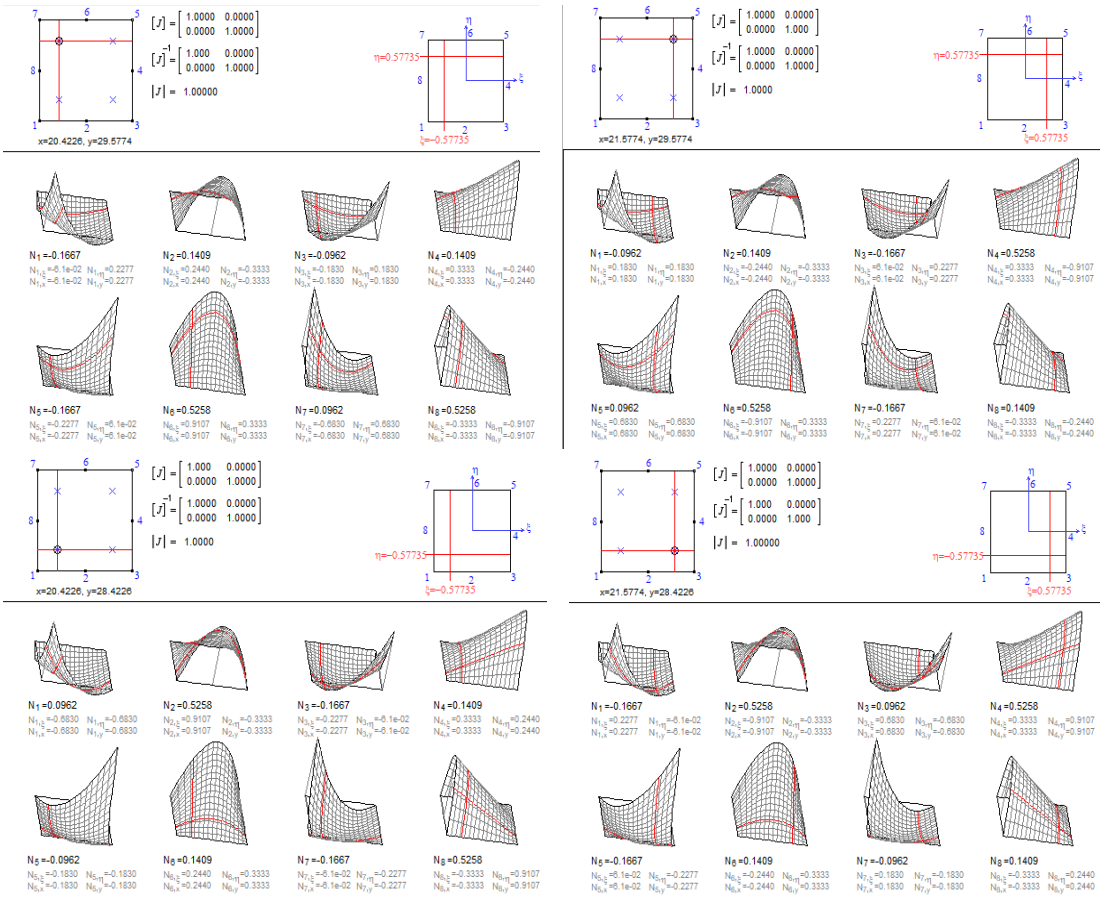

Figure 66: shape function at four integration points

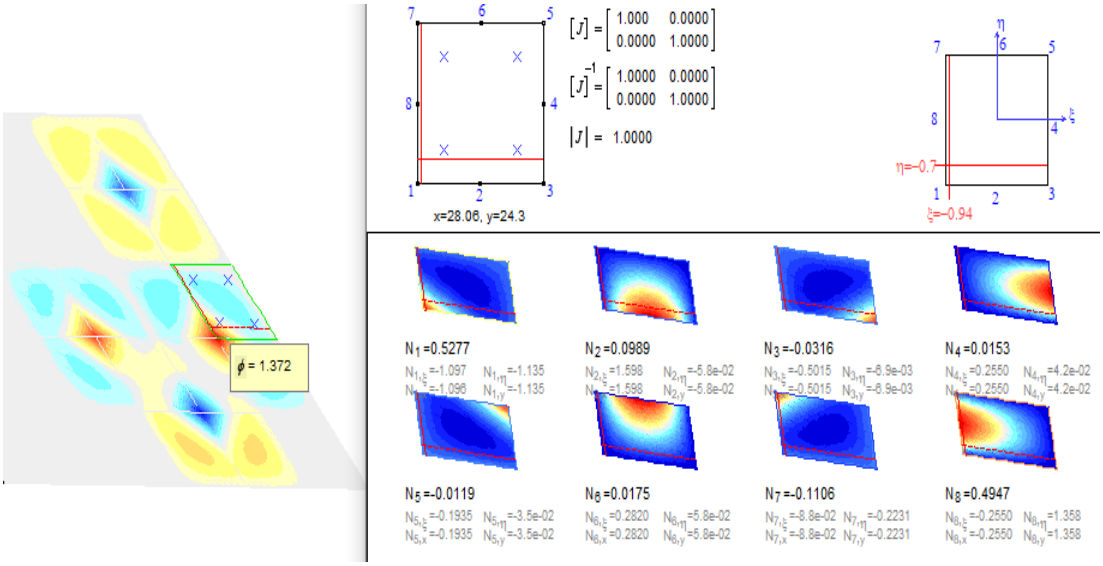

Figure 67: Contour shape function of quadrilateral element

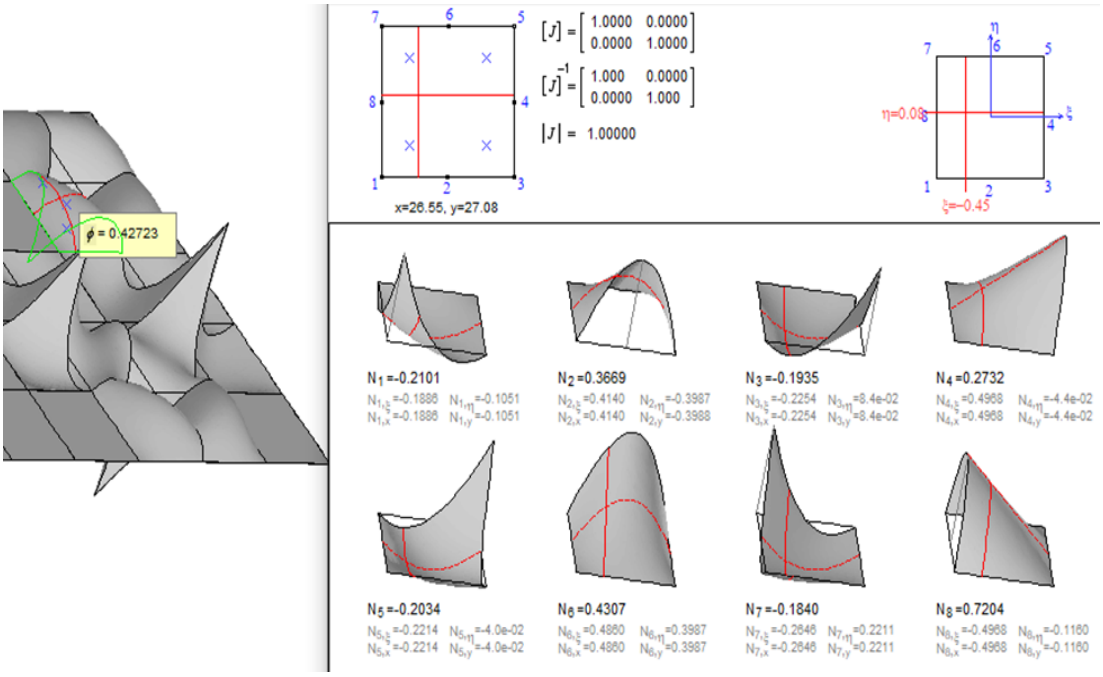

Figure 68: Shading shape function of quadrilateral element